SYNTHESIS OF NANOSTRUCTURED COPPER OXIDE - ZINC OXIDE BY CO-PRECIPITATION PROCESS FOR HUMIDITY SENSOR DEVICE

NATPASIT CHAITHANATKUN

A THESIS SUBMITTED IN PARTIAL FULFILLMENT OF THE REQUIREMENTS FOR THE DEGREE OF MASTER OF SCIENCE IN NANOSCIENCE AND NANOTECHNOLOGY

COLLEGE OF NANOTECHNOLOGY
KING MONGKUT'S INSTITUTE OF TECHNOLOGY LADKRABANG

2017
KMITL-2017-NT-M-001-005

SYNTHESIS OF NANOSTRUCTURED COPPER OXIDE - ZINC OXIDE BY CO-PRECIPITATION PROCESS FOR HUMIDITY SENSOR DEVICE

NATPASIT CHAITHANATKUN

A THESIS SUBMITTED IN PARTIAL FULFILLMENT OF THE REQUIREMENTS FOR THE DEGREE OF MASTER OF SCIENCE IN NANOSCIENCE AND NANOTECHNOLOGY

COLLEGE OF NANOTECHNOLOGY
KING MONGKUT'S INSTITUTE OF TECHNOLOGY LADKRABANG

2017
KMITL-2017-NT-M-001-005

หัวข้อวิทยานิพนธ์	การสังเคราะห์วัสดุคอปเปอร์ออกไซด์-ซิงค์ออกไซด์โครงสร้างระดับนาโนเมตรด้วยวิธีการตกตะกอนร่วม เพื่อประยุกต์ใช้เป็นอุปกรณ์ตรวจวัดความชื้น
นักศึกษา	นายณัฐพสิษฐ์ ไชยธนัทกุล
รหัสประจำตัว	58607013
ปริญญา	วิทยาศาสตรมหาบัณฑิต
สาขาวิชา	นาโนวิทยาและนาโนเทคโนโลยี
พ.ศ.	2560
อาจารย์ที่ปรึกษาวิทยานิพนธ์	ผศ. ดร. เบญจพล ตันฮู้

บทคัดย่อ

ในวิทยานิพนธ์นี้ โครงสร้างระดับนาโนเมตรของคอปเปอร์ออกไซด์-ซิงค์ออกไซด์ถูกเตรียมขึ้นด้วยวิธีการตกตะกอนร่วม ซึ่งได้ทำการศึกษาเงื่อนไขของการเติมปริมาณคอปเปอร์เข้าไปในโครงสร้างของซิงค์ออกไซด์และการเผาในบรรยากาศปกติที่อุณหภูมิต่างๆ จากนั้นทำการตรวจสอบวิเคราะห์ลักษณะทางโครงสร้าง, สมบัติความเป็นผลึก และการวิเคราะห์เชิงเคมีด้วยเทคนิคการเลี้ยวเบนของรังสีเอ็กซ์, กล้องจุลทรรศน์อิเล็กตรอนแบบส่องกราดแบบฟิลด์อิมิชชัน, กล้องจุลทรรศน์อิเล็กตรอนแบบส่องผ่าน, ฟูเรียร์ทรานฟอร์มอินฟราเรดสเปกโตรสโคปี และเอกซเรย์โฟโตอิเล็กตรอนสเปกโตรสโคปี จากผลการทดลองดังกล่าว พบว่าโครงสร้างผลึกของคอปเปอร์ออกไซด์-ซิงค์ออกไซด์มีลักษณะเป็นแบบเฮกซะโกนอลเวอร์ตไซต์ และเมื่อมีการเติมคอปเปอร์เข้าไปในปริมาณที่มากขึ้น จะพบว่ามีลักษณะโครงสร้างแบบโมโนคลินิกของคอปเปอร์ออกไซด์เกิดขึ้นมา อุปกรณ์ตรวจวัดความชื้นสร้างขึ้นโดยการเตรียมชั้นฟิล์มบางของอนุภาคนาโนคอปเปอร์ออกไซด์-ซิงค์ออกไซด์บนขั้วไฟฟ้าด้วยเทคนิคการพ่นด้วยไฟฟ้าสถิต จากการตรวจสอบลักษณะเฉพาะของอุปกรณ์ตรวจความความชื้นพบว่ามีค่าสภาพความไว 279 Ohm/%RH และมีค่าฮิสเทอรีซีสอยู่ที่ 4 %RH เวลาในการดูดซับและคายความชื้นเท่ากับ 26 และ 6 วินาที ตามลำดับ

คำสำคัญ: คอปเปอร์ออกไซด์-ซิงค์ออกไซด์, กระบวนการตกตะกอนร่วม, อนุภาคนาโน, เทคนิคการพ่นด้วยไฟฟ้าสถิต, อุปกรณ์ตรวจวัดความชื้น

Thesis Title	Synthesis of Nanostructured Copper Oxide - Zinc Oxide by Co-Precipitation Process for Humidity Sensor Device
Student	Mr. Natpasit Chaithanatkun
Student ID	58607013
Degree	Master of Science
Program	Nanoscience and Nanotechnology
Year	2017
Thesis Advisor	Asst. Prof. Dr. Benchapol Tunhoo

Abstract

In this dissertation, the nanostructured copper oxide-zinc oxide was prepared by co-precipitation process. The effect of copper content into zinc oxide structure and thermal treatment at various sintering temperature was studied. The morphology, crystal properties and chemical analysis of prepared nanoparticles at various conditions were investigated using X-ray diffraction (XRD), field emission scanning electron microscopy (FE-SEM) and transmission electron microscopy (TEM), Fourier transform infrared spectroscopy (FTIR) and X-ray photoelectron spectroscopy (XPS). The results show that the represent of formation in hexagonal wurtzite phase of zinc oxide and when copper content was increasingly added into the mixture solution found that the feature of monoclinic phase of copper oxide. Humidity sensor has been fabricated from the thin film of copper oxide-zinc oxide nanoparticles by using electrostatic spray deposition technique. The sensor characteristics show the sensitivity of 279 Ohm/%RH, and hysteresis of 4 %RH. The response and recovery time of humidity sensor are 26 and 6 seconds, respectively.

Keywords: Copper Oxide-Zinc Oxide, Co-precipitation process, Nanoparticles, Electrostatic Spray Deposition Technique, Humidity Sensor

Acknowledgement

Now, I am approaching at the end of the long journey toward obtaining my master degree. I have not traveled without the help and encouragement of many people including my advisor, my family, my friends, my colleagues and my teachers. I would like to say thank you very much to my advisor “Asst. Prof. Dr. Benchapol Tunhoo” for advising and supporting me in everything both academic knowledge and living life usages. In addition, he has introduced many scholarships and many chances after I graduate from university. In 2015, I had got a scholarship from Japan Student Services Organization (JASSO) as an exchange student at National Institute of Technology, Anan College in Tokushima Prefecture, Japan for 7 months. I got many experiences with international friends from Taiwan, Japan, Indonesia, Germany, Vietnam and Cambodia and all Japanese teachers for helping me everything when I live in Japan. I would like to say thank you very much to my parents for taking care and supporting me since I was young. I would like to say thank you very much to “Asst. Prof. Dr. Korakot Onlaor”, “Asst. Prof. Dr. Thutiyaporn Thiwawong”, Dr. Sakon Rahong”, and Dr. Mati Horprathum” for being the thesis examination committee and suggesting everything about my research. I would like to say thank you very much to all members of Electronics and Control System for Nanodevice Laboratory (ECSN Lab), lecturers, staffs, seniors and juniors of College of Nanotechnology and King Mongkut’s Institute of Technology Ladkrabang for supporting me to do research many interested academic problems. In addition, I would like to say thank you to Research Center in Thin Film Physics, Thailand Center of Excellence in Physics (ThEP), College of Nanotechnology, King Mongkut’s Institute of Technology Ladkrabang, Scientific, Technological Research Equipment Centre (STREC), Chulalongkorn University, and Chiangmai University for assisting instruments to characterize material for this research. Finally, I would like to say thank you very much to specialists, all books, research journals which help me to understand scientific knowledge for this research.

Natpasit Chaithanatkun

TABLE OF CONTENTS

TABLE OF CONTENTS (CONTINUED)

LIST OF TABLES

LIST OF FIGURES

LIST OF FIGURES (CONTINUED)

Figure **Page**

LIST OF FIGURES (CONTINUED)

Figure **Page**

CHAPTER 1

INTRODUCTION

1.1 Motivation

Nanotechnology is a combination of science, engineering, and technology which involves the tiny things in nanoscale, approximately 1 to 100 nanometers. The usage of the knowledge from interdisciplinary subjects consisting of physics, chemistry, biology, material science and engineering to optimize the properties of nanomaterials and develop the performance of its applications fabricated from nanoscale matters which can be called as "Nanoscience and Nanotechnology". Professor Richard Feynman discoursed the plenary speech entitled "There's plenty of room at the bottom" giving inspirations and concepts about the nanoscience and nanotechnology [1]. In this speech, Prof. Feynman represented the operation which researchers able to manipulate and control the independent atoms and molecules. Over a 10 years later, the phrase "nanotechnology" was designated in the exploration of ultra-precision machine's Professor Norio Taniguchi. The development of the scanning tunneling microscope had been continually improved the performance for many years until it could be seen the individual atoms, that the modern nanotechnology began [2]. Nowadays, scientists and engineers are looking for the variety of routes to intentionally create nanomaterials to take the enhanced properties such as self-cleaning, higher strength, lighter weight, increase the specific surface area, and increase the electrical conductivity.

The quantity of water vapor which held in the air called as "humidity". Humidity is a gasified state. The sudden change of humidity level can affect the hazardousness to the living organism. For instance, the combination of high-level humidity in hot zone that affects un-wellness, particularly for the youngster and elder [3]. The sensor which can find out the detection of water vapor level, it can be called as the humidity sensor. The humidity sensor is used for detecting the amount of humidity level in numerous areas of human life which have become fascinating research fields.

The Humidity sensor is an important electronic device for numerous application fields including food storage, medical application, meteorology, agriculture, electronic manufacturing and so on [4]. The quantitative determination of humidity level has been attention during last three decades. High sensitivity, good selectivity,

short recovery and response time are preferable humidity sensor device characteristics [5]. The ratio of the actual vapor amount to the saturated vapor amount at granted temperature called as “relative humidity”. Relative humidity is the most oftentimes utilized parameter to stipulate the humidity. Numerous concerning consequent the design of humidity sensor device is because of the restriction in the selection of sensing materials and the compatibility with fabricating technologies. There are two common ways to enhance the properties of the sensing material for humidity sensor: exploring novel material and optimization in the property of an original material. The common fabrication of the humidity sensor contains a glass substrate coating with gold inter-digital type electrodes and then coated with humidity sensing material. Response and recovery time mean the time which sensor gauged value at minimum state to maximum state in case of adsorption and reversely in a case of desorption, respectively. Hysteresis is the time delay in the adsorption and desorption which is commonly utilized to evaluate the reliability of humidity sensor. Good reliability of humidity sensor should have hysteresis value less than 4 % RH [6]. Sensing materials comprise ceramic, polymer material and composite materials have been attractive fascinating to fabricate the sensing layer for the humidity sensor.

The humidity sensors were successfully fabricated from inorganic metal oxide nanomaterials like titanium oxide [7] and tin oxide [8] which have emerged as commercial humidity sensors in recent years. Material based on ZnO and CuO are well studied individually for humidity sensing application. Because of ZnO has the limitation in the electrical conductivity for using in the electronic device. Therefore, CuO has higher electrical conductivity compared with ZnO, so it can be used to enhance the superior performance of the sensor. There are many ways to enhance the superior performance of humidity sensor based on semiconducting materials such as doping, mixing or modifying the material.

In this dissertation, the authors have examined the effect of sintering temperature and mix the copper content into the ZnO structure while the preparation via co-precipitation process. Co-precipitation method is used to prepare CuO-ZnO nanoparticles because it is an easy method and inexpensive when compared with another preparation methods. Sintering process can be used to decompose the impurity and increase the crystal quality of the material. After that, the authors used CuO-ZnO nanoparticles to fabricate the sensing material onto ITO coated on the glass substrate via electrostatic spray deposition (ESD) technique. ESD technique is an unsophisticated process, not complicated and not necessary work in the vacuum system. Sensor characteristic of the humidity sensor is the study about

adsorption and desorption processes of water vapor at sensing material film which change the value of electrical conductivity.

1.2 Objective of the study

1. 2. 1 To study the prepared conditions while the synthesis of CuO-ZnO nanostructure via co-precipitation process.

1.2.2 To characterize the properties of prepared nanoparticles using the X-ray diffraction technique, transmission and scanning electron microscopy, energy dispersive X-ray spectroscopy, Fourier transform infrared spectroscopy and X-ray photoelectron spectroscopy.

1.2.3 To fabricate sensing layer of CuO-ZnO nanoparticles film onto ITO coated on the glass slide using ESD technique for humidity sensor device.

1.2.4 To measure the electrical characteristics of CuO-ZnO humidity sensor.

1.3 Scope of the study

1.3.1 Study the influence of prepared conditions while the synthesis of CuO-ZnO nanoparticles via co-precipitation process.

1.3.2 Fabricate sensing films of CuO-ZnO by ESD technique for humidity sensor application.

1.3.3 Study the electrical characteristic of CuO-ZnO humidity sensor device.

1.4 Expected benefit of the study

1. 4. 1 Understand the principle and method of co-precipitation process to synthesize the CuO-ZnO nanostructure.

1. 4. 2 Understand the preparation parameters that affect to the structural property of CuO-ZnO nanostructure via co-precipitation technique.

1.4.3 Understand the thin film fabrication technique to prepare CuO-ZnO film as sensing layer of the humidity sensor.

1.4.4 Understand the sensing mechanism of CuO-ZnO humidity sensor device.

CHAPTER 2

THEORECTICAL BACKGROUND

Zinc oxide (ZnO) is a very broad energy gap material exhibiting numerousness fascinating properties which have obtained a lot of research interests in various backgrounds of material science covering the development of technology in electronic devices. Likewise, Copper oxide (CuO) can be utilized for numerous applications, for instance, sensing material, field emission and photovoltaic cells [9]. In this chapter, the authors demonstrate extensive description of the properties of these materials.

2.1 Zinc oxide material

ZnO is a special semiconducting material which has piezoelectric properties. From these, ZnO has become the attractive material for applications in the future. The general properties of ZnO will be represented followed the crystal structure, optical and electronic properties in this section.

2.1.1 Generally Crystal Properties of ZnO

ZnO material is ordered with wurtzite mode of crystalizing structure which it is an II-VI group compound semiconducting material. For wurtzite form, it ordered zinc atom and oxygen atom into a hexagonal lattice structure which permeates into the crystal structure where Zn^{2+} ion is interconnected with O^{2-} ions. Even though ZnO material bonding with covalent, it possesses essential the personality of ionic well [10]. The ZnO crystal structure of ZnO is configured into a space group $P6_3mc$ of wurtzite crystal structure. Wurtzite structure of ZnO has polar of surface (0001) plane which is illustrated in Figure 2.1. Because of the polar of ZnO crystal has the meta-stable state, these surfaces display numerous fascinating properties such as piezoelectricity, stability in physical and chemical fields and show high sensitivity in the sensor device. The calculated lattice constants of ZnO crystal unit cell from raw data collected by x-ray diffraction technique have values of a = 3.2490 Å, and c = 5.2069 Å, with c/a ratio approximately 1.6018 [11]. The hexagonal wurtzite of ZnO crystal structure will be confirmed by using scientific characterization techniques for discussing in this dissertation.

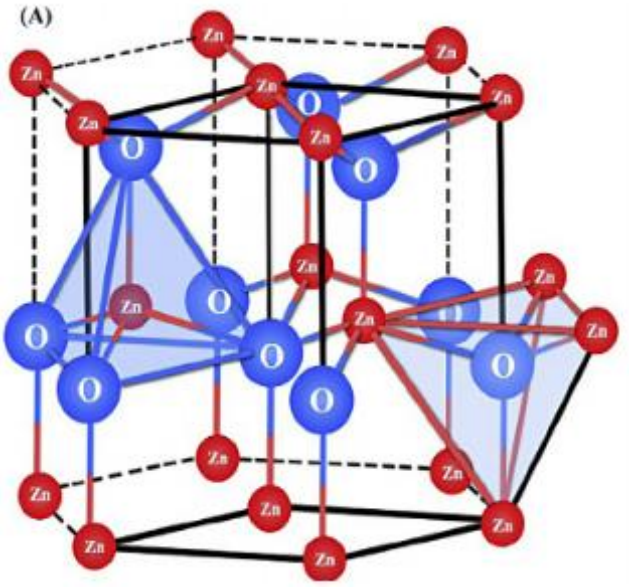

Fig. 2.1 The hexagonal wurtzite of ZnO crystal structure [12].

2.1.2 Electron Band Structure of ZnO

Understanding the electron band structure of used semiconducting compound is the necessary things when this material is considered for device applications. ZnO has the difference between conduction band and valence band approximately 3.37 eV at ambient condition. Because of ZnO has ionic bonding, the lowermost of the conduction band is principally established by 4s-orbital of Zn^{2+}or the antibonding of sp^3 hybridization states, while the valence band is created by the 2p-orbital of O^{2-} or the bonding of sp^3 orbital.

The wide bandgap of ZnO has many important implications in the electronic and optoelectronic fields. For example, ZnO can operate at high power, sustain high breakdown voltages, with maximum electronic noise. Additionally, its wide bandgap can accommodate intrinsic defects that emit various light wavelengths. Also, among other II-VI semiconductors, ZnO possesses a relatively high and stable binding energy of electron-hole pair approximately 60 meV at ambient condition [13]. The large excitonic binding energy of a material ensures that the excitons will recombine radiatively at higher probability.

2.1.3 Optical Properties

As discussed above, ZnO is an optically direct wide energy gap semiconductor, it has numerous of optical characteristics of ZnO which suitable for short wavelength applications. The electron band structure affected directly to the optical properties

of ZnO. Generally, high purity of ZnO is transparent in the visible range of the optical spectrum, with a typical refractive index of 2.008 [12]. Defects were used to modify the energy level of defects within the optical energy band structure of ZnO. These defects including oxygen and zinc vacancies, interstitial of zinc and oxygen and impurities such as Al, Cu and H.

Numerous of researchers on the photoemission of ZnO material have proposed which is inside of the optical energy gap of pure ZnO, there are any defects that are liable for green emission, which has been marked as V_o. While for red emission, it is depicted to interstitial of zinc in ZnO. In addition, the blue emission was attributed to interstitial of zinc and vacancy of zinc, respectively [14] . Understanding the knowledge in defect emissions of ZnO is necessary for modifying energy level of defects within energy bandgap of ZnO in a variety of potential optical applications.

2.1.4 Overview of ZnO properties

In addition, the electronic and optical properties of ZnO material, there are numerous propitious characteristics in this fascinating material, for instance, inexpensive production cost, superabundant sources material and stable in the chemical environment. Besides, ZnO exhibits that it has potential in various electronic device applications such as chemical sensing device, humidity sensing device, photovoltaic cells, and piezoelectric nanodevices. Ordinary details of wurtzite ZnO are concluded at below of Table 2.1.

Table 2.1 Common details about ZnO material [15].

Parameter	Value
Stable phase at 300K	Wurtzite structure
Lattice parametric quantity	a=b=3.2495 Å c=5.2069 Å c/a=1.594-1.6034
Melting temperature	2248 K
Index of refraction	2.008
Band energy width	3.37 electron volt
Excitonic binding energy	60 milli-electron volts

2.2 Copper oxide material

As mentioned earlier [16], Cuprous oxide (Cu_2O) and cupric oxide (CuO) are generally types of copper oxide. They are p-type semiconducting materials which have narrow energy gap. In additions, they can be utilized in numerous applications. Their potential applications including humidity sensor, photovoltaic cells [17], lithium-ion battery [18], superconductor [19], gas sensors [20] and photoconductive systems [21]. Due to its fantastical properties, CuO has been chosen in this thesis work to profit from the unique properties of CuO-ZnO in humidity sensing application.

2.2.1 Cupric Oxide

Cupric oxide (CuO) has a bandgap in the range of approximately 1.21-1.85 eV. The crystal structure of CuO is space group C2/c of monoclinic phase. CuO unit cell consists of Cu^{2+} ions interconnected with four O^{2-} ions in the form of square planar configuration.

The advantages of copper source material are inexpensive manufacturing, high thermal and chemical stability which make CuO a potential material in numerous usages. Therefore, CuO nanomaterials are the fascinating material for various applications such as gas sensing device, the catalyst for environmental fields. Also, the synthesis of CuO-ZnO and their application as good performances of humidity sensor was accomplished. Some of the important properties of CuO material are given in Table 2.2.

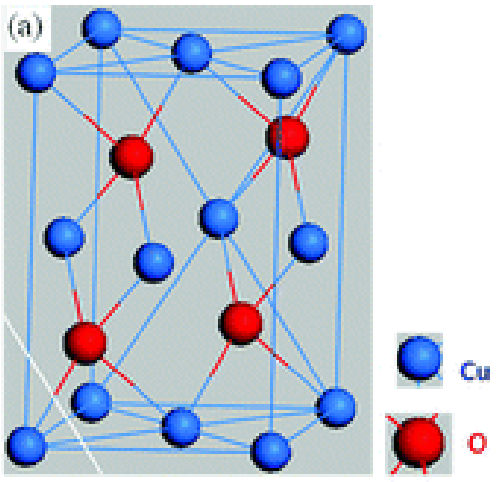

Fig. 2.2 Monoclinic crystal structure of cupric oxide (CuO). [22].

Table 2.2 Common details about CuO material [23].

Parameter	Value
Stable phase at 300K	Monoclinic structure
Lattice parametric quantity	a=4.68 Å b=3.42 Å c=5.13 Å
Melting point	2248 K
Band energy width	1.21-1.85 eV, direct

2.3 Synthesis and Processing of CuO-ZnO nanostructure

Semiconducting nanomaterial can be prepared by either composing atoms to nanomaterials or breaking down bulk material smaller in size. Numerous preparation methods have been developed and utilized for the nanomaterial preparation techniques. In the Top-down, it represents the bulk material is minimized to get the nanoparticles. The common examples of the top-down technique are milling and attrition, lithography. The major disadvantage of the Top-down is non-perfection of the structure. The product from attrition technique has very broad size distribution and numerous geometries of the particle. Besides, it may concern the number of contaminants. In the Bottom-up, the independent atoms or molecules are precisely self-assembly. So, bottom-up techniques are more convenient for the preparation of nanostructure and numerous techniques of Bottom-up have been greatly evolved.

CuO-ZnO nanostructures can be prepared by many routes, for instance, chemical vapor deposition process (CVD), sol-gel technique, hydrothermal process and chemical precipitation method.

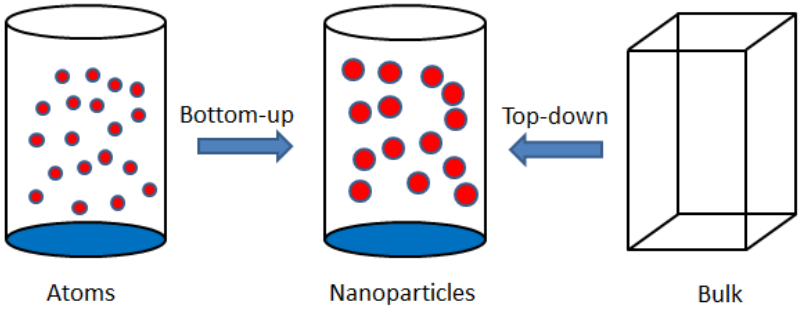

Fig. 2.3 Schematic represents the Bottom-up and Top-down techniques.

2.3.1 Chemical Vapor Deposition

Chemical vapour deposition is a common route for the fabrication of nanostructure on the deposited area with the chemical reaction from vapor phase to deposit solid material such as nanoparticles, thin film, nanotubes, nanowire and so on [24]. The system of general CVD is illustrated in figure 2.4. The CVD reactor provides the preparation of mixing or doped nanoparticles by feeding another precursor at the second stage.

Hong Wan and Harry E. Ruda [25] have prepared ZnO nanowires via CVD route using zinc powder and a combination of ZnO and graphite as precursors. SEM micrographs of fabricated ZnO nanostructure via CVD route is illustrated in figure 2.5.

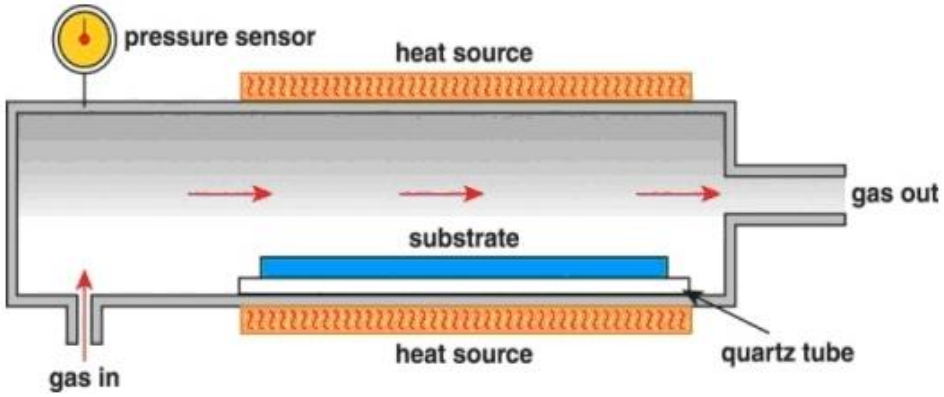

Fig. 2.4 Typical CVD reactor [26].

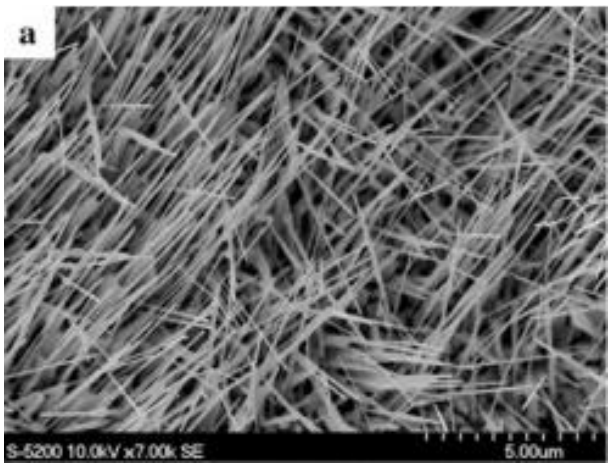

Fig. 2.5 SEM images of fabricated ZnO nanowires via CVD process [25].

2.3.2 Sol-gel

Sol-gel is a common route for synthesizing of low-dimensional materials. It involves the growth of the networks by the establishing of colloidal to connect the network in the liquid state. The main advantage of this route is the modification of the microstructure of product by adjusting the parameters in the chemical reaction. This method is generally used for the preparation of nanomaterials in numerous research groups. The catalyst is utilized for starting the reaction and controlling the value of pH. The schematic of this system is illustrated in figure 2.6.

Riyadh M. Alwan, et. al. [27] prepared ZnO nanoparticles by sol-gel method using zinc acetate as a precursor. The SEM image shows that prepared ZnO nanoparticles in this study are spherical in shape with the smooth surface as shown in figure 2.7.

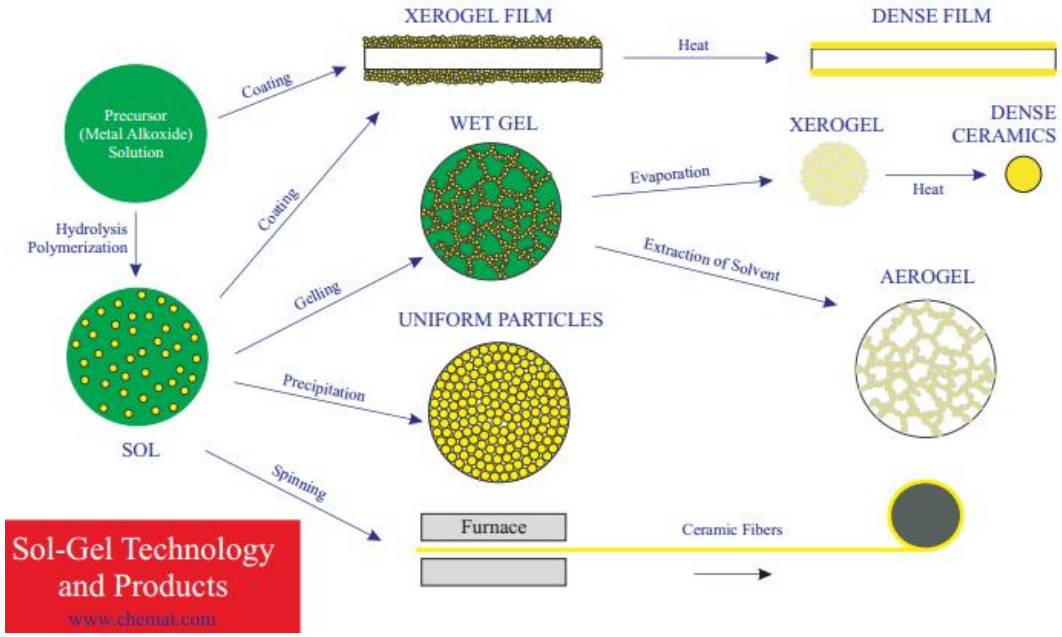

Fig. 2.6 Sol-gel process [28]

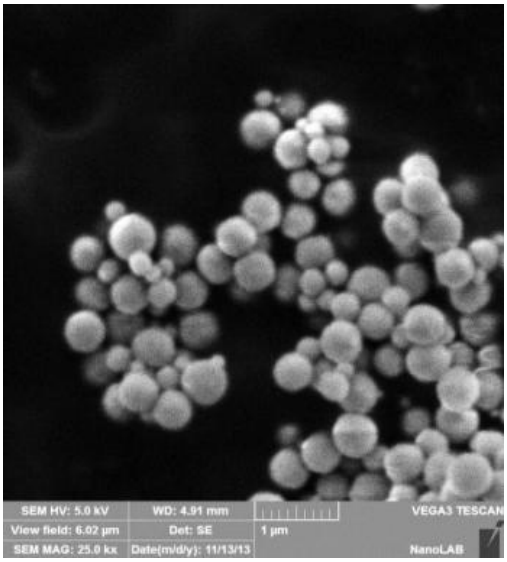

Fig. 2.7 SEM image of ZnO nanoparticles grown by sol-gel method [27].

2.3.3 Hydrothermal

Hydrothermal route is a growth of crystal under high pressure and temperature in water which substances are not soluble under regular temperature and pressure conditions (<100°C, <1 atm) [29].

Kai-Chen et al. [30] synthesized ZnO nanostructures by hydrothermal synthesis on patterned aluminum substrate prepared by colloidal lithography. The nanowires and nanosheets were well-defined as shown in figure 2.8.

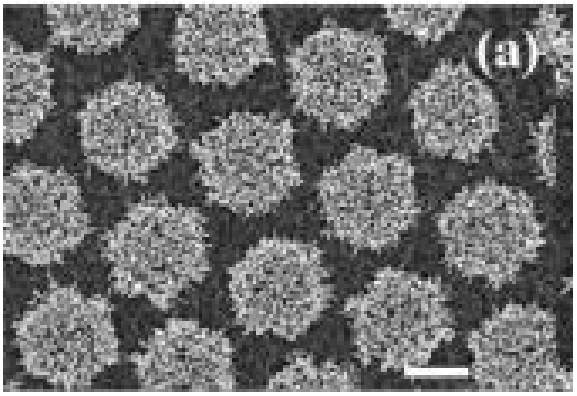

Fig. 2.8 SEM image of ZnO nanowires/nanosheets prepared by hydrothermal process. The scale bar is 2 µm in length [30].

2.3.4 Chemical precipitation

Chemical precipitation route is an uncontrolled process in the kinetics, the nucleation of solid phase and crystal growth process. Thus, collected powders via precipitation route have a broad size distribution, uncontrolled morphologically shape and aggregation of solids. To collect the nanostructures with narrow size distribution, the appropriate concentration of precursor and suitable reaction time are the necessary requirements.

Multi ceramic oxide which generally utilized for the synthesis of nanomaterials called the co-precipitation technique. The solution has then adjusted the value of pH or heat treatment to induce those salts of precursors to be the precipitate. The crystal growth of nanomaterial is depending on the concentration of precursor, reaction temperature and the value of pH. After precipitation process finished, the powder is collected, washed several times and then slowly dried. The applied washing and drying processes affect to the agglomeration of the final product. The dopant is added to the solution of precursor while precipitation reaction. A stabilizer is used to prevent the formed particles. Normally, a step of the annealing process is essential to transform hydroxide into the high crystal quality of metal oxides. The advantages of co-precipitation routes are low operating temperature, inexpensive, fine and uniform product.

Zeljca Petrovic et al. [31] prepared ZnO microstructure via precipitation method using zinc acetylacetonate as the precursor. Figure 2.9 shows the formation of ZnO particles consisting of hexagonal pyramids.

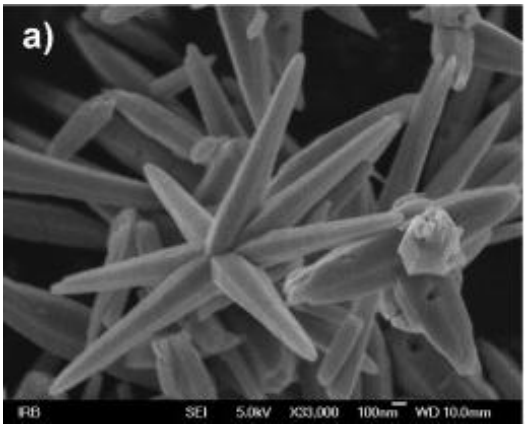

Fig 2.9 SEM image of ZnO microstructure prepared by precipitation method [31].

As mentioned above, the co-precipitation method is chosen for preparing the CuO-ZnO nanostructure in this dissertation because it is simple, inexpensive, prepare in low reaction temperature, not need to prepare under the vacuum system and so on.

2.4 Mixing of Metal oxide nanomaterial

Morphological, structural, luminescence and sensing properties of the nanostructures can be adjusted by mixing of metal oxide atom. The addition of the small amount of mixing material into major material serves different purposes under different desires [32].

Many physical properties of ZnO, such as piezoelectricity, electrical conductivity, and defect structure are much influenced by the presence of the impurity. The mixing of metal oxide has been attracted for researching new special properties from each original metal oxide.

CuO-ZnO has been previously used as active layer in varistor [33], phosphor [34] and surface acoustic wave [35]. The emission spectra of CuO-ZnO extend from ultraviolet to the infrared region depending on the concentration of CuO, defect in ZnO and excitation conditions [36]. Cu^{2+} is the best-chosen impurity because it can form the lowest formation energy due to the smallest ionic size mismatch between Cu^{2+} and Zn^{2+} ions. The structural deformation can be happened by Cu when it replaces or substitutes or interstitial zinc atoms in the lattice of ZnO [37].

2.5 Characterization testing for nanomaterials

In this dissertation, numerous techniques have been exploited to examine the synthesized metal oxide nanoparticles. The analysis of purity of crystal phase, morphological surface and elemental analysis of chemical composition was experimented by X-ray diffractometer (XRD), transmission and scanning electron microscope, X-ray photoelectron testing and Fourier transform-infrared testing respectively.

2.5.1 X-ray Diffractometer

X-ray Diffractometer is the effective testing utilized to measure the orientation of crystal structure occurs in nanomaterials and phase composition, preferred orientation, grain size, microstrain in the structure of these phases.

X-ray beam is directed to crystal structure at angle θ to the atomic planes. X-rays interact with the electrons of atoms which the X-ray reflection process is

appeared by the atomic planes. Part of the X-ray beam can pass through and some of them reflect another direction. Referring to figure 2.10, there is a different path between reflected rays of plane 1 and plane 2 within the crystal structure.

$$2d \sin \theta = n\lambda \qquad (2.1)$$

Where n is the integer number

λ is the X-ray wavelength

d is the spacing of each layer of atoms

θ is the diffracted angle

A general approach of powder Diffractometer is given as follows: The characteristic X-rays from an X-ray generator are rushed to the surface of the sample. The intensity of the signal is collected and convert from analog to appear on the monitor of a personal computer. The machine utilized to maintain the angle and rotate the sample is controlled with a goniometer. XRD pattern was collected by a BRUKER AXS: D8DISCOVER (Figure 2.11) with Ni-filtered Cu-Kα radiation (λ =1.5406 Å).

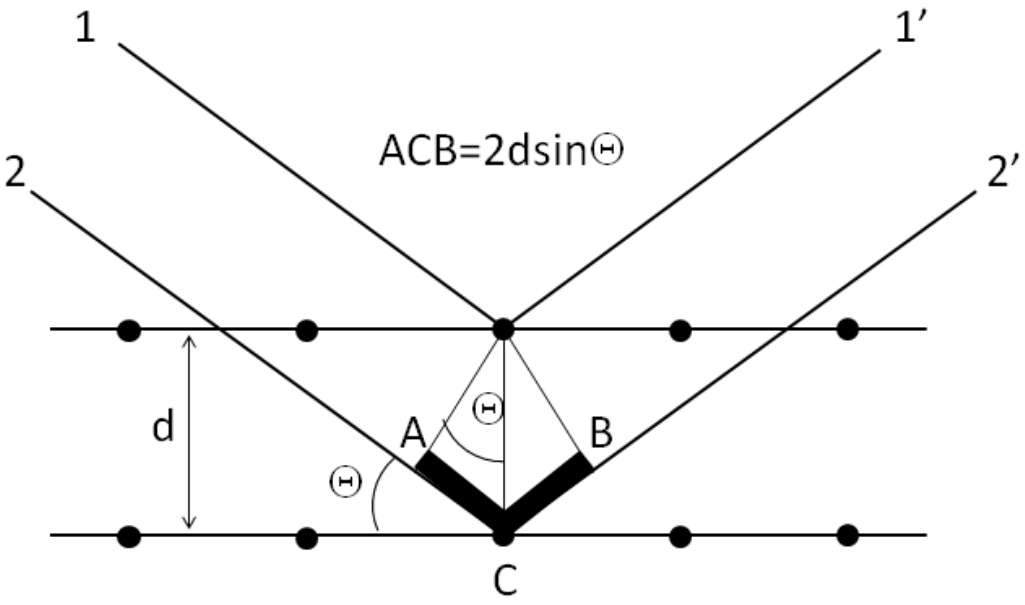

Fig. 2.10 Bragg's law of diffraction.

Fig. 2.11 BRUKER AXS: D8DISCOVER Powder Diffractometer [38].

2.5.2 Transmission Electron Microscope

Transmission electron microscope (TEM) is a machine for carrying out the morphological characteristics of nanomaterials. TEM image offers the morphological information such as size, topography, and crystallographic details. The determination the positions of atoms inside nanomaterials has made by TEM. In this dissertation, a PHILIPS (TECNAI 20) is used to study the morphology of the nanoparticles with a resolution of 1.4-2.7 Å. The samples were examined under the TEM after dispersing them in ethanol and placing a few drops of the mixture in the Cu grid. The photographic image of used transmission electron microscope in this dissertation is shown in Figure 2.12.

Fig. 2.12 Photograph of TEM machine [39].

2.5.3 Scanning Electron Microscope

The scanning electron microscope (SEM) can create high-resolution micrographs of the sample. The SEM micrographs are helpful for considering the morphology of the sample. In a generally SEM, an electron is emitted from tungsten wire or Lanthanum Hexaboride (LaB_6). The typical setup is maintained under high vacuum ambient. The electron beam which has few hundred electron volts to 50 kiloelectronvolt of energy range is condensed by condenser lenses into a beam with very fine spot sized approximately ranging from 1 nm to 5 nm.

The typical produced photographs from SEM machine divided into three types: secondary electron micrograph, backscattered electron micrograph, and X-ray elemental mapping. Secondary and backscattered electrons are generally sorted by the energy of emitted electron. Generally, the secondary electron (SE) has energy not much than 50 eV. Most of the secondary electrons are produced from few nanometers of the surface and provide the information of surface. In this experiment, the SEM micrographs were carried out using the scanning electron microscope with field emission type (Japan Electron Optics Laboratory) JEOL JSM-7001F machine (Figure 2.13).

Fig. 2.13 Photograph of SEM machine [40].

2.5.4 Fourier Transform Infrared Spectrometer

Fourier transform infrared spectrometer (FTIR) serves the details of chemical bonding within nanomaterial. It is especially profitable for the analysis of nanomaterials. The basically of infrared testing is to measure the intensity changing of infrared signals after it interacts with the sample. The frequencies of vibrational motion are the fingerprint of the compounds material and are utilized for the analysis of nanomaterials. The typical infrared spectrometer is developed by adding the Fourier transform technique to the modern FTIR instrument. The pattern collected from two beam interferometers as the difference of path is varied when Fourier transformed. The transformation of the infrared beams is carried out mathematically with computer shown in Figure 2.14.

In our experiment, the infrared pattern was determined using a Perkin Elmer Spectrum One FT-IR by using potassium bromide (KBr) pellet technique. In each preparation for measuring, the sample grind with KBr to form a mixture, and then was made the pellet by compressed technique. This pellet was measured from the wavenumber in the range between 4000-450 cm^{-1}.

Fig. 2.14 Photograph of FT-IR Spectrometer [41].

2.5.5 X-ray Photoelectron Spectroscopy

X-ray photoelectron spectroscopy (XPS) is the characterization of the chemical composition. It is the technique for the analysis of surface with a depth of approximately 50-100 Å. XPS is a chemical composition technique that provides the details of chemical state for digesting the chemical elements. This technique used monochromatic X-rays for radiation to the sample, collected the emitted electrons which the energy of the electron is the fingerprint of elements [42]. The schematic of XPS system is illustrated in figure 2.15. The chemical state is related to the binding energy (BE) of an electron which results to the changing in the value of kinetic energy (KE). The value of BE is the function depending on the value of KE with the equation; BE = $h\nu$ – KE, where $h\nu$ is the energy of photon [43]. The chemical bonding of elements is checked from the shifts of chemical energy. X-ray photoelectron spectroscopy (AXIS Ultra DLD) is utilized in this dissertation as shown in figure 2.16.

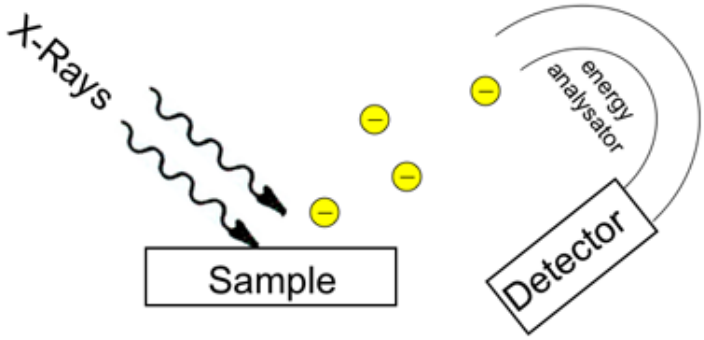

Fig. 2.15 Basically system of X-ray photoelectron spectroscopy [44]

Fig. 2.16 Photograph of XPS machine [45]

2.6 Thin film fabrication

There are many techniques to fabricate thin film layer both physical and chemical processes. In this work, we used the electrostatic spray deposition technique (ESD) to prepare sensing material for humidity sensor application because the ESD technique is a simple method that can be operated at low temperature and without vacuum system, easily adjust preparation parameters such as distance between tip and substrate, substrate temperature, voltage between tip and substrate, flow rate of mixture solution and coating time. Schematic of ESD system is shown in Figure 2.17. On the top part of ESD system is the part of the capillary tube which combines with pump, capillary tube, and metal tip. This part connected with a positive electrode of the high voltage source. The substrate part consists of a metal plate, thermocouple, and heater. A metal plate is used as substrate holder which connected with a negative electrode of high-voltage source. The heater is controlled by a temperature controller.

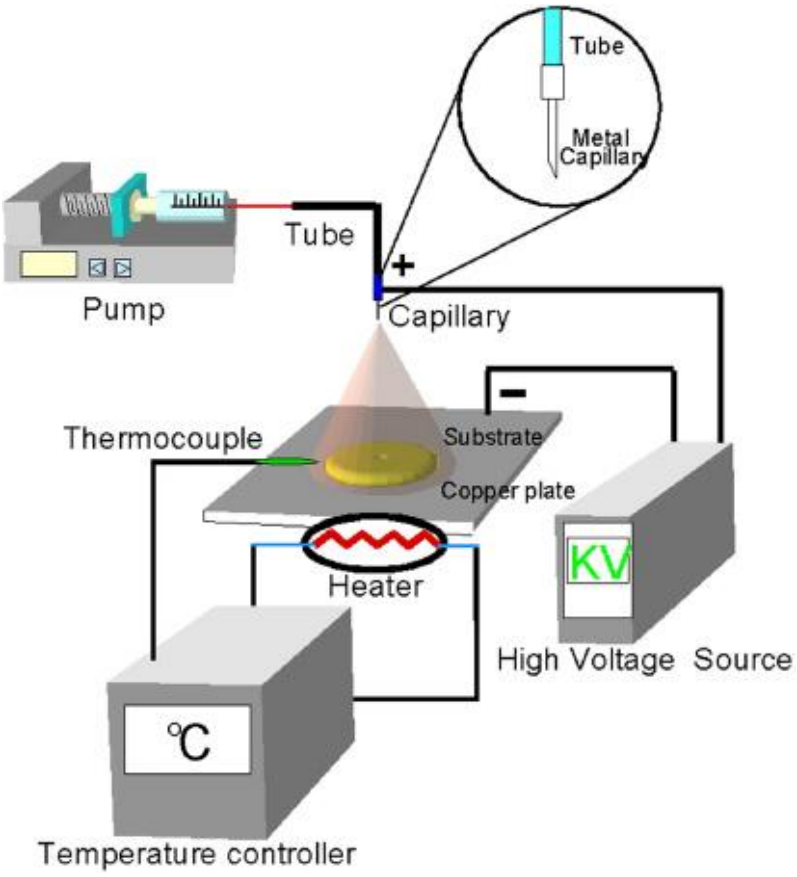

Fig. 2.17 Schematic of ESD system [46]

2.7 Humidity Sensor Device

Humidity is a principal factor in physical, chemical and biological processes. Humidity sensor is widely used in environmental, agricultural, industrial, food storage applications. In the semiconductor industry, humidity is observed in the processing of wafer manufacturer. There are numerous applications, for instance, smart environmental control in building, cooking control in a microwave, laundry and so on. In the industry for automobile, the humidity sensor is utilized in a window for the defogger and assembly of motor lines. In the medical, humidity sensor is utilized in respiratory equipment, incubator, and processing in pharmaceutical. In agricultural, the humidity sensor is utilized for the protection of plantation, monitoring of moisture in the soil, and storage of cereal. In typical industry, the humidity sensor is utilized for the control of humidity level in oven, paper and textile production and food processing.

Science and technology play a significant role in the lives of humans. They can improve the quality of the better human life. There are many innovations made

from knowledge of science and technology. Nanoscience and nanotechnology have been studied and interested in many decades. For example, silver nanoparticles have special optical properties of surface plasmon effect and antimicrobial activity for inhibiting the growth of E. coli bacteria. Metal oxide nanoparticles such as zinc oxide nanoparticles were studied both physical and chemical properties for use as smart material in many applications such as zinc oxide nanomaterial was used as the photocatalytic degradation for managing environmental pollution, gas sensing material, bistable memory device. Sometimes pure nanomaterial has limitation for some applications. Therefore, the pure nanomaterial is necessary to develop and modify by mixing with some potential material for improve performance for those applications. Mixing nanomaterial is a major challenge in the future applications of nanomaterial. The copper oxide - zinc oxide (CuO-ZnO) has been an interesting research in the last few years, due to the attraction properties of both CuO and ZnO [4].

In this dissertation, the authors have experimented the influence of sintering temperatures and added the copper concentration of CuO-ZnO nanoparticles prepared via co-precipitation process. The co-precipitation process was used for preparing CuO-ZnO nanoparticles because it is a simple method and inexpensive. After that, electrostatic spray deposition technique was used to fabricate the layer of CuO-ZnO as sensing material for humidity sensor application.

CHAPTER 3

EXPERIMENTS

3.1 Experimental outline.

In this chapter, the briefly basic and details of the experimental process used to synthesize uniform and high-quality CuO-ZnO nanostructure are described. The process of an experiment is followed by outline as shown in Fig. 3.1. Initially, preparation of CuO-ZnO nanostructure was studied by using co-precipitation process, and then all prepared conditions of CuO-ZnO nanostructure were characterized by using scientific instruments. Then, the humidity sensor made from CuO-ZnO nanostructure is fabricated by using electrostatic spray deposition technique. Finally, characteristic of the humidity sensor is measured for explaining the working mechanism of humidity sensor device.

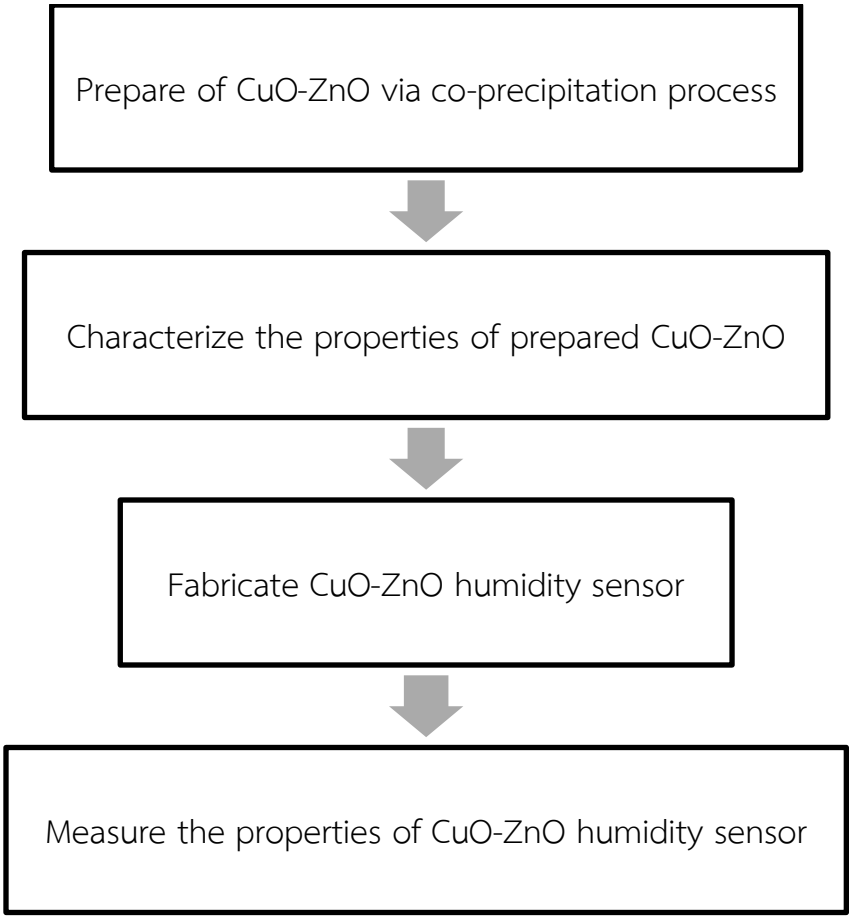

Fig. 3.1 Outline of experimental process.

3.2 Preparation of CuO-ZnO nanostructures via co-precipitation process.

All chemical reagents are analytical chemical grade. Zinc nitrate hexahydrate (Fig.3.2 (a)) and copper nitrate hexahydrate (Fig.3.2 (b)) were bought from Sigma-Aldrich and potassium hydroxide (Fig.3.2 (c)) was bought from UNIVAR. CuO-ZnO nanostructures were synthesized by co-precipitation process using zinc nitrate hexahydrate ($Zn(NO_3)_2$), copper nitrate hexahydrate ($Cu(NO_3)_2$) and potassium hydroxide (KOH) as zinc, copper and hydroxide precursor, respectively. Firstly, a mixture of the amount of $Zn(NO_3)_2$ and $Cu(NO_3)_2$ at different Cu : Zn molar ratio from 0:100 to 10:90 follow by Table 3.1 with 200 ml of deionized water in a beaker. Secondly, 1 molar of KOH was mixed with deionized water in separately beaker. After that, KOH solution was slowly dropped into the mixture solution under stirring with a magnetic stirrer until pH value till 14. The precipitate occurred in the solution. The precipitate was washed twice times with deionized water until pH value was neutral to remove the impurities in solution. The as-prepared precipitate was dried in an oven at 120 °C for 12 hours and then sintered for 2 hours at various temperatures of 500, 600, 700 and 800 °C, respectively followed by Table 3.2.

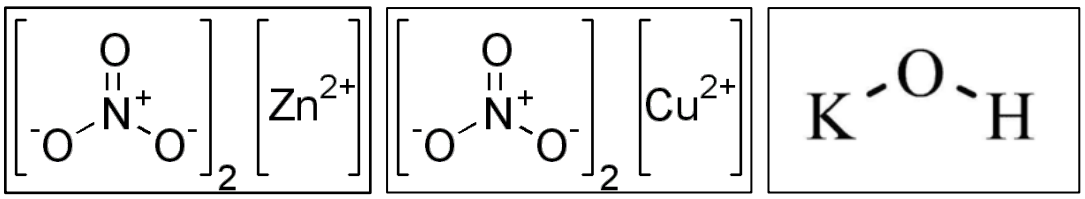

(a) (b) (c)

Fig. 3.2 Chemical structure of (a) zinc nitrate hexahydrate, (b) copper nitrate hexahydrate and (c) potassium hydroxide.

The characterization techniques in this dissertation for measuring the properties of synthesized CuO-ZnO nanostructures consist of X-ray Diffractometer (XRD: Bruker AXS D8 Discovery), field emission scanning electron microscopy (FE-SEM: JSM-7001F) with energy dispersive x-ray spectroscopy (EDX), transmission electron microscopy (TEM: Philips TECNAI 20), Fourier transform infrared spectrophotometer (FT-IR: Perkin-Elmer Spectrum One) and X-ray photoelectron spectroscopy (XPS: AXIS Ultra DLD).

Table 3.1 Synthesized condition of CuO-ZnO nanostructures via co-precipitation process.

Cu : Zn molar ratio	Amount of $Zn(NO_3)_2$ (g)	Amount of $Cu(NO_3)_2$ (g)
0 : 100	5.9498	0.0000
1 : 99	5.8903	0.0483
2 : 98	5.8308	0.0966
4 : 96	5.7118	0.1933
6 : 94	5.5928	0.2899
8 : 92	5.4738	0.3688
10 : 90	5.3548	0.4832

Table 3.2 Sintered conditions of CuO-ZnO nanostructures via co-precipitation process**.**

Cu : Zn molar ratio	As-prepared	Post-sintering temperature [°C]			
		500	600	700	800
0 : 100	✓	✓	✓	✓	✓
1 : 99	✓	✓			
2 : 98	✓	✓	✓	✓	✓
4 : 96	✓	✓			
6 : 94	✓	✓			
8 : 92	✓	✓			
10 : 90	✓	✓			

The preparation of the sample for characterizing with scientific instruments is essential to prepare a sample with the suitable method for each technique. In this dissertation, For XRD technique, the powder sample was packed to a flat surface onto the sample holder. For XPS, SEM and EDX analysis, all samples are not good in electrical conductivity. Therefore, samples should be coated with the gold conductive metal or mounted with carbon tape for reducing charge effect which it will cause images distortion of drift. For the analysis with TEM machine, 20 mg of powder was dispersed with 10 ml of ethanol under ultrasonicate ambient. The droplet of mixture suspension is dropped onto a carbon coated holey film on a copper grid. For the measurement using Fourier transform infrared spectrophotometer, the potassium bromide is the commonly utilized for packing with powder sample due to it can transparent in the infrared region. Thus, it will not

be detected in the infrared spectra. After mixing process, pressure approximately 8 tons is applied to pack the transparent pellet under vacuum ambient for 3 minutes.

3.3 Fabrication of CuO-ZnO humidity sensor via electrostatic spray deposition technique.

In this dissertation, electrostatic spray deposition technique is one of the good choices for the fabrication of CuO-ZnO humidity sensor because this technique can be operated at low temperature and easy to the fabrication setup. A substrate in this study is H-shape structure (Fig. 3.3). H-shape is the simple electrode. Firstly, the Indium doped Tin Oxide (ITO) coated on the glass is wetly etched as H-shape structure using aqua-regia solution. The Aqua-regia is a mixture of nitric acid and hydrochloric acid with 1:3 molar ratio. Secondly, the substrate was cleaned by alcohol process followed by deionized water (DI), acetone, methanol, and isopropanol under ultrasonicated for 15 minutes, respectively. Then, the substrate was stuck with plastic tape to protect the area of a conductive electrode. Mixing solutions were prepared by the mixture of 20 mg of sample powder and 10 ml of ethanol under ultrasonication for 15 minutes. After that, the CuO-ZnO layer was fabricated on the substrate with conditions of voltage between tip and substrate of 8 kV, substrate temperature of 80 ^{o}C to evaporate the alcohol solvent while the fabrication process, distance between tip and nozzle of 40 mm, flow rate = 3 ml/h and fabrication time of 15 minutes. The electrostatic spray deposition (ESD) was used to fabricate the layer of CuO-ZnO as sensing material of humidity sensor in this study. ESD technique is very simple and not necessary used in a vacuum system. The photograph of ESD system is shown in Fig. 3.4.

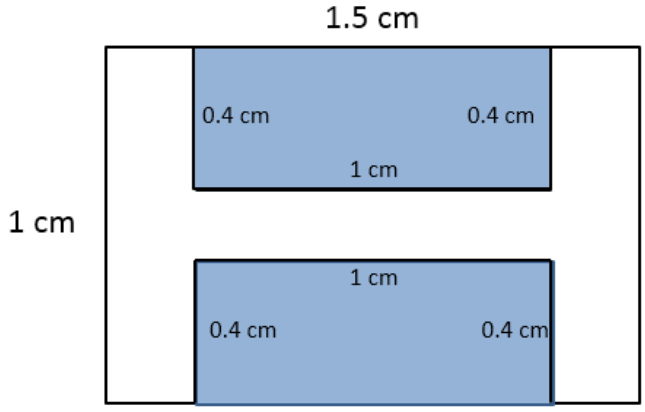

Fig. 3.3 H-shape type.

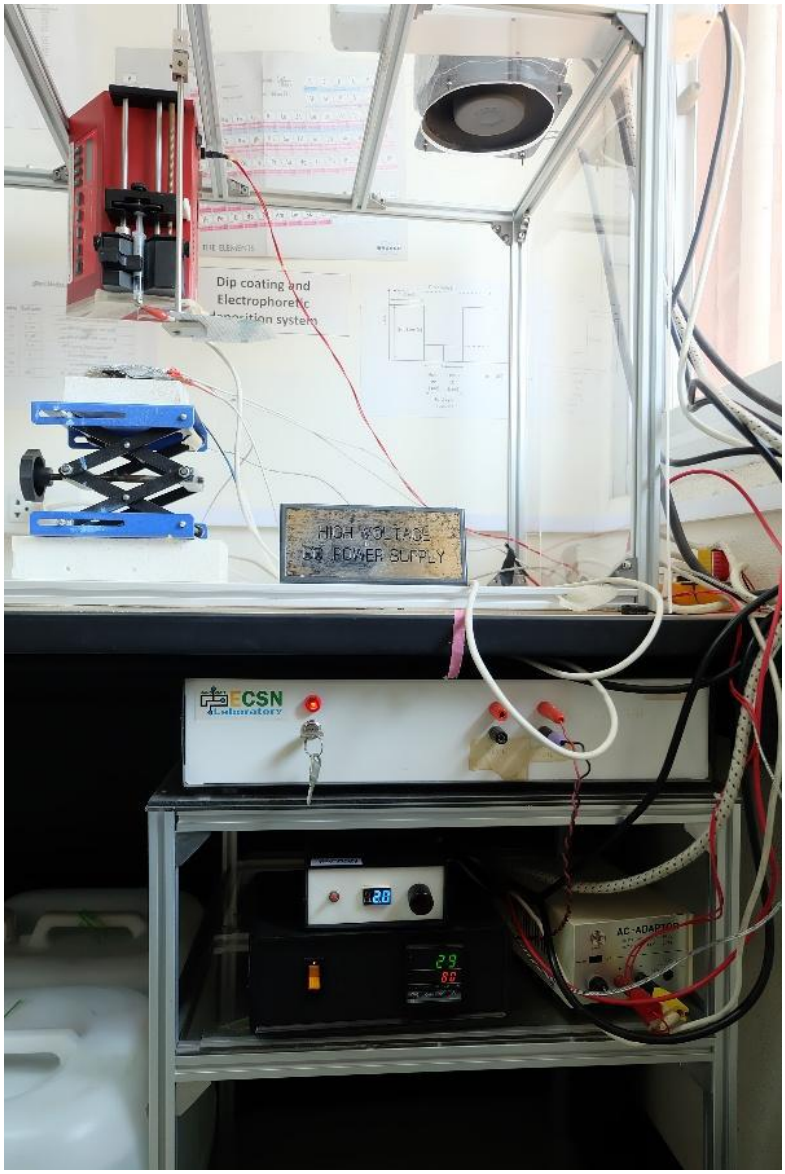

Fig. 3.4 ESD system at ECSN Lab.

3.4 Experiment setup for the measurement of electrical characteristics of CuO-ZnO humidity sensor.

The sensor characteristic was measured by using LCR meter (Fig 3.5) to collect the electrical conductivity of sensor in each value of relative humidity in CuO-ZnO humidity sensor. The general methods for controlling the accurately relative humidity level use either humidity generator or equilibrium of closed space with a salt solution which provides the desired humidity level. Due to humidity generator is expensive and complex. The salt solution system becomes the useful method to provide desired humidity level in closed space or chamber. Each value of relative

humidity was set by the mixture of saturated salt which each saturated salt gives only one value of relative humidity level depending on temperature. The saturated salt solutions were shown in Fig 3. 6. The saturated salt solution mixed with potassium acetate, magnesium chloride, magnesium nitrate, sodium chloride, potassium chloride and potassium nitrate, it provides the relative humidity level of 23, 32.75, 52.89, 75.29, 84.34 and 93 %RH, respectively.

Fig. 3.5 Photograph of LCR meter.

Fig. 3.6 Photograph of saturated salt solution at various level of relative humidity.

CHAPTER 4

RESULTS AND DISCUSSION

In this chapter, it can be divided into 2 parts; Part I study the effect of sintering temperature at the molar ratios of the Cu : Zn content of 0 : 100 and 2 : 98, respectively. Part II is the study of the effect of Cu : Zn molar ratio at as-prepared and post-sintered at temperature of 500 °C for 2 hours, respectively. The condition in this work showed in Table 4.1.

Table 4. 1 Prepared conditions of CuO-ZnO nanostructures via co-precipitation process**.**

Cu : Zn molar ratio	As-prepared	Post-sintering temperature [°C]			
		500	600	700	800
0 : 100	✓	✓	✓	✓	✓
1 : 99	✓	✓			
2 : 98	✓	✓	✓	✓	✓
4 : 96	✓	✓			
6 : 94	✓	✓			
8 : 92	✓	✓			
10 : 90	✓	✓			

4.1 The influence of sintering temperature of pure ZnO

4.1.1 Crystal structure properties

The X-ray diffractograms of the pure ZnO powder as-prepared and sintered at the temperature of 500, 600, 700 and 800 °C for 2 hours are shown in figure 4.1. All samples, there are 9 crystallographic planes indicating to (100), (002), (101), (102), (110), (103), (200), (112) and (201) and these all hkl Bragg diffraction peaks can be indexed to the hexagonal wurtzite structure of ZnO polycrystalline followed The Joint Committee on Powder Diffraction Standards (JCPDS) card no. 36-1451. The influence of the sintering temperature in XRD pattern of the samples can be observed in the variations of intensity and full-width at half maximum (FWHM) of the diffraction peaks of ZnO. When the sintering temperature increases, the intensity of diffraction peak is also increasing due to the high quality of crystallinity. There are no any impurities occur in the XRD pattern of all samples. The crystallite size was

determined from the broadening of X-ray peak using Scherrer equation. The results show the size of crystal increased with the sintering temperature. Crystal size is an estimation of the size of a diffracted domain, and the crystal size is not commonly the same with the particle size due to the occurrence of the aggregate of polycrystalline. Numerous techniques utilized for the estimation of particle size are light scattering testing, scanning electron microscopy (SEM) and transmission electron microscopy (TEM), which in this experiment, the authors used SEM and TEM result to measure the morphology shape and particle size which will be described later [47]. The value of crystallite size is shown in Table. 4.2 which is about 17-28 nm. The temperature increases reach to 700 °C, the size of crystal become bigger and perfectly crystal due to the thermal energy. At a temperature of 800 °C, the thermal energy is excessing for the formation of crystal which results to the size become smaller due to the recrystallization.

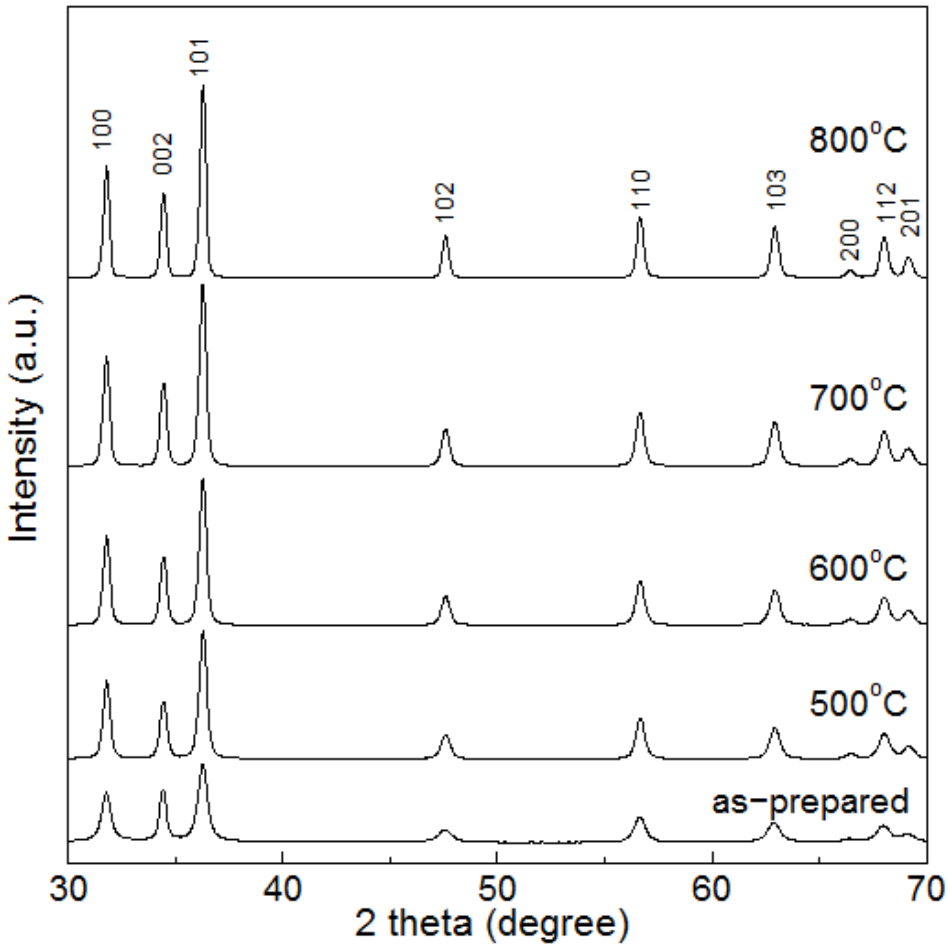

Fig.4.1 XRD diffractograms of pure zinc oxide at different sintering temperatures.

Table 4.2 Calculated crystallite size of pure zinc oxide at different sintering temperatures.

Temperature (°C)	Crystallite size (nm)
As-prepared	17.83
500	23.76
600	26.09
700	28.20
800	27.30

4.1.2 Scanning electron micrograph

All samples are the form of powder. Each sample was mounted onto the carbon tape and then the sample was coated with gold nanoparticles by a sputtering technique for increases the electrical conductivity which is a good benefit for the measurement of SEM images. In this experiment, the used electron gun is the field emission gun. Field emission gun is sharply Muller type which held at several kilovolts. An emitter is made by coating tungsten tip with zirconium oxide which the electrical conductivity is increasing at the higher temperature. Thus, the field emission type is the best type in present for measuring at high magnification. Figure 4. 2 shows the SEM images of pure zinc oxide at as-prepared and with various sintering temperatures of 500, 600, 700 and 800 °C. The morphological shape is little changed from petal-like structure to spherical-like structure and become larger by the influence of thermal energy which is consistent with XRD analysis. From the result, when thermal energy was applied to an as-prepared sample, the particles are break unstable form and reformed it to the bigger size when the supplied thermal energy is increased.

4.1.3 Fourier transform infrared spectrum

The structural characteristics of the pure ZnO at various sintering temperatures were evaluated by Fourier transform infrared spectroscopy (FTIR) using KBr pellet. The FTIR spectra of the pure ZnO at various sintering temperatures are shown in Figure 4.3. The bands at 410-438 cm^{-1} can be assigned to Zn-O stretching mode. The band at 836 cm^{-1} is due to ν_2 vibration mode of the interlayer anion (nitrate). The weak band around 1,638 cm^{-1} and broad band around 3,440 cm^{-1} are attributed to moisture water molecules. It is known that nitrate group is an evaporable anion and decomposed completely at the temperature as high as 400 °C. For the sintered

sample from 500 to 800 °C, the band at nitrate group does not appeared in FTIR spectra.

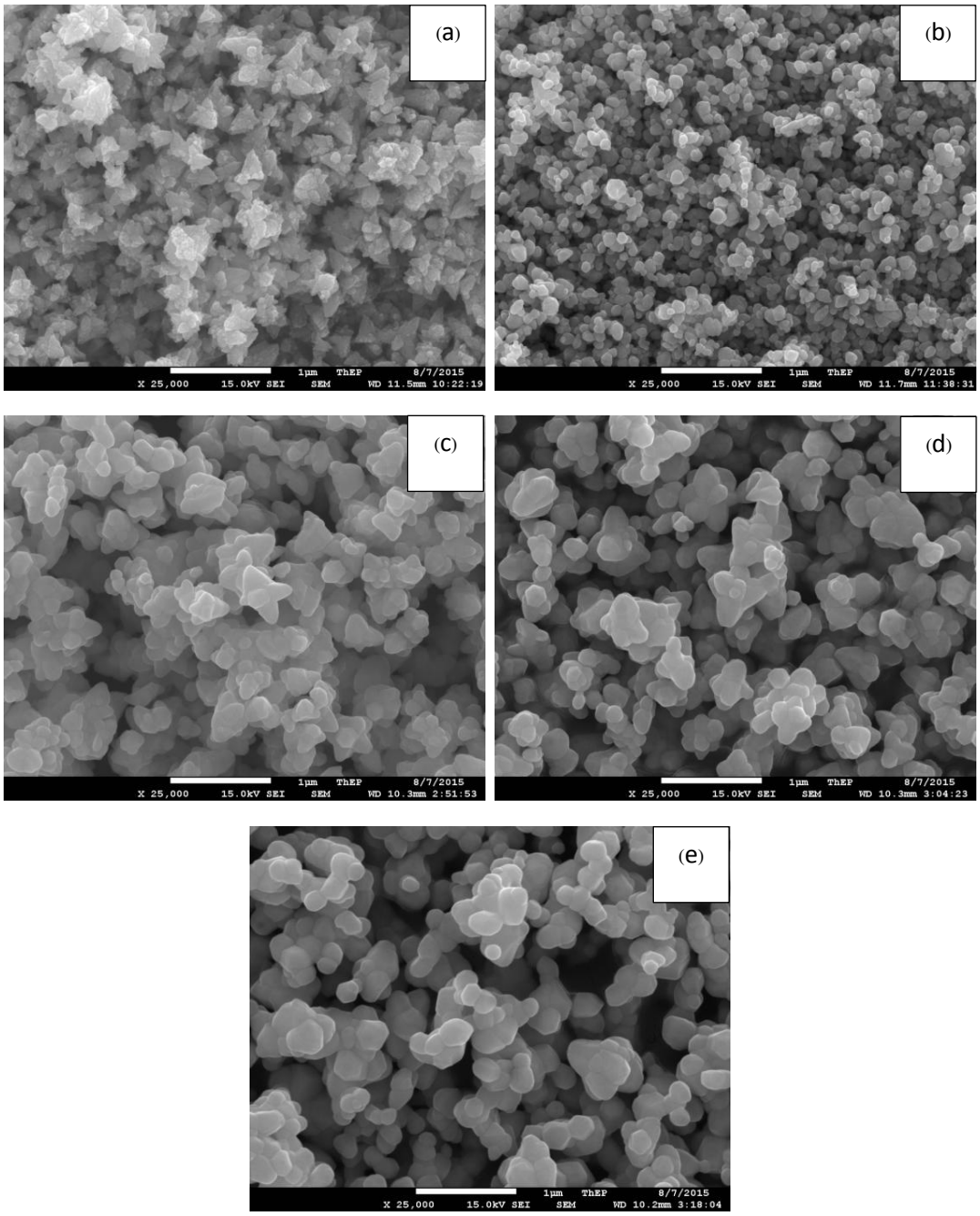

Fig. 4.2 SEM photographs of pure zinc oxide at various sintering temperatures (a) as-prepared, (b) 500 °C, (c) 600 °C, (d) 700 °C and (e) 800 °C.

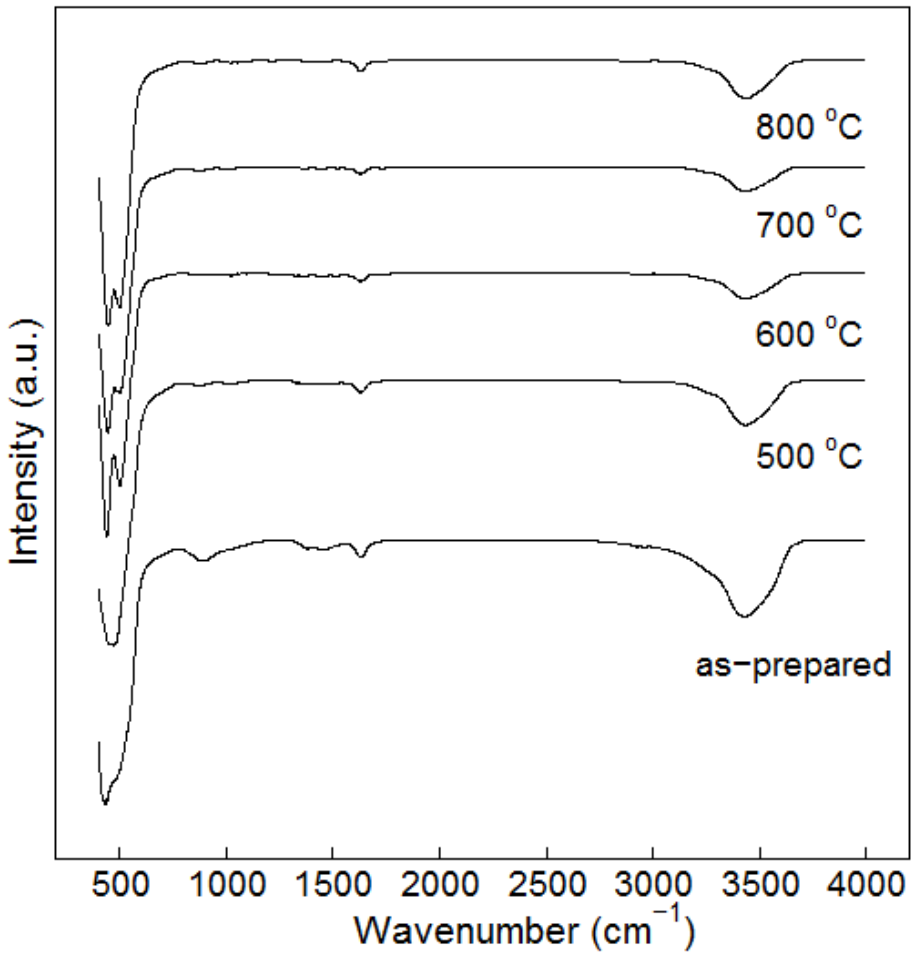

Fig. 4.3 FTIR spectra for pure zinc oxide at different sintering temperatures (a) as-prepared, (b) 500 °C, (c) 600 °C, (d) 700 °C and (e) 800 °C.

4.2 The influence of sintering temperature of added Cu content at molar ratio of Cu : Zn at 2 : 98

4.2.1 Crystal structure properties

The X-ray diffractogram of the CuO-ZnO at a molar ratio of Cu : Zn = 2 : 98 at various post-sintering temperatures is illustrated in figure 4. 4. All peaks in diffractograms are indexed by JCPDS card no. 36-1451 with hexagonal ZnO with wurtzite structure. There are no any diffraction peaks indicating to the crystal of CuO due to the molar ratio of Cu : Zn is a small quantity. There are no any impurities appear in all samples. The value of crystallite size is shown in Table 4.3 which is about 16-39 nm. The increasing in crystallite size at the sintering temperature means that the thermal energy to form bigger and perfectly crystal. The results in this part

are consistent with the results from a previous part which both studies are the influence of thermal energy on the properties of CuO-ZnO nanoparticles.

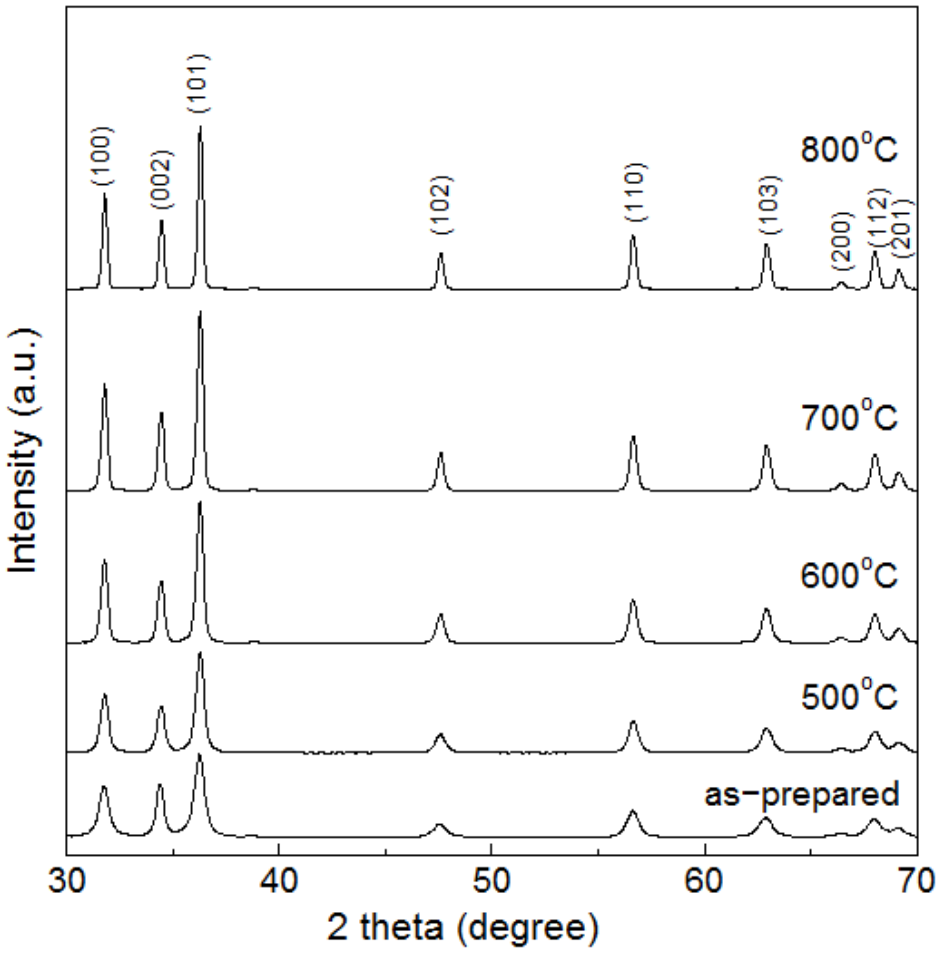

Fig.4.4 X-ray diffractograms of CuO-ZnO at molar ratio of Cu : Zn = 2 : 98 at various sintering temperatures.

Table 4.3 Calculated crystallite size of CuO-ZnO at molar ratio of Cu : Zn = 2 : 98 at various sintering temperatures.

Temperature (°C)	Crystallite size (nm)
As-prepared	16.28
500	19.85
600	24.26
700	27.29
800	39.25

4.2.2 Scanning electron micrograph

The SEM images of CuO-ZnO at a molar ratio of Cu : Zn = 2 : 98 at various sintering temperatures are shown in Figure 4.5 and 4.6, respectively. The shape of particles is a little changed from petal-like structure to the spherical-like structure by the influence of thermal energy. The size of particles in each condition will be described in the part of TEM because it can precisely measure the size more accurately. From the result, when thermal energy was applied to an as-prepared sample, the particles become larger size when the supplied thermal energy is increased.

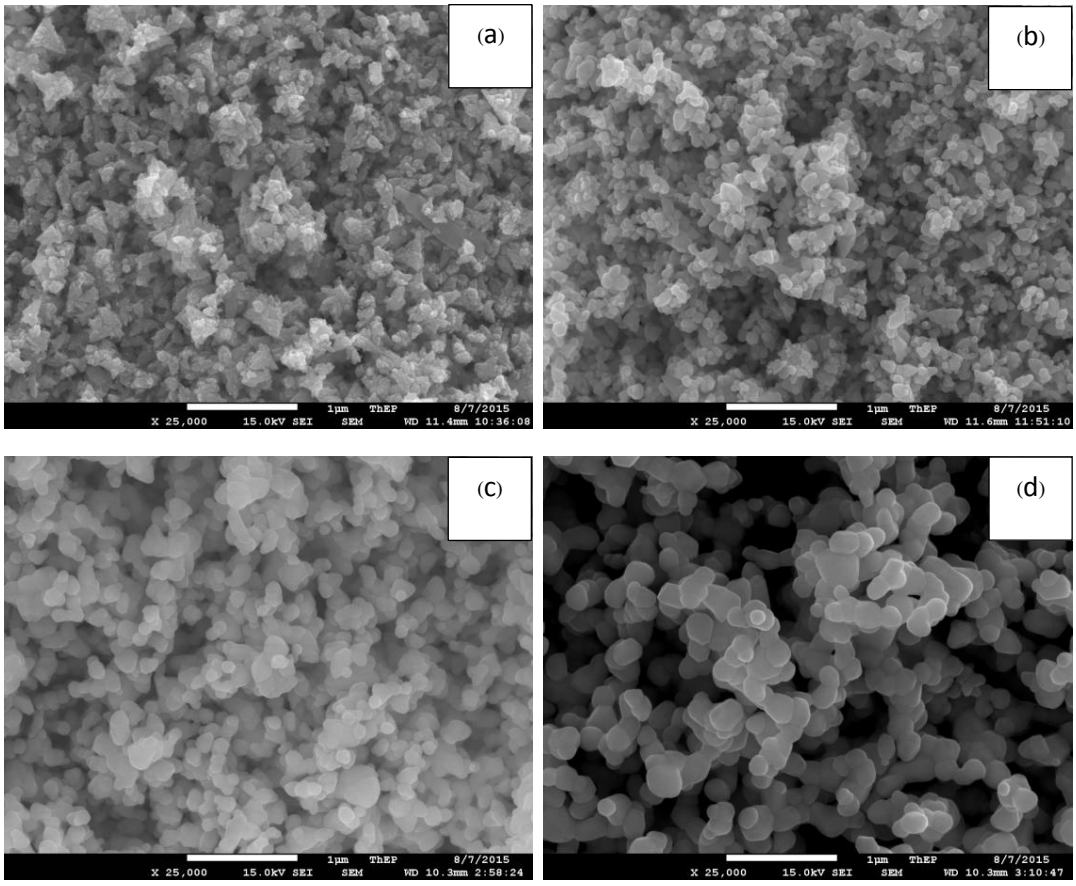

Fig. 4.5 SEM micrographs of CuO-ZnO at molar ratio of Cu : Zn = 2 : 98 at various sintering temperatures (a) as-prepared, (b) 500 °C, (c) 600 °C, (d) 700 °C and (e) 800 °C.

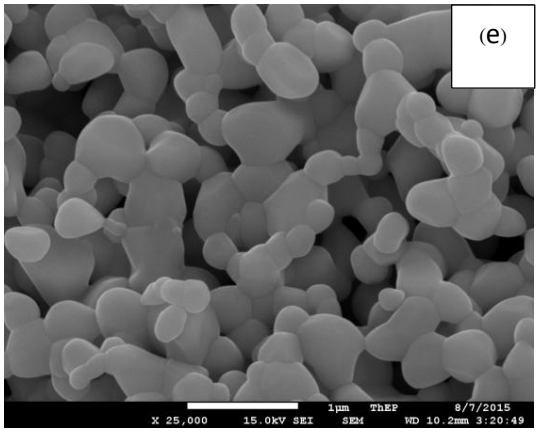

Fig. 4.5 (continued) SEM micrographs of CuO-ZnO at molar ratio of Cu : Zn = 2 : 98 at various sintering temperatures (a) as-prepared, (b) 500 °C, (c) 600 °C, (d) 700 °C and (e) 800 °C.

4.2.3 Transmission electron micrograph

Powder sample was dispersed in ethanol solvent under ultrasonic energy and then dropped onto the carbon coated onto a copper grid and heated to remove the solvent. TEM images of CuO-ZnO at a molar ratio of Cu : Zn = 2 : 98 at various sintering temperatures are shown in Figure 4.6. The average particle sizes of CuO-ZnO are measured with ImageJ software. The average sizes of particles are 28 nm, 49 nm, 117 nm, 156 nm and 272 nm at as-prepared and sintering temperature of 500, 600, 700 and 800 °C, respectively. The particle size is larger with increasing the supplied thermal energy. The shape of particle size was changed from petal-like structure to spherical-like structure with increasing the supplied sintering temperature. Due to the thermal energy can help the forming crystallization, the shape of the nanostructure is transformed to be the shape to decrease the surface energy within a structure for the stable state.

Table 4.4 Average particle sizes of CuO-ZnO at molar ratio of Cu : Zn = 2 : 98 at various temperature. (N=10)

Conditions	Average particle size (nm)
As-prepared	19 ± 5
500 °C	57 ± 11
600 °C	105 ± 20
700 °C	152 ± 21
800 °C	314 ± 37

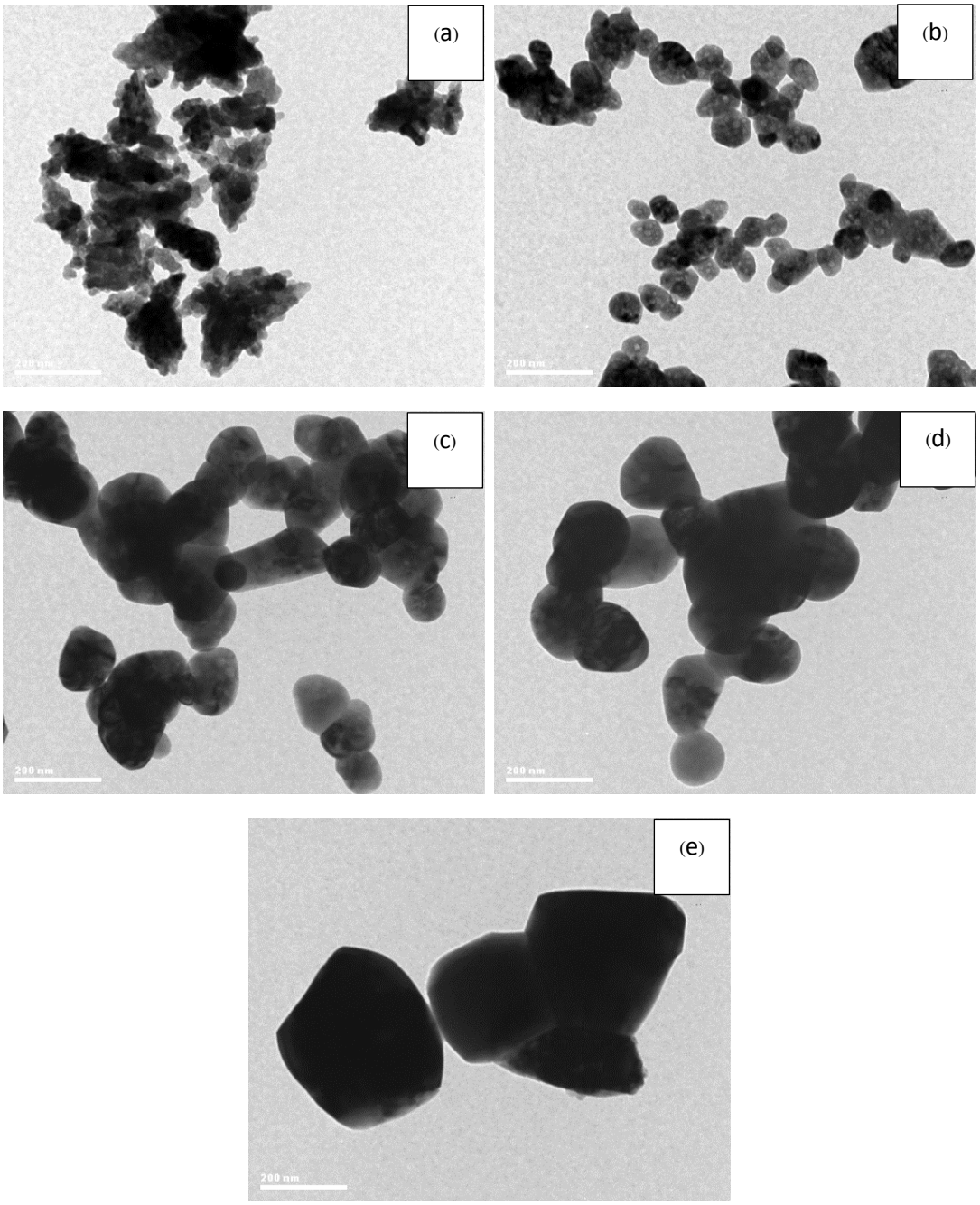

Fig. 4.6 TEM micrographs of CuO-ZnO at molar ratio of Cu : Zn = 2 : 98 at various sintering temperatures (a) as-prepared, (b) 500 °C, (c) 600 °C, (d) 700 °C and (e) 800 °C.

4.2.4 Fourier transform infrared spectrum

Figure 4.7 shows the FTIR spectra of CuO-ZnO at a molar ratio of Cu : Zn = 2 : 98 at various post-sintering temperatures. The bands at 400-600 cm^{-1} centered at 436 cm^{-1} can be assigned to Zn-O and Cu-O stretching mode. The band at 836 cm^{-1} is due to ν_2 vibration mode of nitrate mode. The weak band around 1,638 cm^{-1} and broad band around 3,440 cm^{-1} are attributed to adsorbed water molecules. For the sintered sample from 500 to 800 °C, the band at nitrate group does not appeared in FTIR spectra. At the higher sintering temperature, the water molecules were released by the supplied thermal energy.

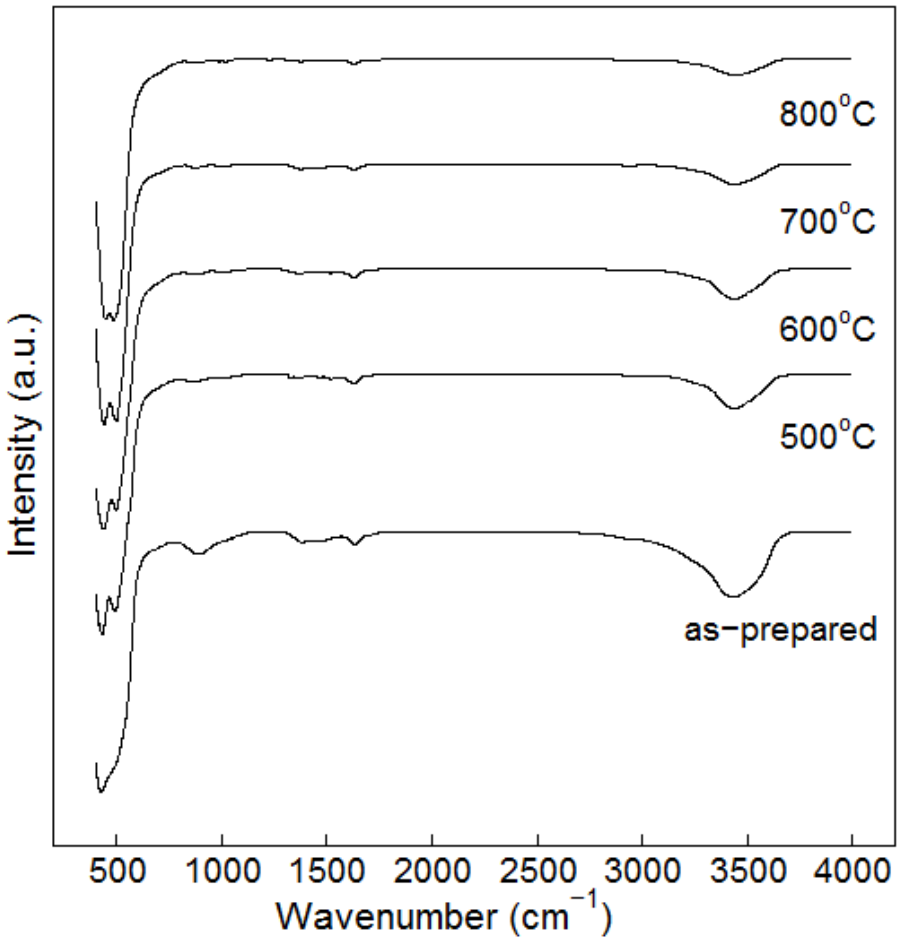

Fig. 4.7 FTIR spectrum of CuO-ZnO at molar ratio of Cu : Zn = 2 : 98 at various sintering temperatures.

4.3 The influence of molar ratio of Cu : Zn of as-prepared CuO-ZnO

4.3.1 Crystal structure properties

XRD diffractogram of as-prepared CuO-ZnO at the various molar ratio of Cu : Zn is shown in Fig. 4.8. All diffraction peaks are indexed by JCPDS card no. 36-1451 with hexagonal ZnO with wurtzite structure. There is a little peak indicating to the crystal of CuO marked with an asterisk. In this part, the authors have studied the influence of the molar ratios of Cu : Zn. At higher ratio of Cu : Zn, XRD technique can collect the CuO crystal on the surface of samples. Therefore, the authors confirm that samples at higher conditions are CuO-ZnO nanostructure. The change in intensity of each diffraction peaks are featured due to the substitution of the copper atom in CuO-ZnO structure because of copper radii and zinc radii have closed size which easily to penetrate together.

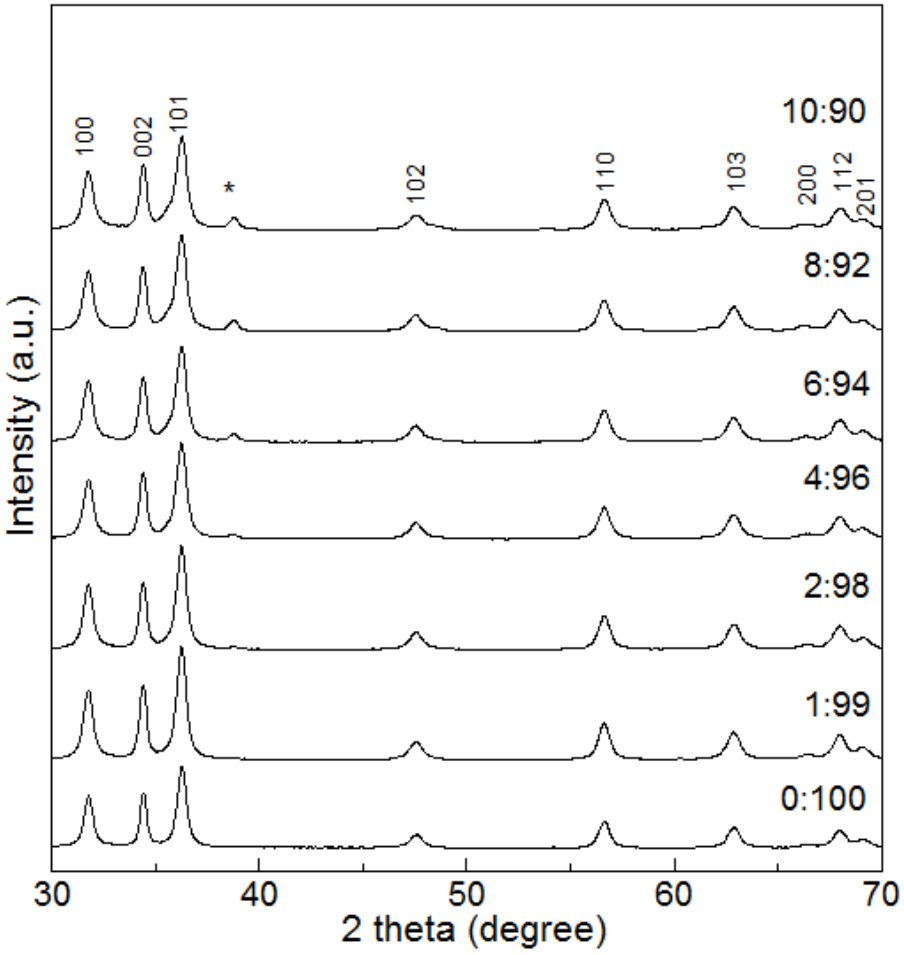

Fig. 4.8 X-ray diffractogram of as-prepared CuO-ZnO at various molar ratio of Cu : Zn.

4.3.2 Scanning electron micrograph and energy dispersive X-ray analysis

Figure 4.9 shows the SEM micrographs of as-prepared CuO-ZnO at various molar ratio of Cu : Zn. The morphological shape of the sample was changed from pure petal-like structure to mixed petal-like structure and needle-like structure of CuO-ZnO at the molar ratio of 0 to 10. In figure 4.10(a) for a pure sample, there are only Zn and O in EDX spectrum. In figure 4.10(b) for CuO-ZnO at a molar ratio of Cu : Zn of 10 : 90, there are only Zn, Cu and O in EDX spectrum. The quantitative values of each spectrum in EDX spectrum result are shown in Table 4.5. From these results, it represents that when the Cu content was added into the CuO-ZnO structure, some added Cu was attached on the nanomaterial which confirmed with EDX spectrum and consistent with the XRD results.

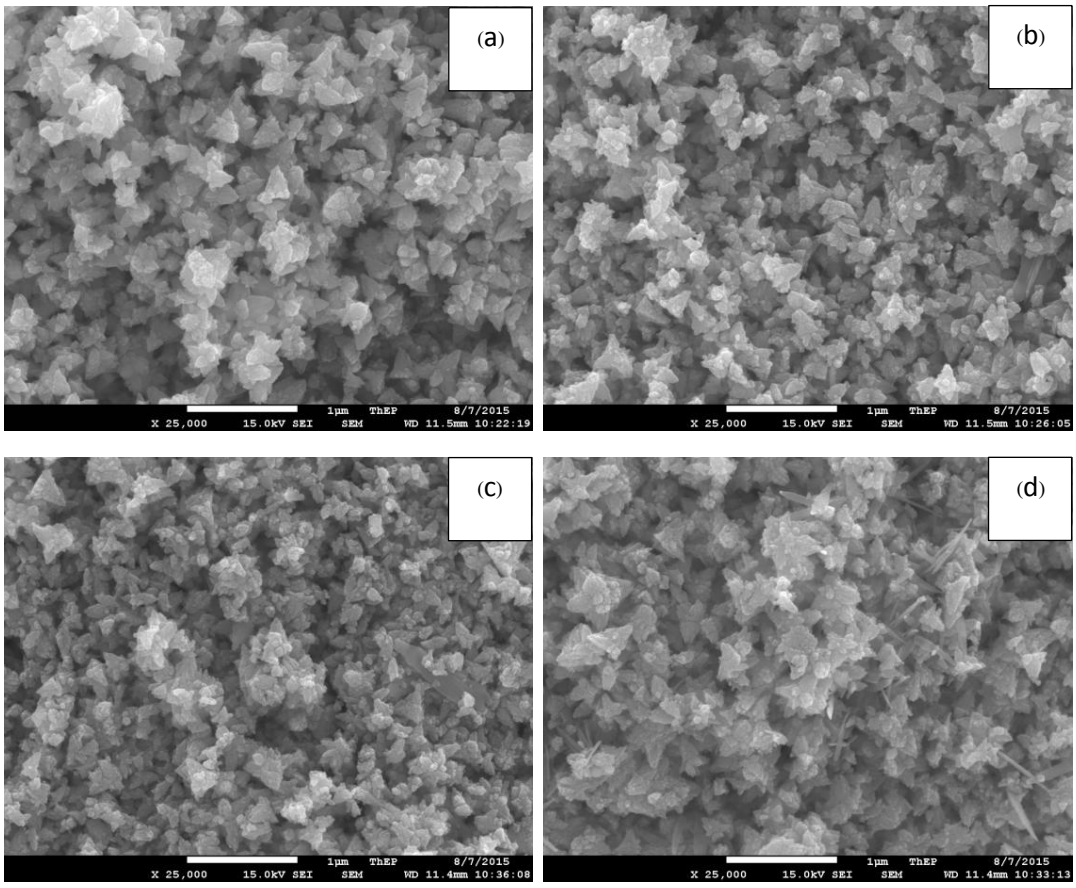

Fig. 4.9 SEM micrographs of as-prepared CuO-ZnO at (a) pure, and various molar ratio of Cu : Zn (b) 1 : 99, (c) 2 : 98, (d) 4 : 96, (e) 6 : 94, (f) 8 : 92 and (g) 10 : 90.

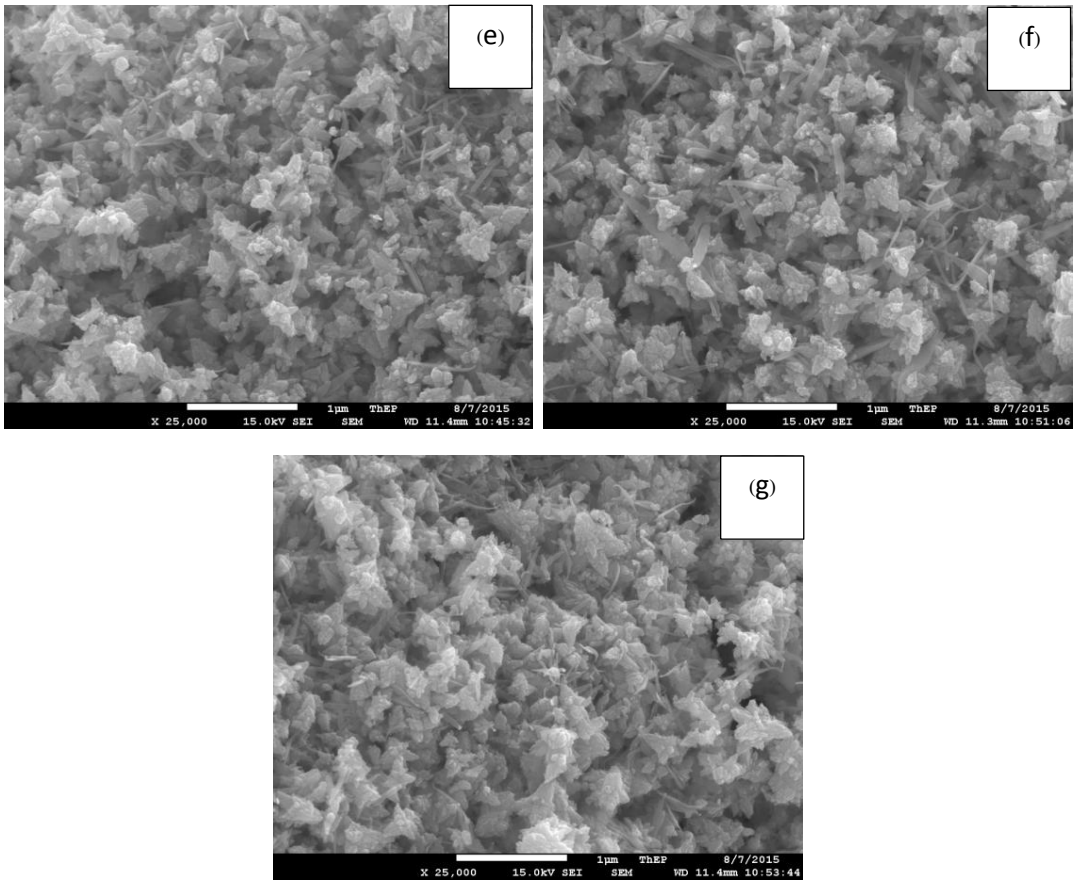

Fig. 4.9 (continued) SEM micrographs of as-prepared CuO-ZnO at (a) pure, and various molar ratio of Cu : Zn (b) 1 : 99, (c) 2 : 98, (d) 4 : 96, (e) 6 : 94, (f) 8 : 92 and (g) 10 : 90.

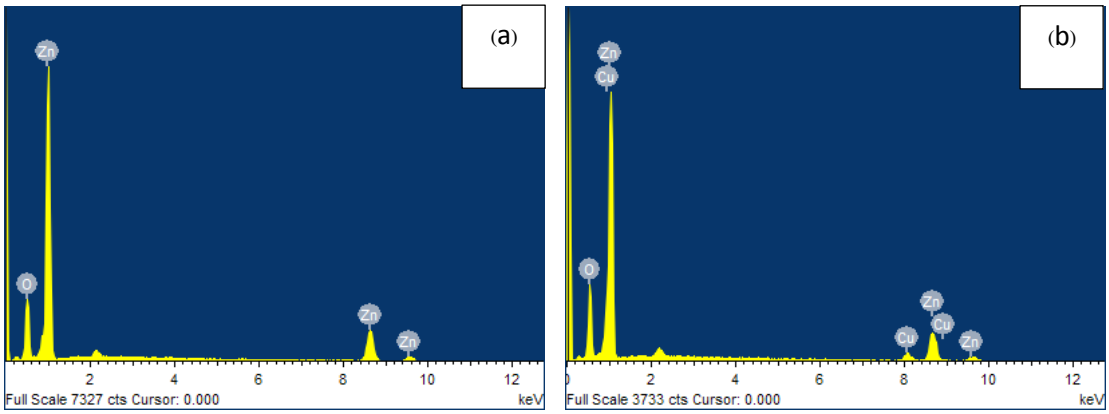

Fig. 4.10 EDX analysis of as-prepared zinc oxide (a) pure and (b) added Cu content at molar ratio Cu : Zn of 10 : 90.

Table 4.5 Quantitative value of EDX spectrum.

Conditions	Atomic percentage (%)		
	Zn	Cu	O
0 : 100	47.83	-	52.17
10 : 90	42.78	5.63	51.58

4.3.3 Transmission electron micrograph

TEM images of as-prepared CuO-ZnO at different molar ratio of Cu : Zn are shown in Figure 4.11. The shape and particle size of all samples are related in the same direction with SEM result which shape was changed from pure petal-like structure to mix phase between petal-like structure and needle-like structure. The morphological shape was changed due to it might be the result from surface energy of the material. From SEM result, it can confirm the morphological shape of nanomaterial. TEM result can be used to measure the size of particle more accuracy. The average particle sizes of nanomaterial were measured by the ImageJ software. These average particle sizes of each condition are shown in Table 4.5. At higher molar ratio of Cu : Zn, there are many needle-like structures compared with the lower molar ratio of Cu : Zn due to the probability of the formation of copper including copper oxide while the preparation process.

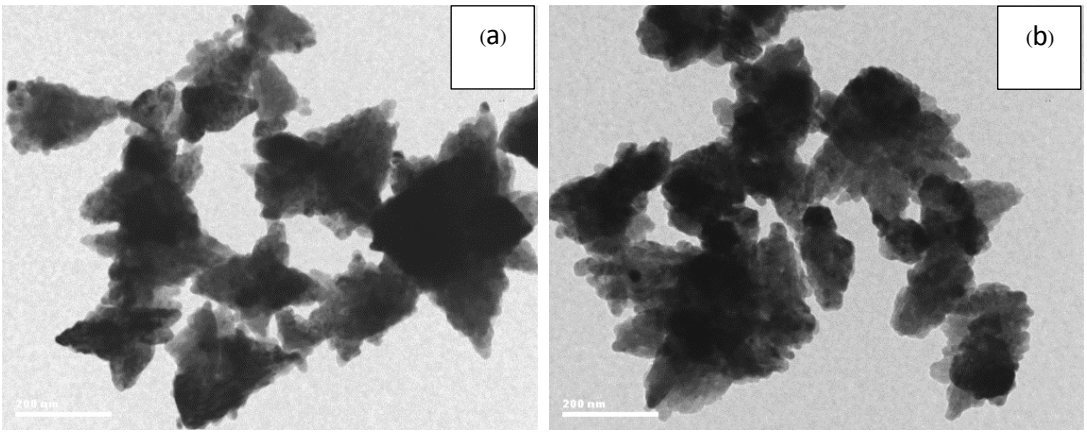

Fig. 4.11 TEM photographs of as-prepared CuO-ZnO at (a) pure, and various molar ratio (b) 1 : 99, (c) 2 : 98, (d) 4 : 96, (e) 6 : 94, (f) 8 : 92 and (g) 10 : 90.

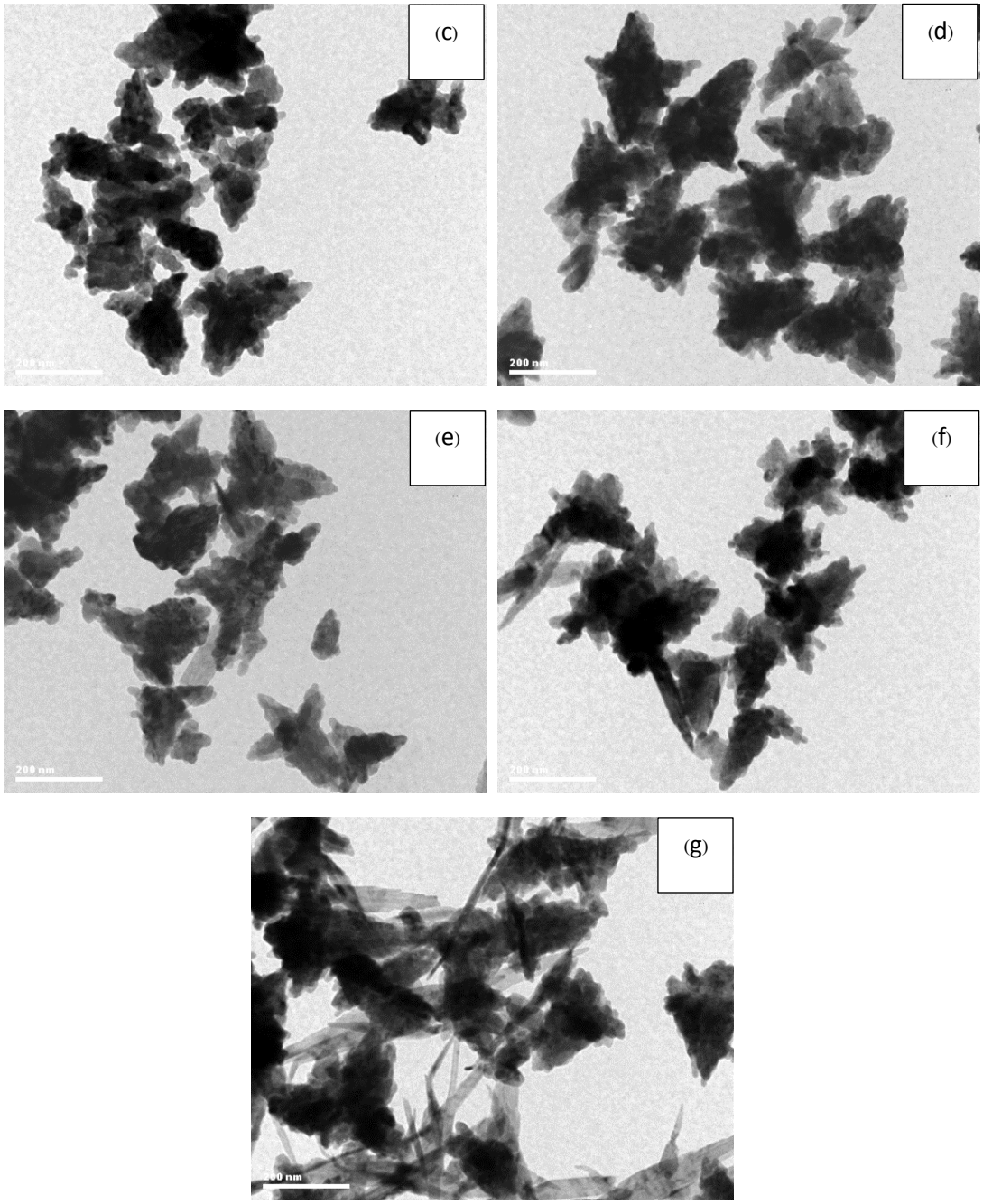

Fig. 4.11 (continued) TEM photographs of as-prepared CuO-ZnO at (a) pure, and various molar ratio (b) 1 : 99, (c) 2 : 98, (d) 4 : 96, (e) 6 : 94, (f) 8 : 92 and (g) 10 : 90.

Table 4.6 Average particle sizes of as-prepared CuO-ZnO at various molar ratio of Cu : Zn. (N=10)

Molar ratio of Cu : Zn	Average particle size (nm)
0 : 100 (Pure)	26 ± 8
1 : 99	23 ± 6
2 : 98	28 ± 3
4 : 96	35 ± 11
6 : 94	29 ± 7
8 : 92	27 ± 7
10 : 90	30 ± 8

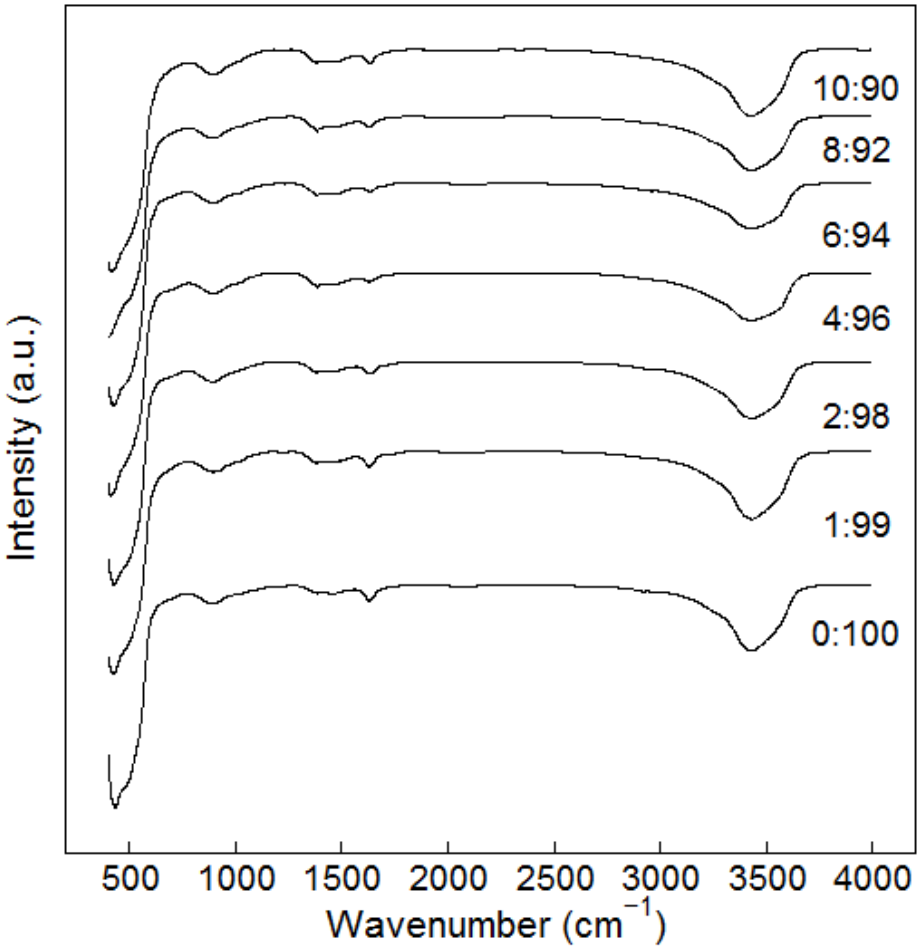

Fig. 4.12 FTIR spectrum of as-prepared CuO-ZnO at various molar ratio of Cu : Zn.

4.3.4 Fourier transform infrared spectrum

Figure 4.12 shows the FTIR spectra of as-prepared CuO-ZnO at the different molar ratios. The Zn-O and Cu-O stretching modes are indicated that the bands around 400-600 cm^{-1} centered at 436 cm^{-1}. The ν_2 vibration mode of nitrate mode band at 836 cm^{-1} is shown in all samples due to without sintering condition. The weak band around 1,638 cm^{-1} and broad band around 3,440 cm^{-1} are attributed to adsorbed water molecules.

4.3.5 X-ray photoelectron spectrum

The as-prepared CuO-ZnO at various molar ratios of Cu : Zn content (a) 0 : 100, (b) 1 : 99, (c) 2 : 98, (d) 4 : 96, (e) 6 : 94, (f) 8 : 92 and (g) 10 : 90 were measured by XPS machine. Fig. 4.13 shows the typical XPS wide survey spectra of as-prepared CuO-ZnO at various molar ratios. Carbon, zinc, and oxygen peaks occurred as shown in the survey spectra in Fig. 4.13, there is Cu 2p region because of the Cu content added to CuO-ZnO structure is enough to detect with XPS machine.

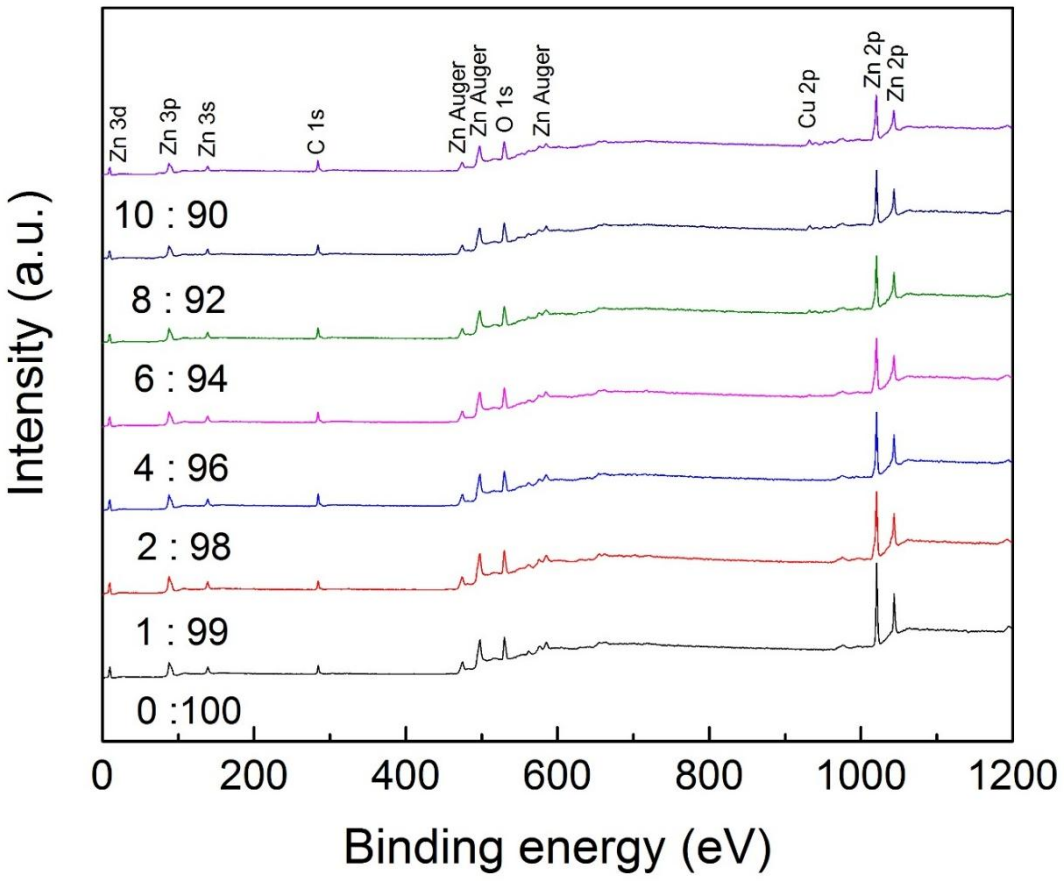

Fig. 4.13 XPS survey spectra of as-prepared CuO-ZnO at various molar ratio of Cu : Zn.

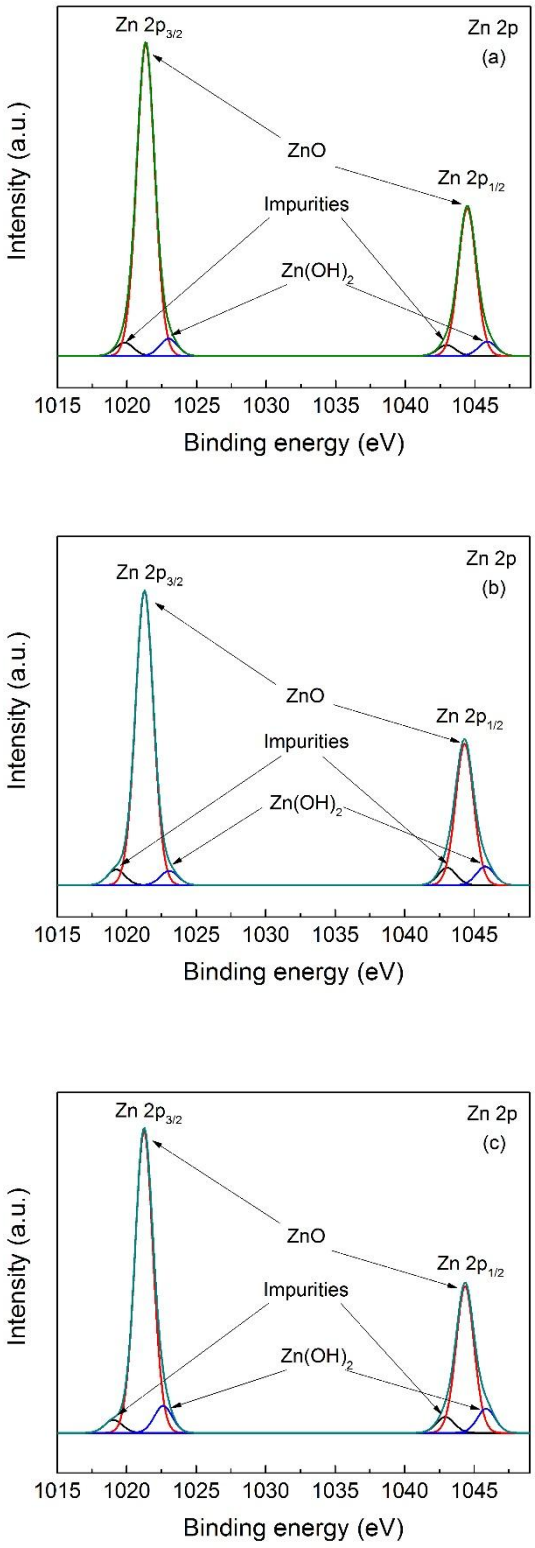

Fig. 4.14 XPS spectra of Zn 2p core-level of as-prepared CuO-ZnO at (a) pure, and various molar ratio of Cu : Zn (b) 1 : 99, (c) 2 : 98, (d) 4 : 96, (e) 6 : 94, (f) 8 : 92 and (g) 10 : 90.

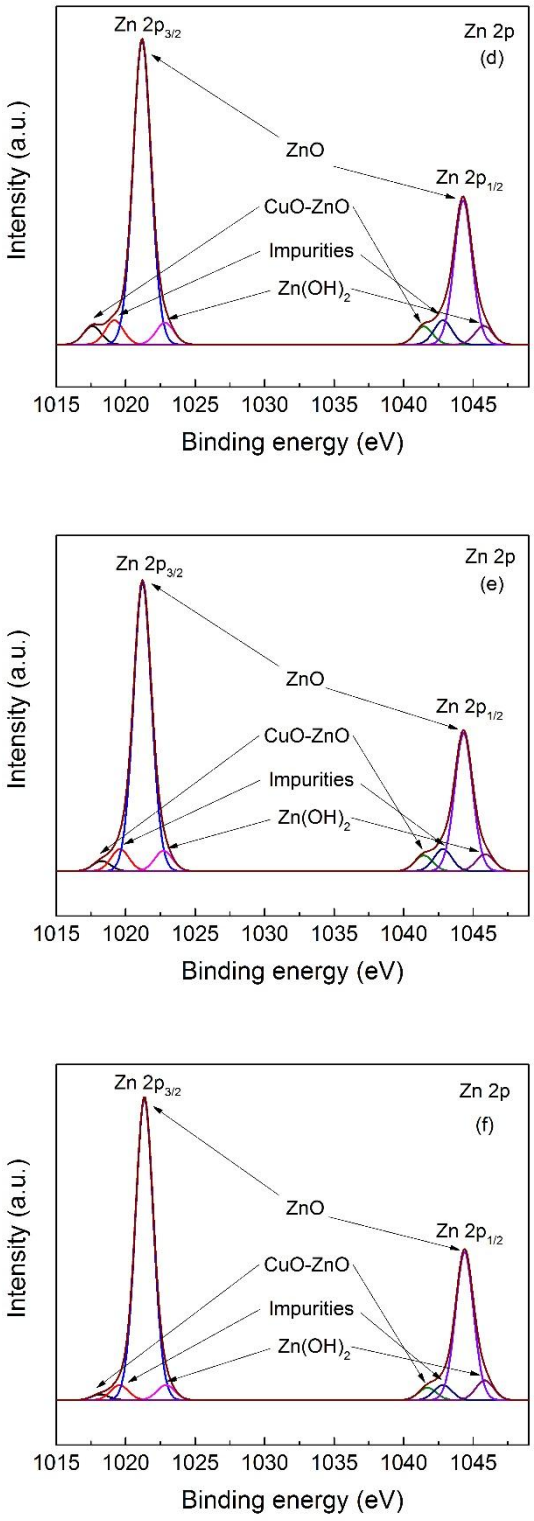

Fig. 4.14 (continued) XPS spectra of Zn 2p core-level of as-prepared CuO-ZnO at (a) pure, and various molar ratio of Cu : Zn (b) 1 : 99, (c) 2 : 98, (d) 4 : 96, (e) 6 : 94, (f) 8 : 92 and (g) 10 : 90.

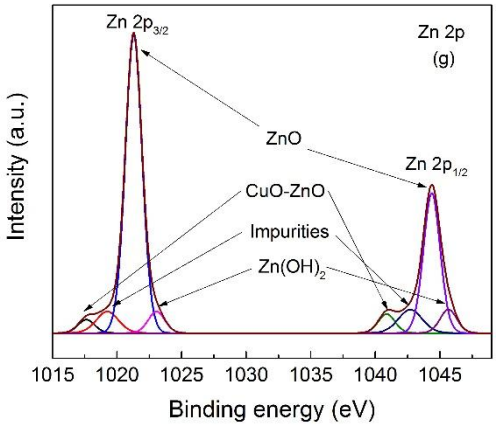

Fig. 4.14 (continued) XPS spectra of Zn 2p core-level of as-prepared CuO-ZnO at (a) pure, and various molar ratio of Cu : Zn (b) 1 : 99, (c) 2 : 98, (d) 4 : 96, (e) 6 : 94, (f) 8 : 92 and (g) 10 : 90.

Fig. 4.14 and Fig. 4.15 demonstrate the comparisons of high-resolution XPS spectra of the Zn 2p and O 1s regions of as-prepared CuO-ZnO at various molar ratios of Cu content. The core level Zn 2p of as-prepared CuO-ZnO at various molar ratios has fitting peaks appeared at approximately 1044.5 and 1021.4 eV depicted to Zn $2p_{1/2}$ and Zn $2p_{3/2}$, respectively. The core level Cu 2p of as-prepared CuO-ZnO at various molar ratio depicted to Cu$2p_{1/2}$ and Cu $2p_{3/2}$, respectively, and these values are consistent with the standard XPS database. The difference of binding energy between the Zn $2p_{1/2}$ and Zn $2p_{3/2}$ is 23.1 eV confirmed to highly quality ZnO nanostructure which consistent with the standard database [48].

After de-convolution the peak of Zn$2p_{3/2}$ of pure ZnO, we observed the occurrence of three peaks at 1019.8, 1021.3, and 1023.0 eV. An occurrence of a prominent peak at 1021.3 eV is represented the common of ZnO crystal. In the hexagonal crystal of ZnO, zinc cation is arranged with four atoms of oxygen and shows peak located at 1021.3 eV. Peak locates at 1023.0 eV is the peak which indicated that is hydroxyl group of nanostructures. For the ideal, there are no any oxygen deficiencies in the structure. However, when the tetrahedrally of oxygen coordinated with ZnO, deficient of oxygen atoms such as hydroxyl group which produce a new peak of binding energy at 1019.8 eV. At higher molar ratio of Cu : Zn content, there is new binding energy peaks appearance at a lower binding energy compared with pure ZnO in the XPS spectra indicating to oxygen deficiency defect in CuO-ZnO structure [49].

Fig 4.15 displays the XPS spectra of O 1s region of as-prepared CuO-ZnO at various molar ratios of Cu : Zn. It is demonstrated in Fig. 4.15 that the O 1s core level spectrum of as-prepared CuO-ZnO at various molar ratio of Cu : Zn has different forms of oxygen. For pure ZnO, the peaks in O 1s region spectra were deconvoluted into five peaks at 530.1, 531.1, 532.0, 532.8 and 533.6 eV by using the Gaussian fitting. The peaks located at 530.1 and 531.1 eV are depicted to the atom of oxygen in the lattice without and with deficiencies oxygen, respectively. The peak located at 532.0 eV is usually attributed to chemisorbed atom of oxygen onto the ZnO nanoparticles, for instance, carbonyl and hydroxyl groups [50]. The peaks at 532.8 and 533.6 eV are high probability corresponding to the adsorbed of water molecules [51]. At higher molar ratio of Cu : Zn content more than 4 : 96, the peak at lower binding energy centered at 529.0 eV indicate that CuO [52]. Because of all samples were not thermal treatment, therefore peak represents the water molecules at the binding energy around 532.8 and 533.6 eV appear in all samples [48,53].

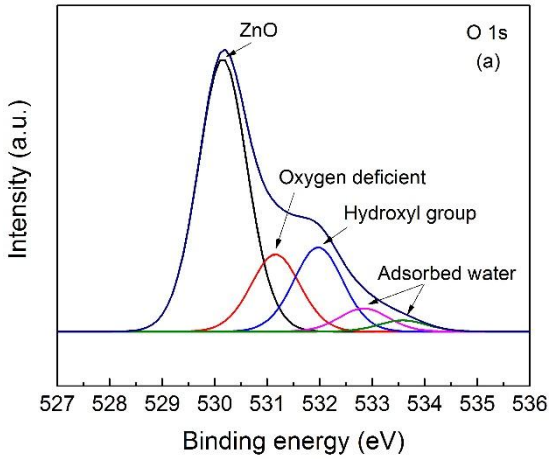

Fig. 4.15 XPS spectra of O 1s core-level of as-prepared CuO-ZnO at various molar ratio of Cu : Zn of (a) 0 : 100, (b) 1 : 99, (c) 2 : 98, (d) 4 : 96, (e) 6 : 94, (f) 8 : 92 and (g) 10 : 90.

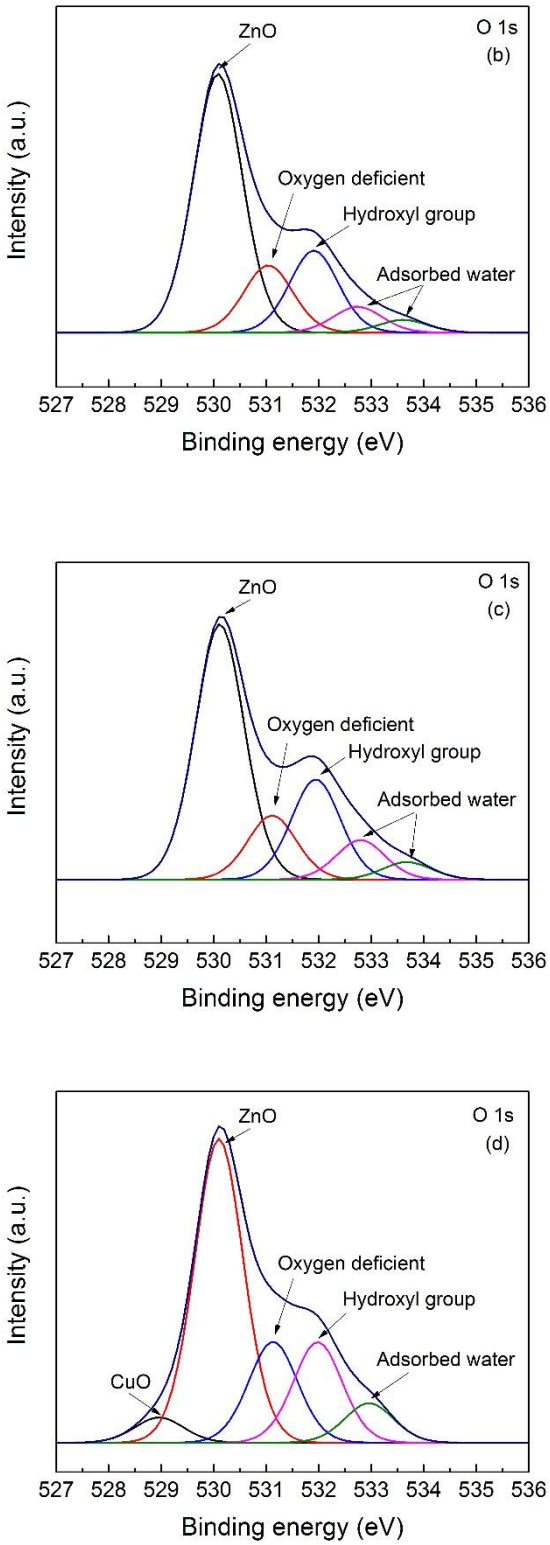

Fig. 4.15 (continued) XPS spectra of O 1s core-level of as-prepared CuO-ZnO at various molar ratio of Cu : Zn of (a) 0 : 100, (b) 1 : 99, (c) 2 : 98, (d) 4 : 96, (e) 6 : 94, (f) 8 : 92 and (g) 10 : 90.

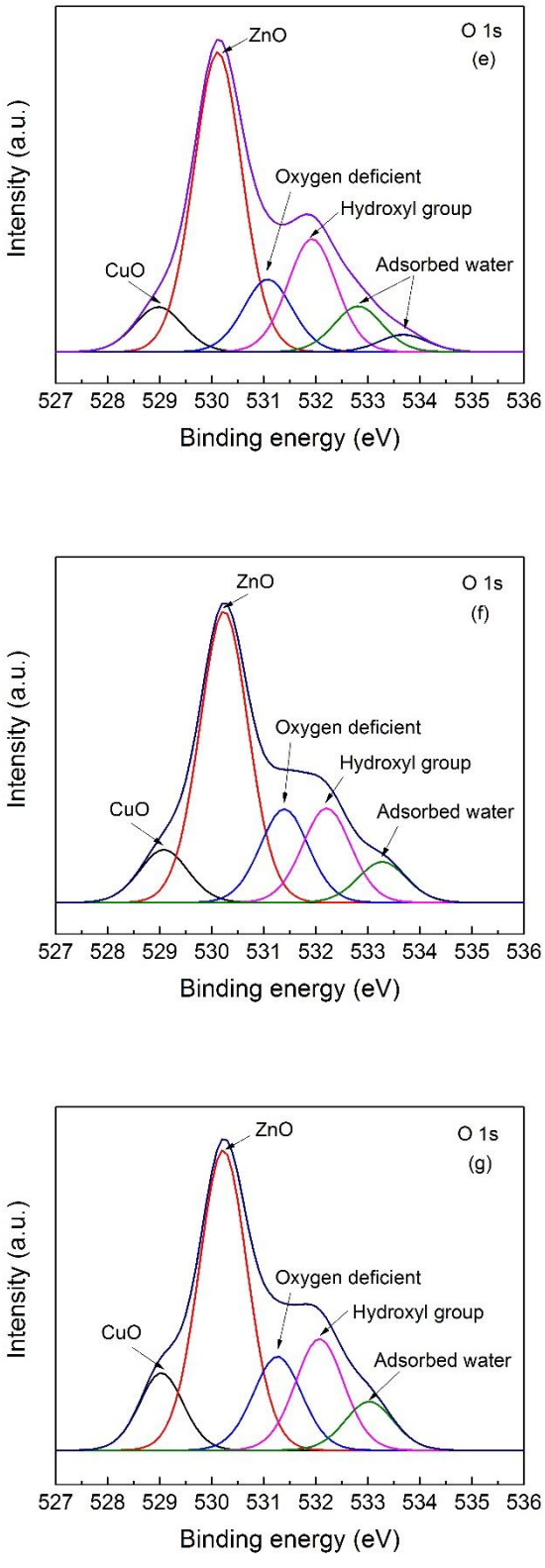

Fig. 4.15 (continued) XPS spectra of O 1s core-level of as-prepared CuO-ZnO at various molar ratio of Cu : Zn of (a) 0 : 100, (b) 1 : 99, (c) 2 : 98, (d) 4 : 96, (e) 6 : 94, (f) 8 : 92 and (g) 10 : 90.

Fig. 4.16 shows the deconvoluted XPS spectra of high-resolution Cu 2p core-level of as-prepared CuO-ZnO at various molar ratio of Cu : Zn depicted to Cu $2p_{1/2}$ and Cu $2p_{3/2}$, respectively [53]. The peaks at 932.0 and 952.0 eV are attributed to Cu $2p_{3/2}$ and Cu $2p_{1/2}$, respectively, indicating that the existence of CuO nanoparticles in the CuO-ZnO nanostructures [54]. There are three peaks at 931.3, 932.5, and 933.5 eV which indicating to the mixture of CuO and ZnO nanostructure, the lattice of CuO crystal, and copper hydroxide, respectively [54]. At higher molar ratio of Cu : Zn content, the intensity of Cu 2p peaks become sharper which confirmed that there is much mixing phase between CuO and ZnO in CuO-ZnO nanostructure [55]. In additions, there is more peaks at 930.9 eV which occurs only in the sample at condition of molar ratio of Cu : Zn of 10 : 90 indicating to excess of copper in the nanostructure.

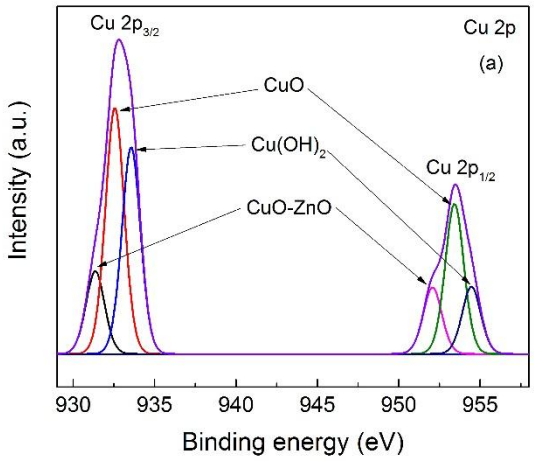

Fig. 4.16 XPS spectra of Cu 2p core-level of as-prepared CuO-ZnO at various molar ratio of Cu : Zn of (a) 4 : 96, (b) 6 : 94, (c) 8 : 92 and (d) 10 : 90.

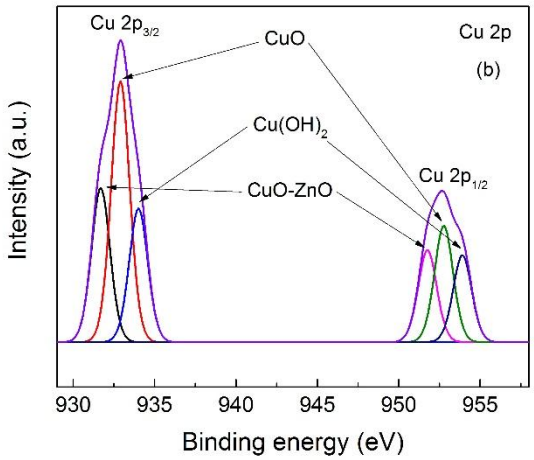

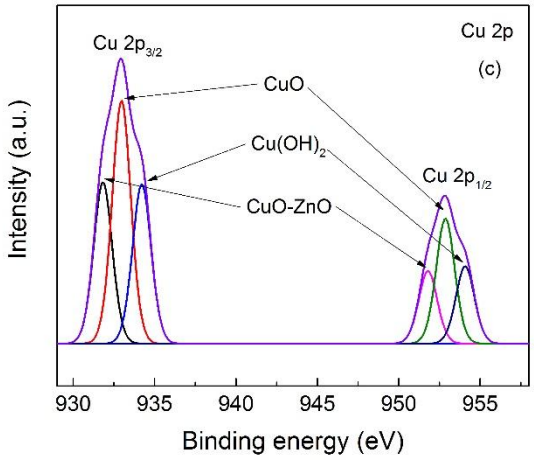

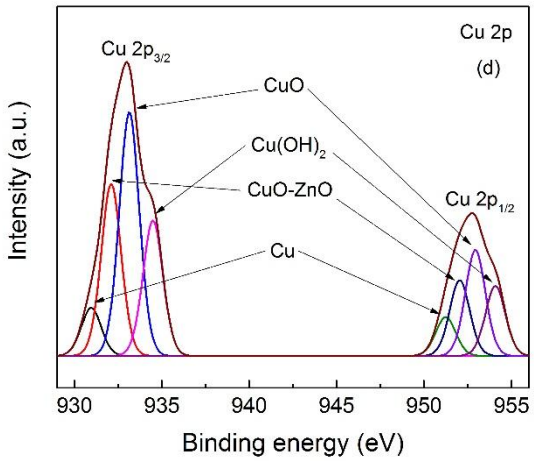

Fig. 4.16 (continued) XPS spectra of Cu 2p core-level of as-prepared CuO-ZnO at various molar ratio of Cu : Zn of (a) 4 : 96, (b) 6 : 94, (c) 8 : 92 and (d) 10 : 90.

4. 4 The influence of molar ratios of Cu : Zn in the CuO-ZnO nanoparticles sintered at temperature of 500 °C for 2 hours.

4.4.1 Crystal structure properties

Figure 4.17 shows the X-ray diffractogram of CuO-ZnO at various molar ratios of Cu : Zn content sintered at 500 °C. All diffraction peaks are indexed by JCPDS card no. 36-1451 with hexagonal ZnO with wurtzite structure. There is a little peak indicating to the crystal of CuO in the sample which has the molar ratio of Cu : Zn much than 6 : 94. There are no any impurities appear in all samples.

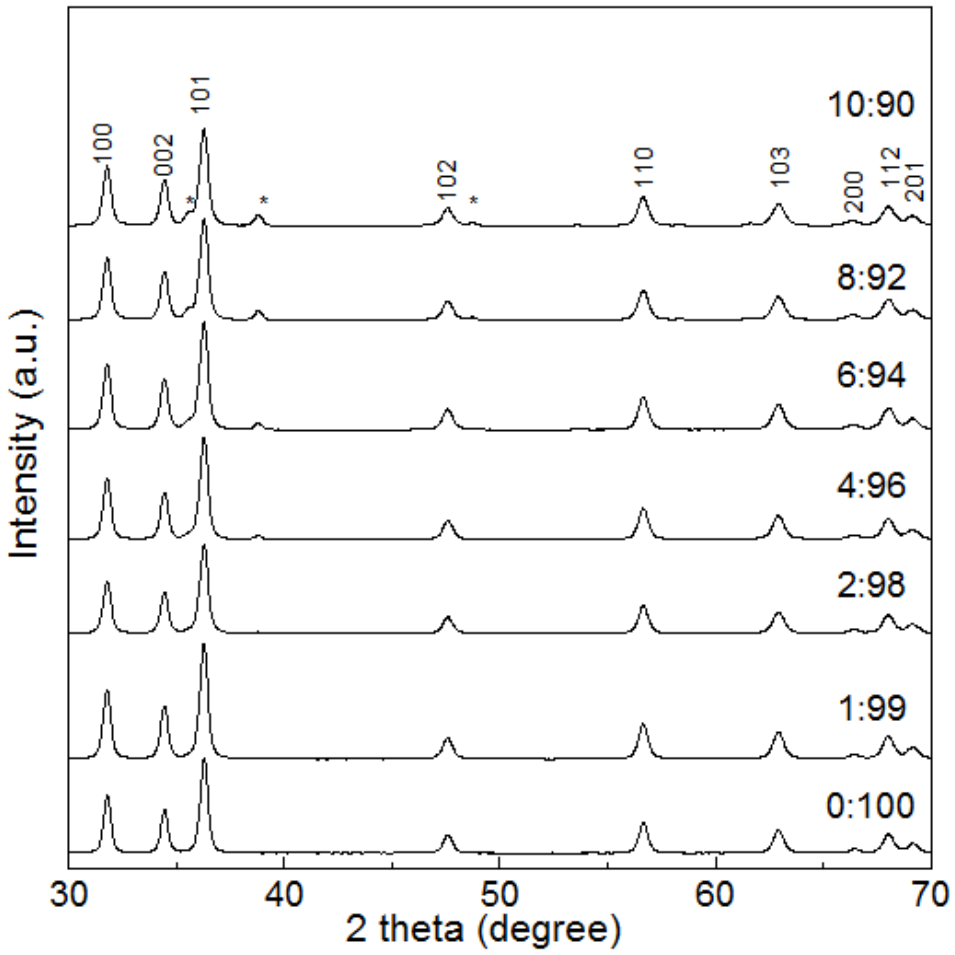

Fig. 4.17 X-ray diffractogram of CuO-ZnO at various molar ratios of Cu : Zn sintered at 500 °C.

4.4.2 Scanning electron micrograph

SEM micrographs of CuO-ZnO at various molar ratios of Cu : Zn content sintered at a temperature of 500 °C for 2 hours are shown in Figure 4.18. The shape was not changed in few molar ratios of Cu : Zn content into zinc oxide and changed to mix phase between spherical-like structure and needle-like structure in the added copper condition at a molar ratio of Cu : Zn at 10 : 90. The comparison of particles size of each molar ratios of Cu : Zn contents, the size of particles is not significantly changed for all samples

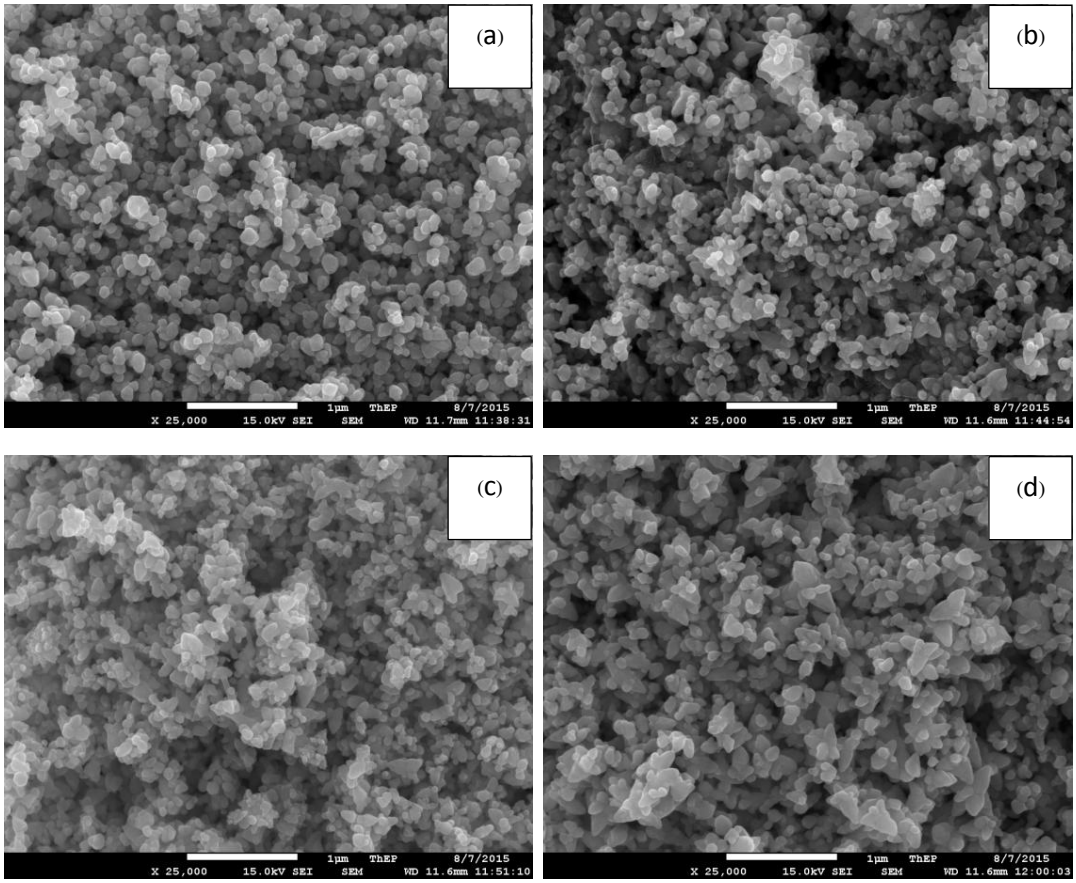

Fig. 4.18 SEM micrographs of CuO-ZnO at various molar ratios of Cu : Zn content sintered at 500 °C (a) 0 : 100, (b) 1 : 99, (c) 2 : 98, (d) 4 : 96, (e) 6 : 94, (f) 8 : 92 and (g) 10 : 90.

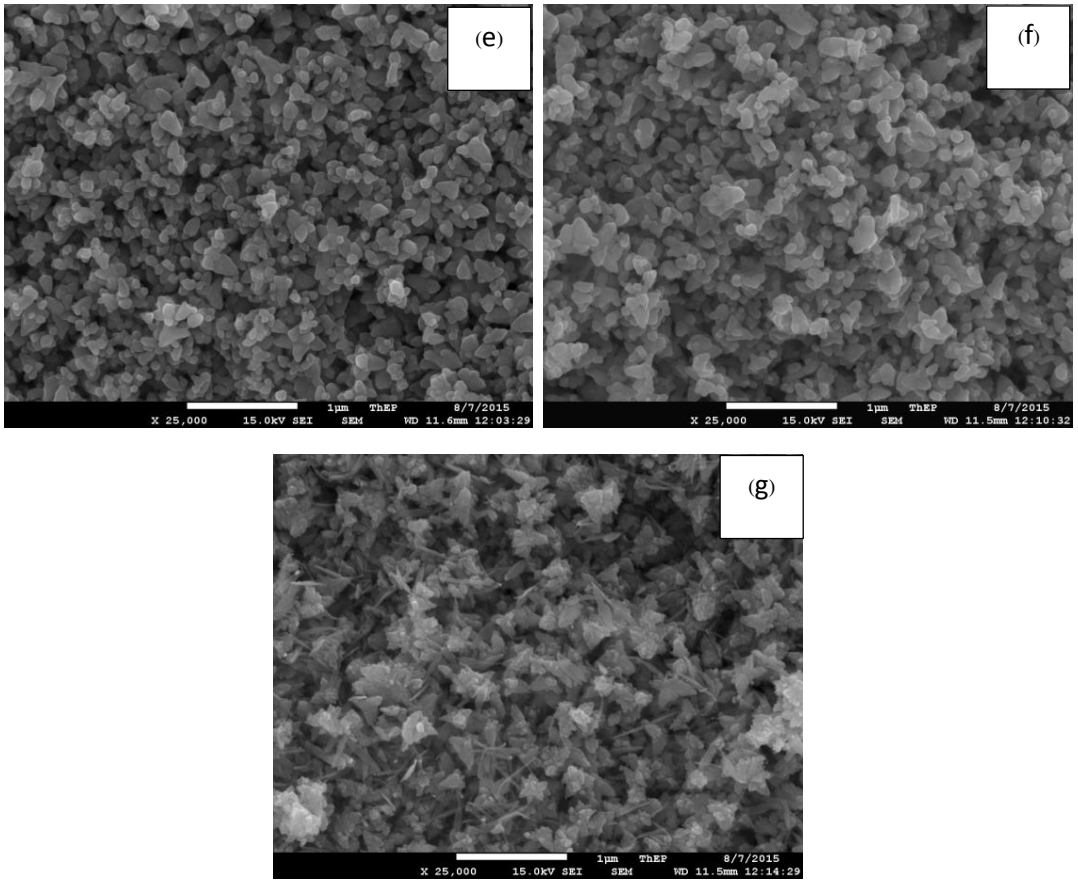

Fig. 4.18 (continued) SEM micrographs of CuO-ZnO at various molar ratios of Cu : Zn content sintered at 500 °C (a) 0 : 100, (b) 1 : 99, (c) 2 : 98, (d) 4 : 96, (e) 6 : 94, (f) 8 : 92 and (g) 10 : 90.

4.4.3 Fourier transform infrared spectrum

Figure 4.19 shows the FTIR spectra of at various molar ratios of Cu : Zn into the CuO-ZnO nanostructure sintered at 500 °C. The Zn-O and Cu-O stretching modes are indicated that the bands around 400-600 cm^{-1} centered at 436 cm^{-1}. The ν_2 vibration mode of nitrate mode band at 836 cm^{-1} is not shown in all samples because as high as 400 °C, the nitrate can be decomposed. The weak band around 1,638 cm^{-1} and broad band around 3,440 cm^{-1} are attributed to adsorbed water molecules.

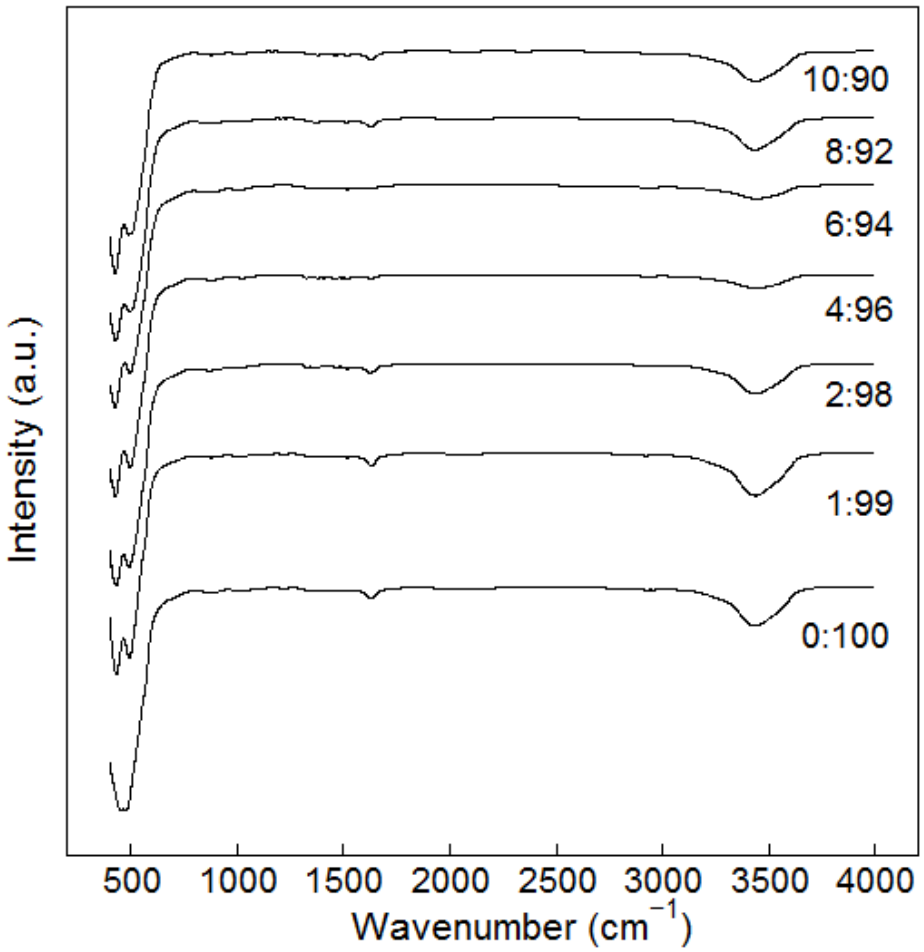

Fig. 4.19 FT-IR spectrum of CuO-ZnO at different molar ratio of Cu : Zn sintered at 500 °C.

4.4.4 X-ray photoelectron spectrum

The sintered CuO-ZnO at 500 °C at various molar ratio of Cu : Zn content (a) 0 : 100, (b) 1 : 99, (c) 2 : 98, (d) 4 : 96, (e) 6 : 94, (f) 8 : 92 and (g) 10 : 90 were measured by XPS machine. Fig. 4.20 shows the common wide survey XPS spectra of sintered CuO-ZnO at a temperature of 500 °C for 2 hours at various molar ratios of Cu : Zn. Zinc, oxygen and carbon peaks were collected in the survey spectra, there is Cu 2p region because of the Cu content added to CuO-ZnO structure is enough to detect with XPS machine.

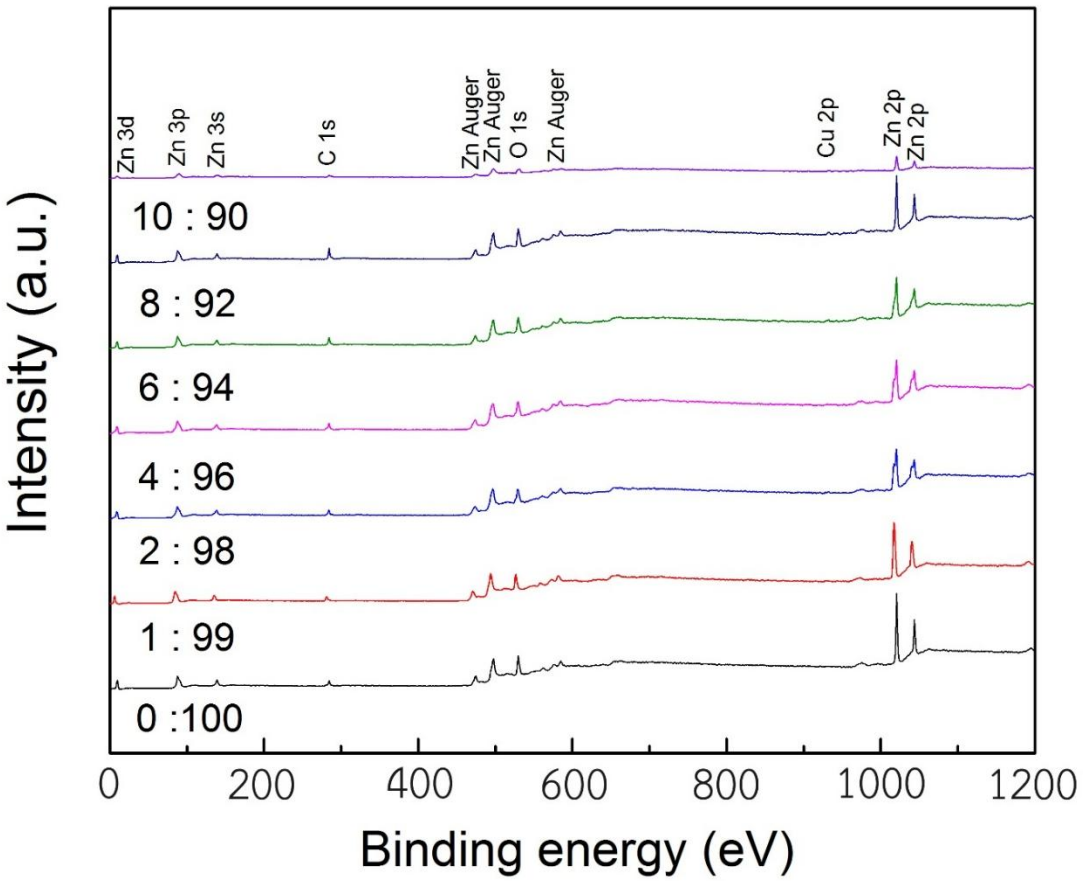

Fig. 4.20 XPS survey spectra of sintered CuO-ZnO at 500 °C at various molar ratio of Cu : Zn.

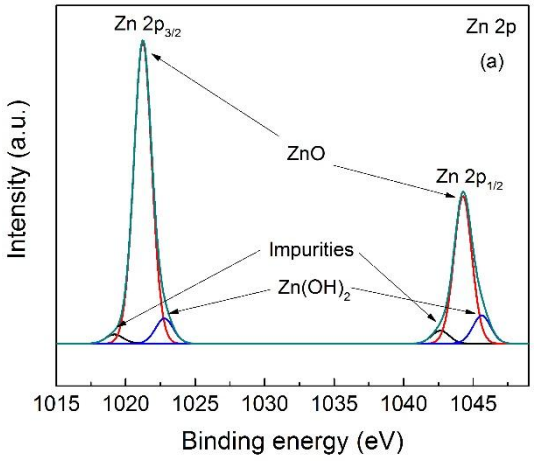

Fig. 4.21 XPS spectra of Zn 2p core-level of sintered CuO-ZnO at 500 °C at various molar ratio of Cu : Zn content of (a) 0 : 100, (b) 1 : 99, (c) 2 : 98, (d) 4 : 96, (e) 6 : 94, (f) 8 : 92 and (g) 10 : 90.

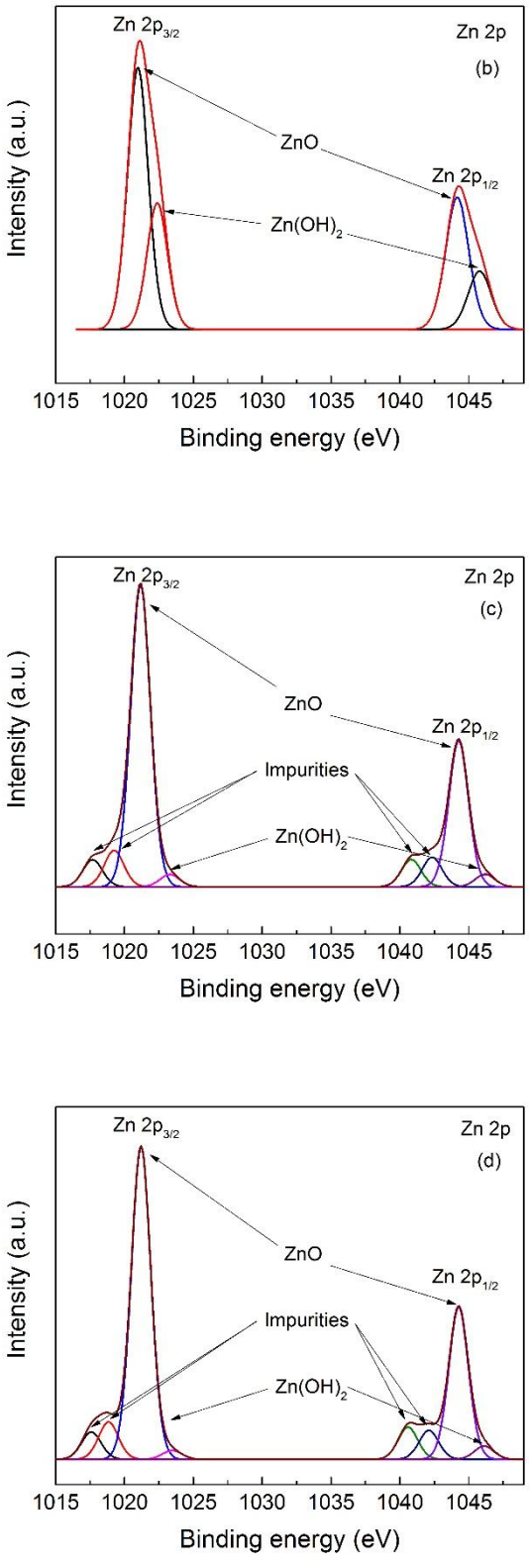

Fig. 4.21 (continued) XPS spectra of Zn 2p core-level of sintered CuO-ZnO at 500 °C at various molar ratio of Cu : Zn content of (a) 0 : 100, (b) 1 : 99, (c) 2 : 98, (d) 4 : 96, (e) 6 : 94, (f) 8 : 92 and (g) 10 : 90.

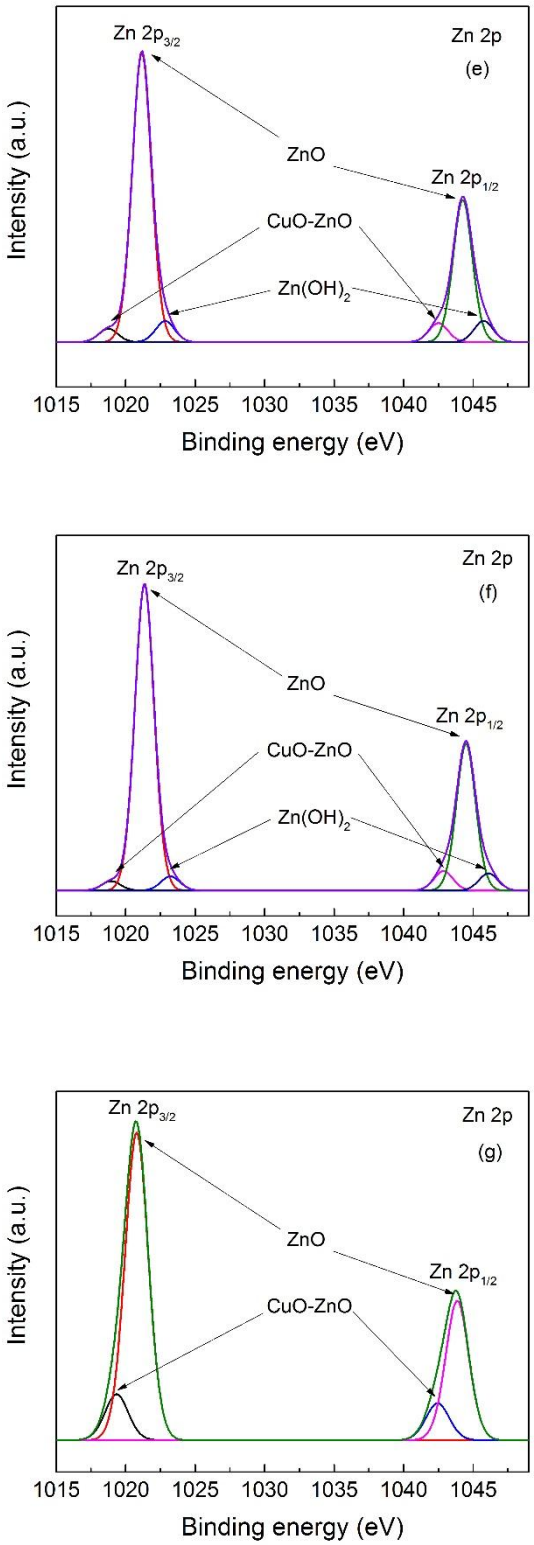

Fig. 4.21 (continued) XPS spectra of Zn 2p core-level of sintered CuO-ZnO at 500 °C at various molar ratio of Cu : Zn content of (a) 0 : 100, (b) 1 : 99, (c) 2 : 98, (d) 4 : 96, (e) 6 : 94, (f) 8 : 92 and (g) 10 : 90.

Fig. 4.21 and Fig. 4.22 show the comparison of the high resolution of XPS spectra, the Zn 2p and O 1s regions of as-prepared CuO-ZnO at various molar ratios of Cu : Zn content. The core level Zn 2p of as-prepared CuO-ZnO at various molar ratios of Cu : Zn has fitting peaks at approximately 1044.3 and 1021.2 eV which corresponding to Zn $2p_{1/2}$ and Zn $2p_{3/2}$, respectively. The Cu 2p core-level of as-prepared CuO-ZnO at various molar ratio of Cu : Zn depicted to Cu$2p_{1/2}$ and Cu $2p_{3/2}$, respectively. The difference of binding energy between the Zn $2p_{1/2}$ and Zn $2p_{3/2}$ is 23.1 eV, well agree with a database.

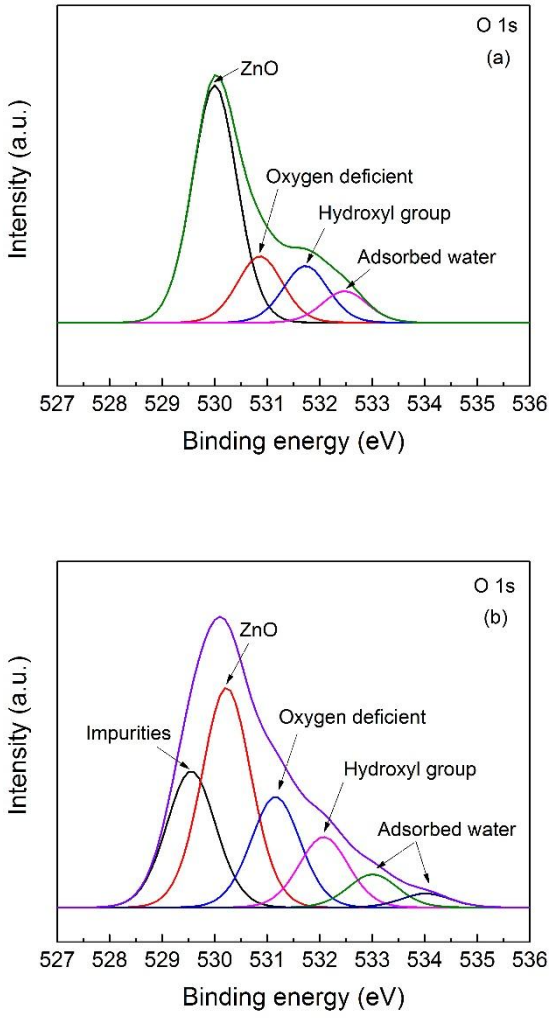

Fig. 4.22 XPS spectra of O 1s core-level of sintered CuO-ZnO at 500 °C at various molar ratio of Cu : Zn content of (a) 0 : 100, (b) 1 : 99, (c) 2 : 98, (d) 4 : 96, (e) 6 : 94, (f) 8 : 92 and (g) 10 : 90.

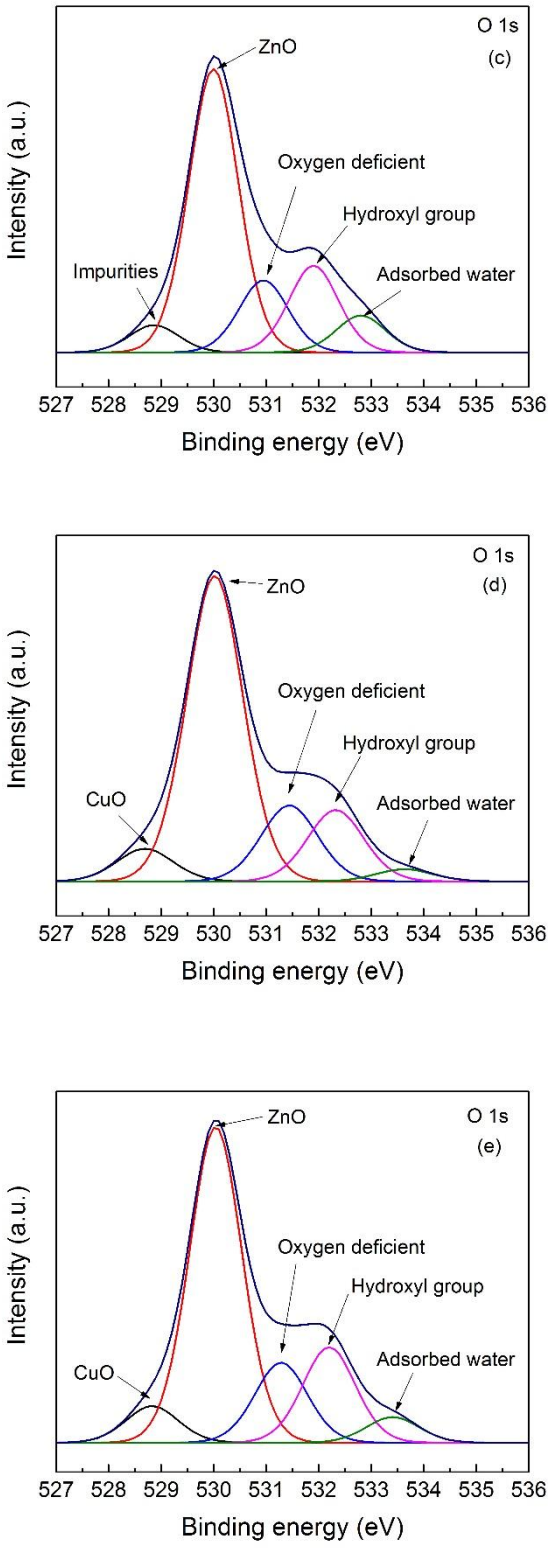

Fig. 4.22 (continued) XPS spectra of O 1s core-level of sintered CuO-ZnO at 500 °C at various molar ratio of Cu : Zn content of (a) 0 : 100, (b) 1 : 99, (c) 2 : 98, (d) 4 : 96, (e) 6 : 94, (f) 8 : 92 and (g) 10 : 90.

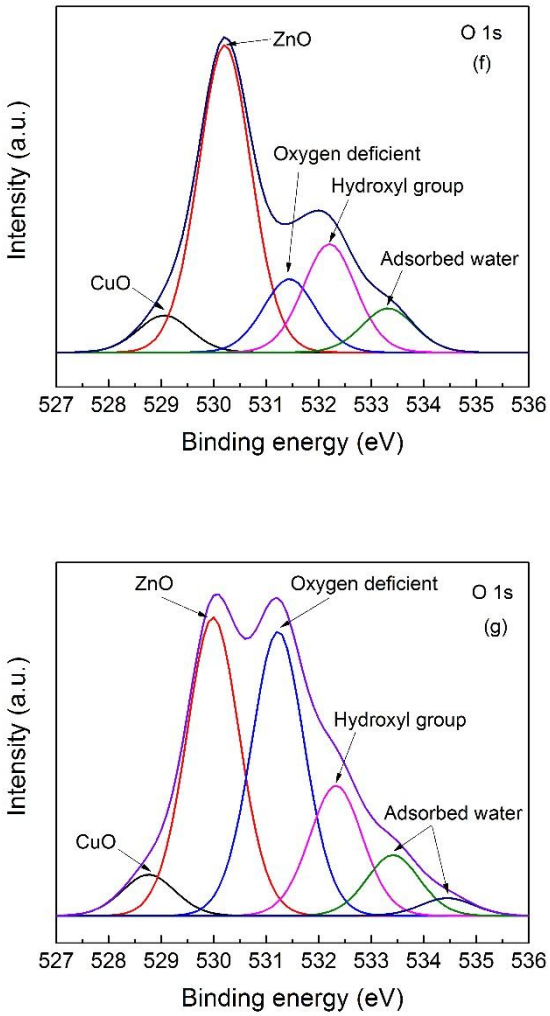

Fig. 4.22 (continued) XPS spectra of O 1s core-level of sintered CuO-ZnO at 500 °C at various molar ratio of Cu : Zn content of (a) 0 : 100, (b) 1 : 99, (c) 2 : 98, (d) 4 : 96, (e) 6 : 94, (f) 8 : 92 and (g) 10 : 90.

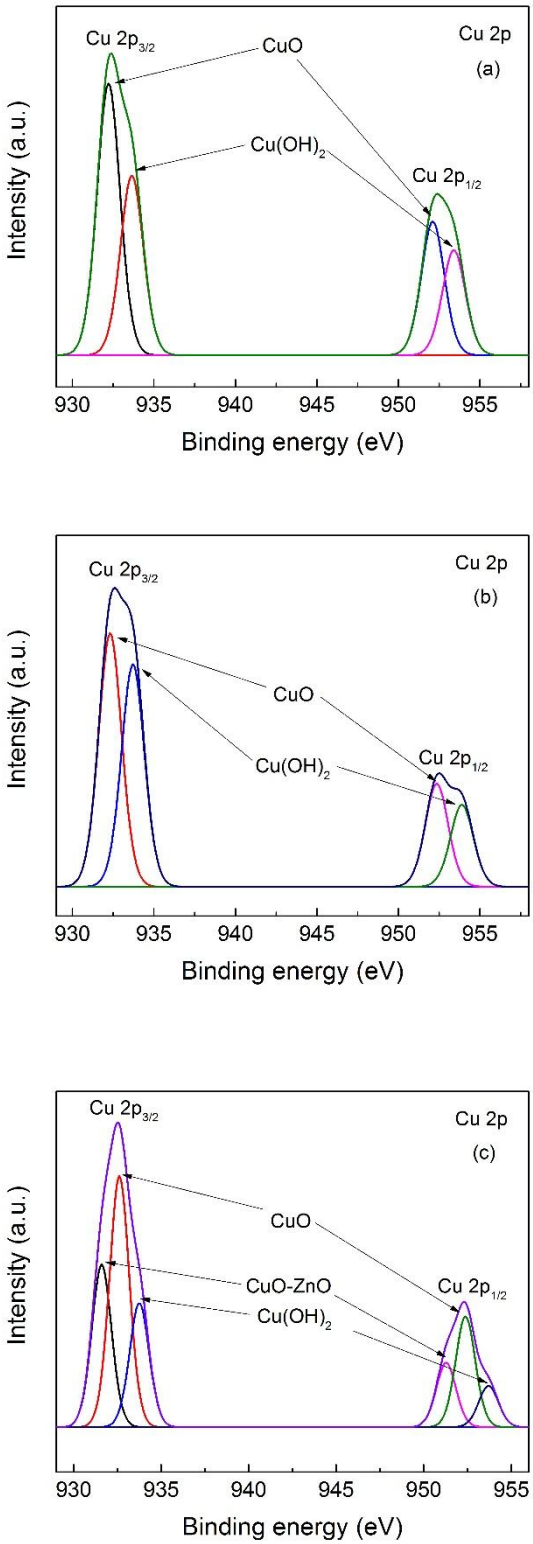

Fig. 4.23 XPS spectra of Cu 2p core-level of sintered CuO-ZnO at 500 °C at various molar ratio of Cu : Zn content of (a) 6 : 94, (b) 8 : 92 and (c) 10 : 90.

After deconvolution, the authors observed the occurrence of three peaks located at 1019.2, 1021.2, and 1022.8 eV. An occurrence of a prominent peak at 1021.2 eV is corresponding to the common of ZnO crystal peak. In the hexagonal ZnO crystal, zinc cation is coordinated with four oxygen atoms tetrahedrally and shows a peak at 1021.2 eV. For the ideal, there are no any oxygen deficiencies in the structure. However, when the tetrahedrally of oxygen coordinated with ZnO, deficient of oxygen atoms or impurities produce a new peak of binding energy at 1019.2 eV. A peak occurs at 1022.8 eV is indicated that the hydroxide of zinc ($Zn(OH)_2$). At higher molar ratio of Cu : Zn, there is new binding energy peaks appearance at a lower binding energy compared with pure ZnO in the XPS spectra indicating to oxygen deficiency defect in CuO-ZnO structure, in this case, it might be the appearance of the formation between the copper atom and zinc atom to form a complex compound.

Fig 4.22 displays the XPS spectra of O 1s region of as-prepared CuO-ZnO at various molar ratio of Cu : Zn. It is demonstrated in Fig. 4.23 that the spectra of O 1s level in samples of as-prepared CuO-ZnO at various molar ratio of Cu : Zn have different forms of oxygen. For pure ZnO, the peaks in O 1s region were de-convoluted with Gaussian fitting. Peak centered at 530.0 and 530.8 are corresponded to the atoms of oxygen in the lattice oxide without and with oxygen deficiencies, respectively. Peak located at 531.7 eV is generally depicted to chemisorbed of oxygen atoms onto the CuO-ZnO nanoparticles, such as carbonyl and hydroxyl groups [50]. The weak peaks at 533.6 and 533.0 eV are depicted to the probably correspond to the adsorbed water which only as-prepared condition has a peak at this position and so at the higher sintering temperature, water molecules were evaporated to the atmosphere [51]. At higher molar ratio of Cu : Zn content more than 6%, the peak at a lower binding energy about 528.8 eV indicate that CuO lattice is shown in Fig. 4.23. Because of all samples have been treated with thermal energy at 500 $^{\circ}$C, therefore peak represents the water molecules at the binding energy around 533 eV become lower intensity for all samples.

Fig. 4.23 shows the deconvoluted XPS spectra of the Cu 2p core-level of sintered CuO-ZnO at a temperature of 500 $^{\circ}$C for 2 hours at various molar ratios depicted to Cu$2p_{1/2}$ and Cu $2p_{3/2}$, respectively [53]. The Cu 2p core-level can be measured at molar ratio of Cu : Zn content above 6 : 94 into the CuO-ZnO structure. The center of peaks located at 932.0 and 952.0 eV is attributed to Cu $2p_{3/2}$ and Cu $2p_{1/2}$, respectively, indicating that the existence of CuO nanoparticles in the CuO-ZnO nanostructures [54]. The observed binding energy of Cu $2p_{3/2}$ at 931.6 eV confirms that Cu in the CuO-ZnO nanostructure belongs to CuO phase [54]. The peaks locate

at 932.3 and 933.7 eV are indicating to the oxide lattice and hydroxide of copper, respectively. Also, at high molar ratio of Cu : Zn content added into CuO-ZnO, the Cu 2p peak becomes higher intensity due to the substitution of the copper ion into structure [56]. At higher molar ratio of Cu : Zn content, the intensity of Cu 2p peaks become sharper which confirmed that there is much mixing phase between CuO and ZnO in CuO-ZnO nanostructure [55].

4.5 Characterization of CuO-ZnO humidity sensors

From the synthesis part of this chapter, at a molar ratio of Cu : Zn content about 6 is the starting point that XPS machine can detect the CuO-ZnO content and another reason is at above 500 °C, the water molecules were evaporated to the atmosphere. Therefore, we choose 3 conditions from above reasons. These conditions were 0 : 100, 6 : 94 and 10 : 90 at sintering temperature of 500 °C.

From figure 4.24, The responses of CuO-ZnO humidity sensors in the various relative humidity levels are measured by LCR meter. The result from LCR meter feature in the function of impedance (Ohm) and time (second). At the low relative humidity level (23 %RH) in all sensors, the value of impedance around 10^8 Ohm. At high relative humidity level (93 %RH) in all sensors, the value of impedance around 10^6 Ohm. Therefore, all samples have the ratio of the value of impedance at low humidity level to value of impedance at high humidity level about 2 orders. In my previous research, the authors used to research pure ZnO making humidity sensor but it does not. All samples have the ratio that is not significantly different. It can summary that all sensors based on CuO-ZnO can be fabricated for humidity sensor applications.

The hysteresis measurement of CuO-ZnO humidity sensors in all samples is shown in Fig. 4.25. This measurement was measured at from lower relative humidity level (23 %RH) to higher relative humidity level (93 %RH) marked as black color and from higher relative humidity level (93 % RH) to lower relative humidity level (23 % RH) marked as red color. From these results are used for checking the adsorption and desorption of sensing material that the value at the black point (lower humidity level to higher humidity level) and red point (higher humidity level to lower humidity level) are the same value. Because we didn't measure at all relative humidity level from 0 % RH to 100 % RH, then we check the linearity for making calibration curve of all relative humidity level. From the result, at 10 : 90 sample has the highest value of R-square (R^2) about 0.9902 (value calculated by using Excel software).

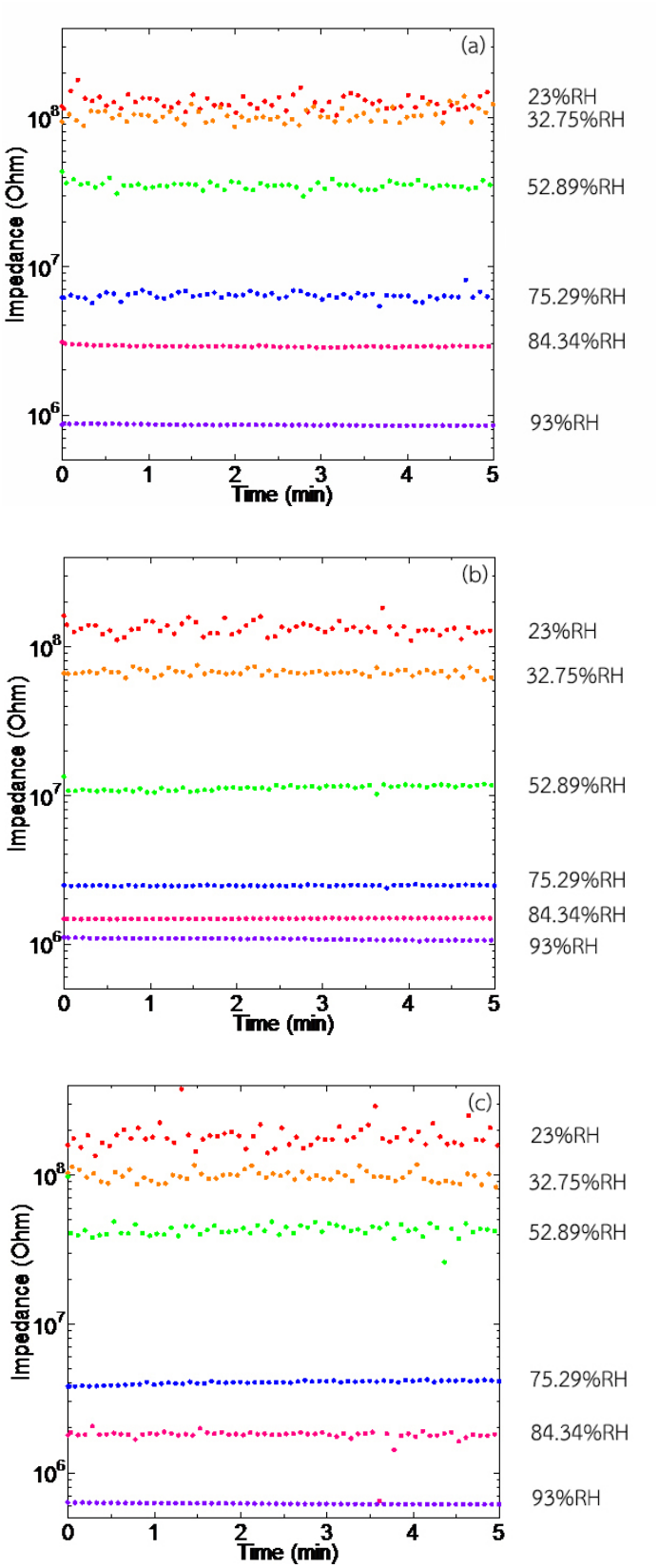

Fig. 4.24 Responses measurement of CuO-ZnO humidity sensors at various relative humidity levels of (a) 0 : 100, (b) 6 : 94 and (c) 10 : 90 of Cu : Zn molar ratio content.

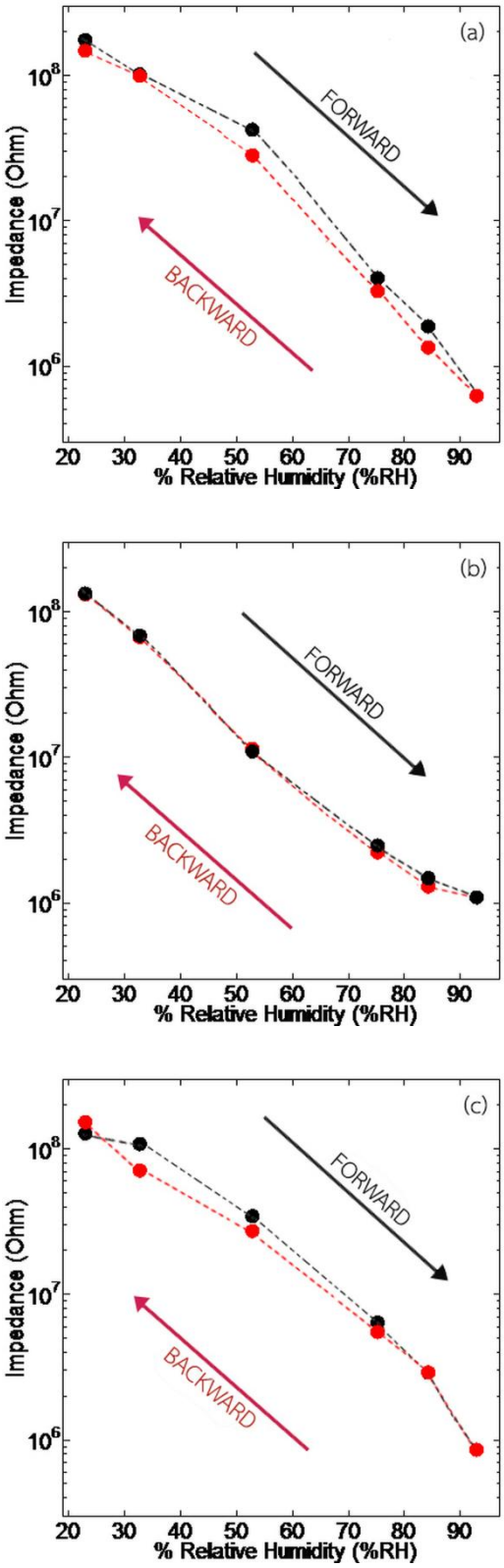

Fig. 4.25 The hysteresis characteristics measurement of CuO-ZnO humidity sensors at various relative humidity level of (a) 0 : 100, (b) 6 : 94 and (c) 10 : 90 of Cu : Zn molar ratio content.

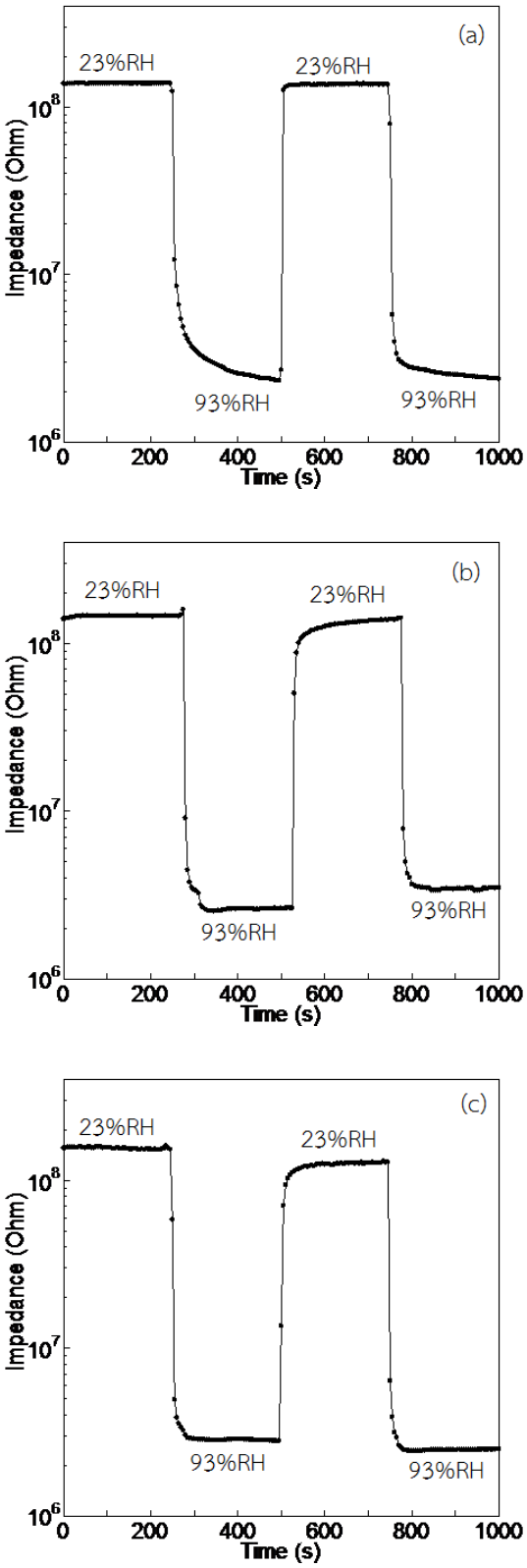

Fig. 4.26 The comparison of measurement on the humidity cycle testing from 23-93 %RH of CuO-ZnO humidity sensors at various relative humidity level of (a) 0 : 100, (b) 6 : 94 and (c) 10 : 90 of Cu : Zn molar ratio content.

Fig. 4.26 shows the response cycle measurement of CuO-ZnO humidity sensors with response time lower than 30 seconds for both the rising and falling changes in the relative humidity levels from high value of relative humidity (93 % RH) to low value of relative humidity (23 %RH) and low value of relative humidity to high value of relative humidity. The best value of response and recovery times for all samples of CuO-ZnO humidity sensors is humidity sensor in the condition of 10 : 90.

The sensing mechanism of CuO-ZnO humidity sensor is examined by the measurement with the complex impedance experiment. Cole-Cole plot at each value of relative humidity level was displayed in Fig. 4.27 (a) 0 : 100, (b) 6 : 94 and (c) 10 : 90. From results, it was found that all samples show two mechanisms of humidity sensors. At the low value of relative humidity level, it represents the semi-circle shape which the width of the semi-circle is depending on the level of relative humidity. From the Fig. 4.27, at the value of relative humidity regions from 23-53 %, it shows the large semi-circle which it can be seen with the linear relation. For the high value of relative humidity, it shows the semi-circle connected with a linear line. From these results, the mechanism of chemisorption was found at a low level of relative humidity. The mechanism in this dissertation is explained by the using of the equivalent circuit, which is illustrated in Fig. 4.27(d). For the high-level of relative humidity, the number of water moisture molecules were adsorbed on the surface of CuO-ZnO nanomaterial film with the formation of hydroxyl groups. Therefore, the changing in the value of impedance output was also small. Besides this, the mechanism of physisorption was found at the high-level of relative humidity level and the equivalent circuit for high-level of relative humidity level is illustrated in Fig.4.27(e). For the equivalent circuits, there is the resistance (R_p), the capacitance (C_p) and contact resistance (R_s) of these CuO-ZnO humidity sensors. In a case of high-level of relative humidity, the Warburg impedance (Z_w) in series with R_p was inputted into the equivalent circuit. At a higher level of relative humidity, the water moisture molecules could penetrate to the interlayer of CuO-ZnO. This process produces a substantial change in the value of the impedance of humidity sensor device.

Understanding the mechanisms of the sensitivity of humidity sensor, the authors model the equivalent circuit of resistor and capacitor for explaining the diagrams of complex impedance as shown in Fig 4.27 (d), (e).

At the low-level of relative humidity, the amount of the moisture is low. Moisture molecules will be adsorbed at the active area form the hydroxyl functional group. Proton can move from surface of hydroxyl to the moisture molecule to form the hydronium ion (H_3O^+). Therefore, at low-level of relative humidity, the electrical

conduction process influenced by the charged carriers and bounded electrons. Charged carriers may come from H_3O^+ and the sensing materials.

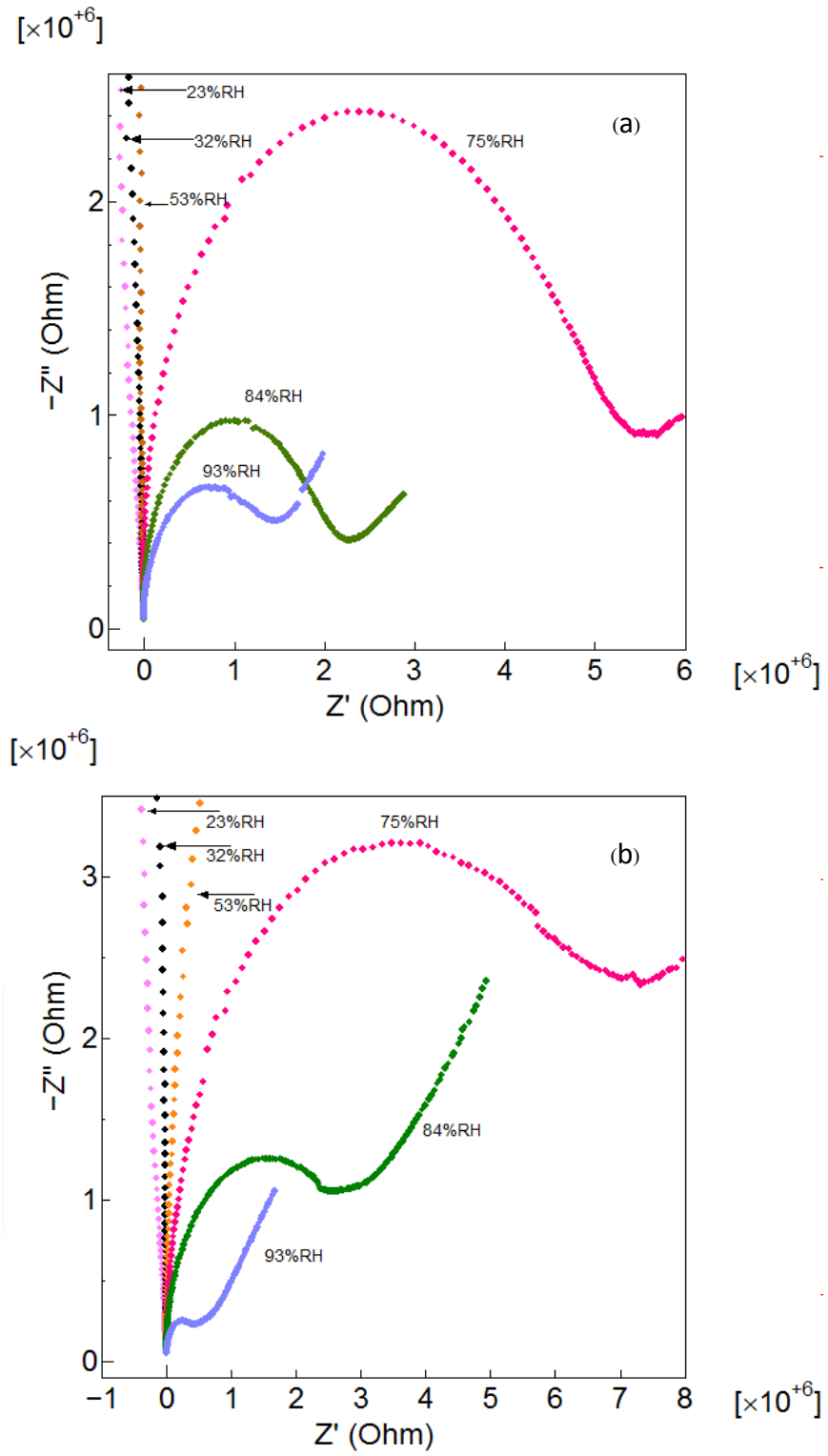

Fig. 4.27 Cole-Cole plot of CuO-ZnO humidity sensors at various relative humidity levels of (a) 0 : 100, (b) 6 : 94, (c) 10 : 90 and the equivalent circuits of the sensor at the region of (d) low and (e) high relative humidity level.

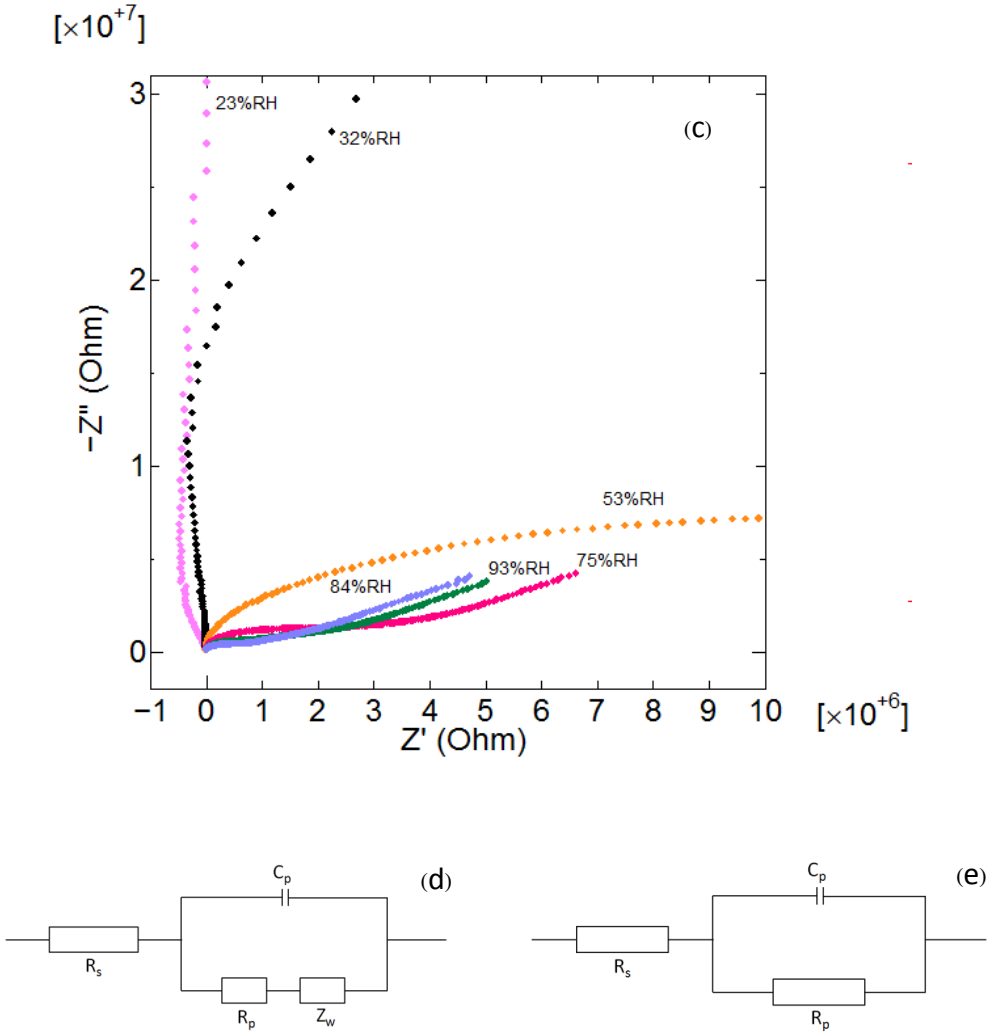

Fig. 4.27 (continued) Cole-Cole plot of CuO-ZnO humidity sensors at various relative humidity levels of (a) 0 : 100, (b) 6 : 94, (c) 10 : 90 and the equivalent circuits of the sensor at the region of (d) low and (e) high relative humidity level.

When the relative humidity is increasing, the increased quantity of adsorbed moisture reduces the resistances from grain boundary and interface between electrodes and sensing material of the humidity sensor. Meanwhile, the moistures are changed, which increases the value of capacitance within the sensor. At the high-level value of relative humidity, the H_3O^+ molecule is reduced into the H_2O and H^+. And then, high quantity of hydrogen ions became the prominent carrier of the electrons move from the sensing material. Therefore, at high-level of relative humidity, the electrical conductivity process is mainly due to adsorbed moistures. There is another semicircle shape appears, the electrical conductivity becomes larger when the level of relative humidity increases.

CHAPTER 5

CONCLUSION

The present thesis dealt mainly with CuO-ZnO, study the synthesis preparation of CuO-ZnO nanomaterial using co-precipitation method, choosing the CuO-ZnO as humidity sensing material for the humidity sensor application.

In the first part of this research, our work on the synthesis of nanostructured of CuO-ZnO using the low-temperature wet chemical route namely as co-precipitation process with starting precursor of zinc nitrate and copper nitrate. There are two major conditions for studying the effect on the properties of CuO-ZnO nanostructure such as annealing temperature from 500, 600, 700, 800 $^{\circ}$C for 2 hours and added copper content into the structure of CuO-ZnO at molar ratio of Cu : Zn of 0 : 100, 1 : 99, 2 : 98, 4 : 96, 6 : 94, 8 : 92 and 10 : 90. X-ray diffractogram showed that all samples have a higher intensity of all diffraction peaks at the higher annealing temperature and there are some peaks depict to CuO crystal structure shown at the higher amount of added copper content in the CuO-ZnO structure. SEM and TEM micrographs show the changing in the shape and size of nanostructure by the influence of thermal energy and amount of copper contents. FTIR result show the vibrational property which represent to the high quality CuO-ZnO nanostructure. In additions, XPS spectra confirms the successfully synthesis of CuO-ZnO nanostructure by co-precipitation process. From all results in the first part, the authors chose the condition at temperature of 500 $^{\circ}$C due to some functional groups were decomposition from the nanostructure which confirmed with the FTIR result. From XPS results, the authors chose the conditions at 0-100, 6-94 and 10-90 which represent the pure ZnO, small amount which Cu 2p core level of XPS appear in data, and highest amount of Cu : Zn in this experiment, respectively. In the second part of this research on the fabrication of CuO-ZnO layer as sensing material in humidity sensor application using electrostatic spray deposition technique. The suitable sensor in this study has the value of the sensitivity of 279 Ohm/ % RH and hysteresis of 4 % RH. The response and recovery time of humidity sensor are 26 and 6 seconds, respectively.

Bibliography

[1] United States National Nanotechnology Initiative. **What is Nanotechnology?** [Online]. Available: https://www.nano.gov/nanotech-101/what/definition

[2] The Future of Human Evolution. **History of Nanotechnology.** [Online]. Available: http://futurehumanevolution.com/history-of-nanotechnology-updated

[3] Wonderopolis. **What is humidity?** [Online]. Available: http://wonderopolis.org/wonder/w hat-is-humidity

[4] Vedhakkani Jeseentharani, Boniface Jeyaraj, John Pragasam, Arunachalam Dayalan, Karach alacheruvu Seetharamaiah Nagaraja. 2010. "Humidity Sensing Properties of CuO, ZnO and NiO Composites." **Sensors & Transducers.** 113(2):48-55.

[5] Shun Hua Xiao, Hai Jun Xu, Jin Hu, Wei Fen Jiang and Xin Jian Li. 2008. "Structure and hu- midity sensing properties of barium strontium titanate/silicon nanoporous pillar array composite films." **Thin Solid Films.** 517(2):929-932.

[6] Baochang Cheng, Baixiang Tian, Cuicui Xie, Yanhe Xiao and Shuijin Lei. 2011. "Highly sen- sitive humidity sensor based on amorphous Al_2O_3 nanotubes." **Materials Chemistry.** 21:1907-1912.

[7] M. Li and Y. Chen. 1996. "An investigation of response time of TiO_2 thin film oxygen sens- ors." **Sens. Actuators B**. 32(1):83-85.

[8] P. Chauhan, S. Annapoorni and S. K. Trikha. 1999. "Humidity sensing properties of nanocr- ystalline haematile thin film prepared by sol-gel processing." **Thin Solid Film.** 346(1-2):266-268.

[9] D. Zappa, E. Comini, R. Zamani, J. Arbiol, J.R. Morante and G. Sberveglieri. 2011. "Copper oxide nanowires prepared by thermal oxidation for chemical sensing." **Procedia Engineering.** 25:753-756.

[10] U. Ozgur, Y. I. Alivov, C. Liu, A. Teke, M. A. Reshchikov, S. Dogan, V. Avrutin, S. J. Cho and H. Morkoc. 2005. "A comprehensive review of ZnO materials and devices." **J. Appl Phys.** 98:041301-041103.

[11] V. A. Coleman, C. Jagadish, 2006. “Chapter 1 – Basic Properties and Applications of ZnO, Zinc Oxide Bulk, Thin Films and Nanostructures, Elsevier Science” **Oxford.** 1-20.

[12] Archana S. Kamble, Bhavesh B. Sinha, Kookchae Chung, Myeng G. Gil, Vishal Burungale, Chan-Jin Park, Jin H. Kim and Pramod S. Patil. 2014. “Effect of hydroxide anion generating agents on growth and properties of ZnO nanorod arrays.” **Electrochimica Acta.** 149:386-393.

[13] C. Klingshirn. 2007. “ZnO: Material, Physics and Applications.” **ChemPhysChem.** 8:782-803.

[14] A. B. Djurisic, Y. H. Leung, K. H. Tam, L. Ding, W. K. Ge, H. Y. Chen and S. Gwo. 2006. “Gre- en, yellow, and orange defect emission from ZnO nanostructures: Influence of excitation wavelength.” **Appl Phys Lett.** 88:103107.

[15] Klaus Ellmer and Andreas Klein. 2008. “Transparent Conductive Zinc Oxide: Basics and Applications in Thin Films.” **Springer.**

[16] Luoyang Tongrun Info Technology CO. LTD. **A brief introduction of Copper Oxide.**
[Online]. Available: http://www.icanz.net/News/A-brief-introduction-of-Copper-Oxide.html

[17] A. Mittiga, E. Salza, F. Sarto, M. Tucci and R. Vasanthi. 2006. “Heterojunction solar cell with 2% efficiency based on a Cu[sub 2]O substrate.” **Appl Phys Lett.** 88:163502.

[18] Z. Da-Wei, Y. Tang-Hong and C. Chun-Hua. 2005. “Cu nanoparticles derived from CuO electrodes in lithium cells.” **Nanotechnology.** 16:2338.

[19] B. G. John. 2003. “Bond-length fluctuations in the copper oxide superconductors.” **J. Physics: Condensed Matter.** 15:R257.

[20] Y. Sui, Y. Zeng, W. Zheng, B. Liu, B. Zou and H. Yang. 2012. “Synthesis of polyhedron hollow structure Cu_2O and their gas-sensing properties.” **Sensors and Actuators B: Chemical.** 171-172:135-140.

[21] E. Fortin and F. L. Weichman. 1962. “Photoconductivity in Cuprous Oxide Single Crystals.” **Canadian Journal of Physics.** 40:1703-1713.

[22] Xiaoxue Xu, Hong Yang and Yinong Liu. 2012. "Self-assembled structures of CuO primary crystals synthesized from $Cu(CH_3COO)_2$-NaOH aqueous systems." **CrystEngComm.** 14:5289-5298.

[23] EDN network. **White LEDs Printed on Paper – A Doctoral Thesis- Part I.** [Online]. Available: http://www.edn.com/Home/PrintView?contentItemId= 4391796**.**

[24] Namita Rajput. 2015. **"Methods of Preparation of Nanoparticles – A Review"** International Journal of Advances in Engineering & Technology. 7(4) : 1806-1811.

[25] Hong Wan and Harry E. Ruda. 2010. **"A study of the growth mechanism of CVD-grown ZnO nanowires"** Journal of Materials Science: Materials in Electronics. 21(10) : 1014-1019.

[26] Strem Chemicals, Inc. 2013. **"Application of Metal Amidinate Precursors in CVD/ALD"** [saved from URL:http://www.azonano.com/article.aspx?ArticleID=3 428].

[27] Riyadh M. Alwan, Quraish A. Kadhim, Kassim M. Sahan, Rawaa A. Ali, Roaa J. Mahdi, Noor A. Kassim and Alwan N. Jassim. 2015. **"Synthesis of Zinc Oxide Nanoparticles via Sol-Gel Route and Their Characterization"** Journal of Nanoscience and Nanotechnology. 5(1) : 1-6.

[28] Chemat Technology. **A Total Sol-gel Solution.** [Online]. Available : http://www.chema t.com/chemattechnology/SolGel.aspx

[29] Hiromichi Hayashi and Yukiya Hakuta. 2010. **"Hydrothermal Synthesis of Metal Oxide Nanoparticles in Supercritical Water"** Materials. 3(7) : 3794-3817.

[30] Kai Chen, Dao D. Thang, Satoshi Ishii, Ramu P. Sugavaneshwa and Tadaaki Nagao. 2015. **"Selective patterned growth of ZnO nanowires/nanosheets and their photoluminescence properties"** Optical Materials Express. 5(2) : 353-360.

[31] Zeljka Petrovic, Mira Ristic, Svetozar Music and Martin Fabian. 2015. **"Nano /microstructure and optical properties of ZnO particles precipitated from zinc acet- ylacetonate"** Journal of Molecular Structure. 1090 : 121-128.

[32] Arshid M. Ali, Ayyaz Muhammad, Amir Shafeeq, Hafiz M. A. Asghar, Syed N. Hussain, Hamid Sattar. 2012. **"Doped Metal Oxide (ZnO) and Photocatalysis: A Review"** Journal of Pakistan Institute of Chemical Engineers. 40(1) : 11-19.

[33] T. G. Kryshtab, V. S. Khomchenko, V. P. Papusha, M. O. Mazin and Yu A. Tzyrkunov. 2002. **"Thin ZnS:Cu,Ga and ZnO:Cu,Ga film phosphors"** Thin Solid Films. 403-404 : 76-80.

[34] T. R. N. Kutty and N. Raghu. 1989. **"Varistors based on polycrystalline ZnO:Cu"** Applied Physics Letters. 54 : 1796-1798.

[35] Jin-Bock Lee, Hye-Jung Lee, Soo-Hyung Seo and Jin-Seok Park. 2001. **"Characterization of undoped and Cu-doped ZnO films for surface acoustic wave applications"** Thin Solid Films. 398-399 : 641-646.

[36] C. X. Xu, X. W. Sun, X. H. Zhang, L. Ke and S. J. Chua. 2004. **"Photoluminescent properties of copper-doped zinc oxide nanowires"** Nanotechnology. 15 : 856-861.

[37] S. Fabbiyola, L. John Kennedy, J. Judith Vijaya, M. Bououdina and Steve Dunn. 2016. **"Structural, Optical and Magnetic Properties of Cu-Doped ZnO Nanoparticles by Co-Precipitation Method"** Journal of Nanoscience and Nanotechnology. 16 : 9722-9730.

[38] XRD, King Mongkut's University of Technology Thonburi. **X-Ray Diffractometer.**
[Online]. Available : http://www.mt.kmutt.ac.th/xrd/Above%20The%20Light.html

[39] Microscopic center, Faculty of Science, Burapha university. **Transmission Electron Microscope.**
[Online]. Available : http://www.microscopic.center.sci.buu.ac.th/service.html

[40] Thailand Center of Excellence in Physics. **Field Emission Scanning Electron Microscope (JSM-7001F).**
[Online]. Available : http://thep-center.org/src/machine_fe-sem.php

[41] Scientific and Technological Research Equipment Centre. **Fourier transform infrared spectroscopy.**
[Online]. Available : http://www.strec.chula.ac.th/

[42] EAG Laboratory. **X-ray photoelectron spectroscopy.** [Online]. Available : http://www.ea g.com/xps-esca/

[43] Kratos Analytical. **X-ray photoelectron spectroscopy (XPS).** [Online]. Available : http:// www.kratos.com/applications/techniques/x-ray-photoelectron-spectroscopy

[44] Department of Physics, Technical University of Munich. **Photoelectron spectroscopy.** [Online]. Available : https://www.e20.ph.tum.de/en/techniques/photoelectron-spectroscopy/

[45] Thailand Center of Excellence in Physics. **X-ray photoelectron spectroscopy.** [Online]. Available : http://thep-center.org/src/machine_xps.php

[46] B. S. Barros, R. Barbosa, N. R. dos Santos, T. S. Barros and M. A. Souza. 2006. **"Synthesis and X-ray Diffraction Characterization of Nanocrystalline ZnO Obtained by Pechini Method"** Inorganic Materials. 42(12) : 1348-1351.

[47] P. Bindu and Sabu Thomas. 2014. **"Estimation of lattice strain in ZnO nanoparticles: X-ray peak profile analysis"** J. Theor Appl Phys. 8 : 123-134.

[48] R. Al-Gaashani, S. Radiman, A.R. Daud, N. Tabet and Y. Al-Douri. 2012. **"XPS and optical studies of different morphologies of ZnO nanostructures prepared by microwave methods"** Ceramics International. 39(3): 2283-2292.

[49] Tridib Kumar Bhowmick, Akkihebbal K. Suresh, Shantaram G. Kane, Ajit C. Joshi and Jayesh R. Bellare. 2008. **"Physicochemical characterization of an Indian traditional medicine, Jasada Bhasma: detection of nanoparticles containing non-stoichiometric zinc oxide"** J. Nanoparticle Research. 11(3):655-664.

[50] Chao Chen, Ti Wang, Hao Wu, He Zheng, Jianbo Wang, Yang Xu and Chang Liu. 2015. **"Room-temperature electrically pumped near-infrared random lasing from high-quality m-plane ZnO based metal-insulator-semiconductor devices"** J. Nanoscale Research Letter. 10:100

[51] Ulugbek Shaislamov, Karthikeyan Krishnamoorthy, Sang Jae Kim, Amir Abidov, Bunyod Allaberqenov, Sungjin Kim, Sooseok Choi, Rai Suresh, Waqar Muhammad Ahmed and Heon-Ju Lee. 2015. **"Highly stable hierarchical p-CuO/ZnO nanorod/nanobranch photoelectrode for efficient solar energy conversion"** International Journal of Hydrogen Energy. 41(4):2253-2262.

[52] D.A. Svintsitskiy, A.I. Stadnichenko, D.V. Demidov, S.V. Koscheev and A.I. Boronin. 2011. **"Investigation of oxygen states and reactivities on a nanostructured cupric oxide surface"** J. Applied Science Surface. 257:8542-8549.

[52] Nguyen Duc Hoa, Nguyen Van Quy, Hyuck Jung, Dojin Kim, Hyojin Kim and Soon-Ku Hong. 2010. **"Synthesis of porous CuO nanowires and its application to hydrogen detection"** Sensors and Actuators B: Chemical. 146:266-272.

[53] Panneerselvam Sathishkumar, Ramaswamy Sweena, Jerry J. Wu and Sambandam Anandan. 2011. **"Synthesis of CuO-ZnO nanophotocatalyst for visible light assisted degradation of a textile dye in aqueous solution"** Chemical Engineering Journal. 171:136-140.

[54] K. Milenova, I. Stambolova, V. Blaskov, A. Eliyas, S. Vassilev and M. Shipochka. 2013. **"The effect of introducing copper dopant on the photocatalytic activity of ZnO nanoparticles"** Journal of Chemical Technology and Metallurgy. 48(3):259-264.

[55] Chunyang Zhou, Lin Xu, Jian Song, Ruiqing Xing, Sai Xu, Dali Liu and Hongwei Song. 2014. **"Ultrasensitive non-enzymatic glucose sensor based on three-dimensional network of ZnO-CuO hierarchical nanocomposites by electrospinning"** Scientific Reports. 4:7382.

Biography

My name is Natpasit Chaithanatkun. I was born in Songkhla province, which is a big city in the south of Thailand. My hometown is in Sungai-Kolok district in Narathiwat province which is in the south of Thailand.

Education information

- 2015 – Present **King Mongkut's Institute of Technology Ladkrabang**, College of Nanotechnology, Master of Science Program in Nanoscience and Nanotechnology.
- 2011 – 2014 **King Mongkut's Institute of Technology Ladkrabang**, College of Nanotechnology, Bachelor of Engineering Program in Nanomaterial Engineering, GPA 3.20.
- 2007 – 2010 **Suankularb Wittayalai Rangsit School**, GPA 3.07

ISI Journal

- K. Onlaor, **N. Chaithanatkun** and B. Tunhoo, Electrical mechanisms of bi-stable memory devices based on an Al/PVK:ZnO NPs/ITO structure with different ZnO NPs annealing temperatures, Current Applied Physics 16 (2016) 1418-1423.

Scopus Journal

- **N. Chaithanatkun**, K. Onlaor and B. Tunhoo, The Influence of Annealing Temperature on Structural Properties of Zinc Oxide Nanoparticles Synthesized by Precipitation Method, Key Engineering Material 728 (2017) 215-220.
- **N. Chaithanatkun**, K. Onlaor, T. Thiwawong and B. Tunhoo, Modification of Structural and Vibrational Properties of ZnO Nanoparticles Prepared by Simple Chemical Precipitation Method, Key Engineering Material, 675-676 (2016) 138-141.

SJR Journal

- **N. Chaithanatkun**, K. Onlaor, T. Thiwawong and B. Tunhoo, Effect of Hydroxide Concentration and Adding Ascorbic Acid on Morphology shape of Zinc Oxide Nanostructure Prepared by Simple Chemical Precipitation Method, Applied Mechanics and Materials 848 (2016) 76-79.

International Conference Proceeding

- **N. Chaithanatkun**, D. Chantarawong, P. Songkeaw, K. Onlaor, T. Thiwawong and B. Tunhoo, Effect of Ascorbic Acid on Structural Properties of ZnO Nanoparticles Prepared by Precipitation Process, Proceedings of the 10th IEEE International Conference on Nano/ Micro Engineered and Molecular Systems (IEEE-NEMS 2015), Xi'an, China, April 7-11, 2015.
- **N. Chaithanatkun**, D. Chantarawong, P. Songkeaw, K. Onlaor, T. Thiwawong and B. Tunhoo, Electrical Bistable Properties of ZnO Nanoparticles Thin Film Prepared by Electrostatic Spray Deposition Technique, Proceedings of the 10th IEEE International Conference on Nano/Micro Engineered and Molecular Systems (IEEE-NEMS 2015), Xi'an, China, April 7-11, 2015.
- **N. Chaithanatkun**, K. Onlaor and B. Tunhoo, Comparative Study of Post-sintering Temperature on Properties of Copper Doped Zinc Oxide Nanoparticles Prepared by Co-precipitation Process, Materials Today Proceeding (accepted).
- **N. Chaithanatkun**, T. Fujihara, M. Kamano, T. Konishi, N. Uehara, K. Onlaor, B. Tunhoo and T. Kozai, Influence of Post-Annealing Temperature on the Morphological, Structural and Optical Properties of Spin coated Zinc Oxide Thin Films, Materials Today Proceeding (accepted).

Biography

My name is Natpasit Chaithanatkun. I was born in Songkhla province, which is a big city in the south of Thailand. My hometown is in Sungai-Kolok district in Narathiwat province which is in the south of Thailand.

Education information

- 2015 – Present **King Mongkut's Institute of Technology Ladkrabang**, College of Nanotechnology, Master of Science Program in Nanoscience and Nanotechnology.
- 2011 – 2014 **King Mongkut's Institute of Technology Ladkrabang**, College of Nanotechnology, Bachelor of Engineering Program in Nanomaterial Engineering, GPA 3.20.
- 2007 – 2010 **Suankularb Wittayalai Rangsit School**, GPA 3.07

ISI Journal

- K. Onlaor, **N. Chaithanatkun** and B. Tunhoo, Electrical mechanisms of bi-stable memory devices based on an Al/PVK:ZnO NPs/ITO structure with different ZnO NPs annealing temperatures, Current Applied Physics 16 (2016) 1418-1423.

Scopus Journal

- **N. Chaithanatkun**, K. Onlaor and B. Tunhoo, The Influence of Annealing Temperature on Structural Properties of Zinc Oxide Nanoparticles Synthesized by Precipitation Method, Key Engineering Material 728 (2017) 215-220.
- **N. Chaithanatkun**, K. Onlaor, T. Thiwawong and B. Tunhoo, Modification of Structural and Vibrational Properties of ZnO Nanoparticles Prepared by Simple Chemical Precipitation Method, Key Engineering Material, 675-676 (2016) 138-141.

SJR Journal

- **N. Chaithanatkun**, K. Onlaor, T. Thiwawong and B. Tunhoo, Effect of Hydroxide Concentration and Adding Ascorbic Acid on Morphology shape of Zinc Oxide Nanostructure Prepared by Simple Chemical Precipitation Method, Applied Mechanics and Materials 848 (2016) 76-79.

International Conference Proceeding

- **N. Chaithanatkun**, D. Chantarawong, P. Songkeaw, K. Onlaor, T. Thiwawong and B. Tunhoo, Effect of Ascorbic Acid on Structural Properties of ZnO Nanoparticles Prepared by Precipitation Process, Proceedings of the 10th IEEE International Conference on Nano/ Micro Engineered and Molecular Systems (IEEE-NEMS 2015), Xi'an, China, April 7-11, 2015.
- **N. Chaithanatkun**, D. Chantarawong, P. Songkeaw, K. Onlaor, T. Thiwawong and B. Tunhoo, Electrical Bistable Properties of ZnO Nanoparticles Thin Film Prepared by Electrostatic Spray Deposition Technique, Proceedings of the 10th IEEE International Conference on Nano/Micro Engineered and Molecular Systems (IEEE-NEMS 2015), Xi'an, China, April 7-11, 2015.
- **N. Chaithanatkun**, K. Onlaor and B. Tunhoo, Comparative Study of Post-sintering Temperature on Properties of Copper Doped Zinc Oxide Nanoparticles Prepared by Co-precipitation Process, Materials Today Proceeding (accepted).
- **N. Chaithanatkun**, T. Fujihara, M. Kamano, T. Konishi, N. Uehara, K. Onlaor, B. Tunhoo and T. Kozai, Influence of Post-Annealing Temperature on the Morphological, Structural and Optical Properties of Spin coated Zinc Oxide Thin Films, Materials Today Proceeding (accepted).